STRUCTURAL INSIGHTS INTO PHOSPHOLIPASE Cε FUNCTION

by

Ngango Yvon Rugema

A Dissertation

Submitted to the Faculty of Purdue University

In Partial Fulfillment of the Requirements for the degree of

Doctor of Philosophy

Department of Chemistry

West Lafayette , Indiana

August 2019

THE PURDUE UNIVERSITY GRADUATE SCHOOL
STATEMENT OF COMMITTEE APPROVAL

Dr. Angeline Lyon, Chair
Department of Chemistry
Dr. Christine A. Hrycyna
Department of Chemistry
Dr. Nicholas N. Noinaj
Department of Biology
Dr. Val J. Watts
Department of Medicinal Chemistry and Molecular Pharmacology

Approved by:
Dr. Christine A. Hrycyna
Head of the Graduate Program

TABLE OF CONTENTS

LIST OF TABLES

LIST OF FIGURES

ABSTRACT

Author: Rugema, Ngango Yvon. PhD
Institution: Purdue University
Degree Received: August 2019
Title: Structural Insights into Phospholipase Cε Function
Committee Chair: Angeline Lyon

Phospholipase Cε (PLCε) is a member of the PLC family of enzymes, which hydrolyze phosphatidylinositol lipids following the activation of G protein coupled receptors (GPCRs) and receptor tyrosine kinases (RTKs). PLCε is unique among the PLC superfamily as it contains an N-terminal CDC25 domain, which has a guanine nucleotide exchange factor (GEF) activity for the small G protein Rap1A, and two C-terminal Ras association (RA) domains that bind scaffolding proteins and activated G proteins. PLCε activity plays an important role in cardiomyocyte contractility and survival. The best-characterized pathway of PLCε activation is mediated by β-adrenergic (β-AR) receptors. Stimulation of these receptors culminates in the activation of the small GTPase Rap1A, which binds to PLCε at the sarcoplasmic reticulum. There, PLCε hydrolyzes phosphatidylinol-4-phosphate (PI_4P) to produce diacylglycerol (DAG). Prolonged activation of this pathway results in increased Ca^{2+}-induced Ca^{2+} release (CICR) and increased expression of hypertrophy-related genes. However, the structural basis of PLCε basal activity, and the mechanism of Rap1A activation are largely unknown. We have now obtained the first high-resolution structure of PLCε. These studies, together with biochemical validation of our structure-based hypotheses, provide the first molecular insights into this enzyme.

CHAPTER 1. INTRODUCTION

1.1 Phospholipase C Subfamilies

PLC enzymes canonically hydrolyze the inner membrane lipid phosphatidylinositol-4,5-bisphosphate (PIP_2) [1], producing the important second messengers diacylglycerol (DAG) and inositol triphosphate (IP_3). DAG remains at the membrane, while IP_3 binds receptors to promote intracellular Ca^{2+} release [2,3]. DAG activates numerous effectors, including protein kinase C (PKC) [4 5], Ras guanyl-releasing protein (RasGRP), and protein kinase D (PKD) [6] **(Fig. 1. 1)**.

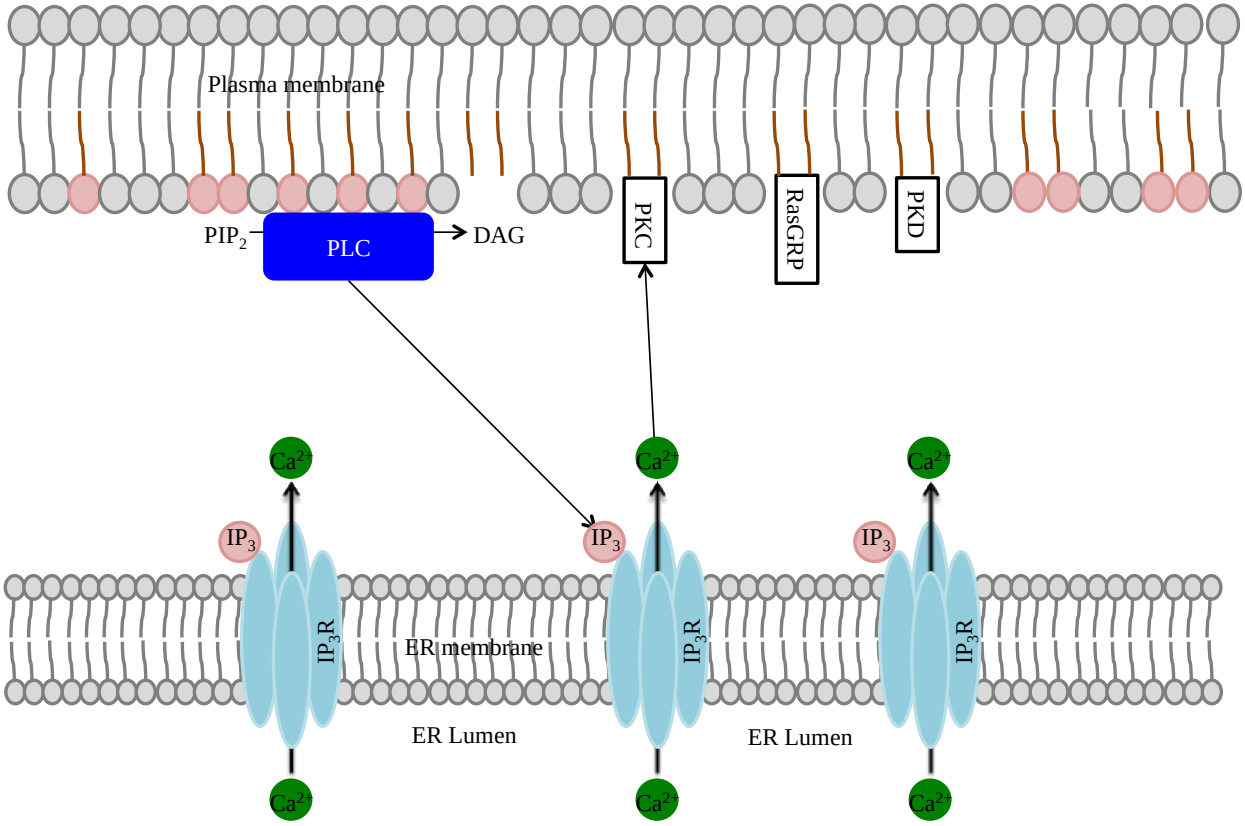

Figure 1.1 Phospholipase Cs classically hydrolyze phosphatidylinositol-4,5-bisphosphate. PLC enzymes hydrolyze PIP2 to produce the second messengers diacylglycerol (DAG) and inositol-1, 4, 5-triphosphate (IP3). DAG remains at the membrane and elicits cellular responses through effector proteins including protein kinase C (PKC), Ras guanyl nucleotide-releasing proteins (RasGRPs), and protein kinase D (PKD). IP_3 binds receptors at the endoplasmic or sarcoplasmic reticulum, triggering the release of Ca^{2+} from internal stores, and further activates PKC enzymes.

To date, thirteen isoforms of mammalian PLCs have been discovered, and are divided into six subfamilies: γ, δ, ζ, β, η, and ε [7,8] **(Fig. 1. 2A)**. Nearly all PLC enzymes contain a pleckstrin homology (PH) domain, and all contain four tandem EF hand repeats, a triose phosphate isomerase (TIM) barrel domain that houses the active site, and a C2 domain [9]. Additional domains, usually at the N- or C-termini of these enzymes, are required for subfamily specific-regulation.

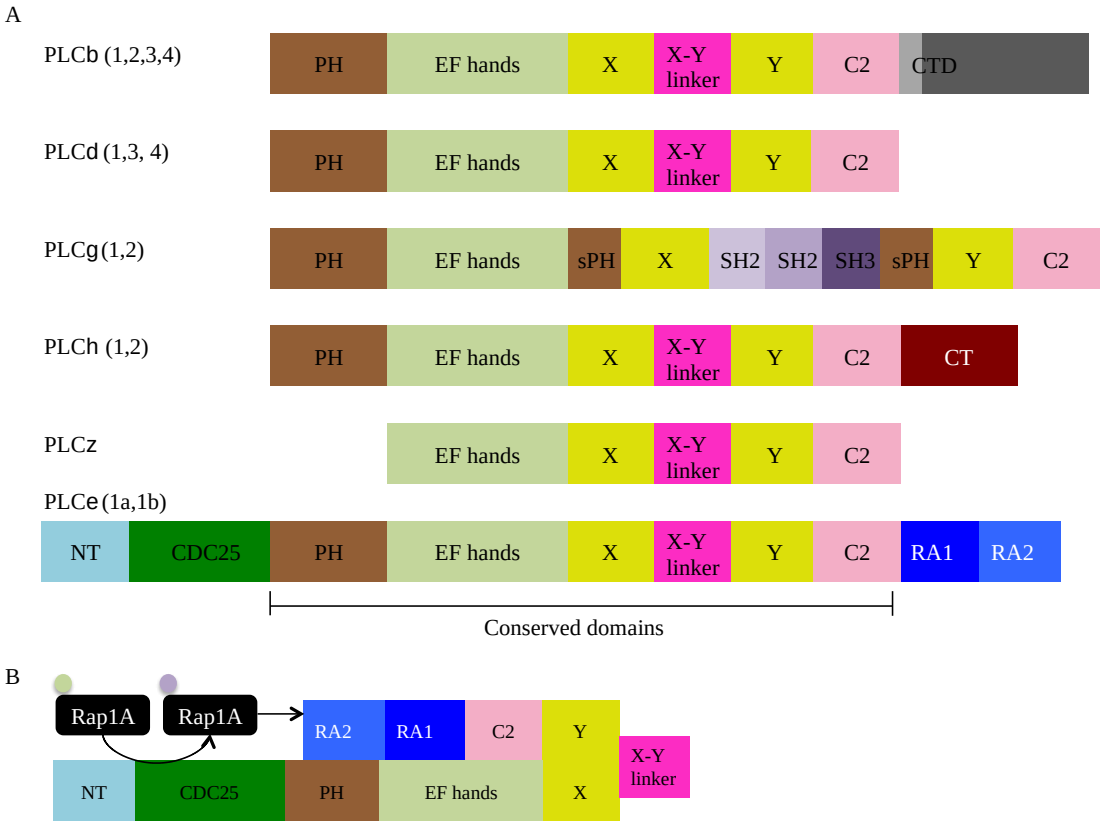

Figure 1.2 Phospholipases Cs are divided into six subfamilies

A. PLC enzymes are divided into six subfamilies based on their domain architecture. The conserved PLC core contains the PH-C2 domains, which are thought to represent the minimal fragment that retains lipase activity. Pleckstrin homology (PH), split PH (sPH), Src Homology (SH) domain, proximal C terminal domain (light grey CTD), distal C terminal domain (dark grey CTD), C-terminal unknown element (CT in burgundy), N-terminal unknown element (NT), cell division cycle protein 25-like homology domain (CDC25), Ras association (RA) domain. B. Schematic of the Rap1A–PLCε feed forward activation loop. The CDC25 domain activates the small GTPase Rap1A, which can then bind the RA2 domain. Green and purple circles correspond to GDP and GTP, respectively.

1.2 Structural Insights into the PLC Subfamilies

Structural and functional studies have provided a wealth of information regarding how these enzymes are regulated under basal and activating conditions. The best characterized PLC subfamily is the PLCβ subfamily, which have been crystallized alone and in complex with the activators Rac1 and the heterotrimeric G protein subunit $G\alpha_q$. Rac1 binds to the PH domain, and may regulate lipase activity by optimizing interactions between the PLCβ active site and the membrane [10,11]. The structures of $G\alpha_q$–PLCβ complexes revealed that $G\alpha_q$ allosterically activates PLCβ by displacing an autoinhibitory helix from the proximal C-terminal domain (CTD) from the core of the enzyme. In addition, interactions between $G\alpha_q$, the PLCβ core, and the distal CTD are proposed to help orient the activated complex at the membrane for efficient catalysis [12,13,14]. The EF hands 3/4 of PLCβ also interact with $G\alpha_q$ to increase the rate of GTP hydrolysis and terminate $G\alpha_q$ signaling [15]. Structures and biochemical studies of PLCδ have shown its PH and C2 domains bind PIP_2, helping to anchor the protein to the membrane and increase catalysis [16,17,18]. In PLCγ, its tandem Src homology (SH) domains are autoinhibitory [19]. Binding of the PLCγ SH2 and SH3 domains to receptor tyrosine kinases (RTKs) leads to phosphorylation of the SH2 domain and activation of the enzyme [19–21,22]. A structure of a phosphorylated PLCγ peptide bound to the SH2 domain revealed that activation must require a conformational change[19]. The small GTPase Rac has also been proposed to regulate activity through interactions with the split PH (sPH) domain of PLCγ [23]. There is no published structural information for the PLCη and PLCζ subfamilies. In PLCε, the only structural information available comes from nuclear magnetic resonance (NMR) structures of the C-terminal Ras association (RA) domains, and a crystal structure of the activator H-Ras·GTP in complex with the isolated RA2 domain [24].

The PLCε subfamily is the largest of the PLC isozymes **(Fig. 1. 2A)**, and contains four important regulatory elements. It contains a CDC25 homology domain that has guanine nucleotide exchange factor (GEF) activity for small GTPases (**Fig. 1. 2B**), a Y-box insertion within the TIM barrel that is required for activation by the small GTPase RhoA, and two C-terminal Ras association (RA) domains (**Fig. 1. 2B**). Biochemical data have shown that the C-terminal RA1 domain interacts with the scaffolding protein muscle-specific A-kinase anchoring protein (mAKAP) in cardiomyocytes, and thus contributes to subcellular localization [25,26]. The RA2 domain binds activated small GTPases, including Rap1A [27] **(Fig. 1. 2B)**, Rap2B [28–30] and H-Ras [24,31]. There are two reported PLCε splice variants that differ at the N-terminus, but both variants retain all known domains [32]

1.3 GPCR- and RTK-Dependent Activation of PLCε

Under basal conditions, PLCε is located in the cytosol [31], and is poised to integrate signals from both G protein-coupled receptors (GPCRs) and receptor tyrosine kinases (RTKs). Depending on the activation pathway, PLCε translocates to the plasma membrane [31], endoplasmic reticulum, sarcoplasmic reticulum [33,34], Golgi [26,35], or the perinuclear envelope[25,36]. This subcellular localization of PLCε has diverse physiological impacts, including increased cardiomyocyte hypertrophy-related gene expression [25,26,35,37], stimulation of Ca^{2+}-induced-Ca^{2+} release (CICR)[33,34,38], and activation of inflammatory pathways [39–41].

PLCε is activated downstream of GPCRs via signaling through the heterotrimeric G proteins Gβγ, $G\alpha_{12/13,}$ and $G\alpha_s$. Gβγ activates PLCε following stimulation of the endothelin-1 receptor (ET-1R) [35]. When mice with conditional deletions of PLCε were subjected to transverse aortic constriction (TAC) to induce cardiac hypertrophy [42], their hearts were smaller than wild-

type [26] and they had reduced expression of protein kinases linked to cardiac hypertrophy. Further studies focused on mapping the pathway linked Gβγ to PLCε activity. Following activation of ET-1R, Gβγ binds to PLCε and translocates the enzyme to the perinuclear membrane. There, PLCε hydrolyzes perinuclear phosphatidylinositol 4-phosphate (PI_4P), generating a local pool of DAG. DAG activates PKC, which in turn activates PKD and Ca^{2+}/calmodulin-dependent protein kinase (CaMKII). This results in phosphorylation of histone deacetylase (HDAC) and increased expression of genes involved in cardiac hypertrophy [26,43]**(Fig. 1. 3 left)**.

PLCε is also activated downstream β-adrenergic receptors (β-AR) through the heterotrimeric G protein $G\alpha_s$[26,33,34,38]. Following agonist binding to the βAR, $G\alpha_s$ is released and activates adenylyl cyclase (AC) to produce cyclic AMP (cAMP). The increased cAMP activates Epac (exchange protein directly activated by cAMP), which is a GEF for Rap1A. Rap1A·GTP binds the PLCε RA2 domain, and translocates the activation complex to the perinuclear Golgi where PI_4P is hydrolyzed [25,26]. This pathway is required for normal Ca^{2+}-induced Ca^{2+}-release (CICR) [33,34,44]. However, chronic activation of this pathway increases the expression of genes required for cardiac hypertrophy (**Fig. 1. 3 center**).

GPCRs coupled to $G\alpha_{12/13}$, such as the thrombin receptor, activate PLCε through the small GTPase RhoA[39–41,45–47]. Activation of thrombin receptors releases $G\alpha_{12/13,}$ which activates RhoGEFs, which in turn activate RhoA. RhoA binds to PLCε, translocating the complex to the Golgi, where PI_4P hydrolysis activates PKD. PKD phosphorylates the scaffold protein PEA15, which associates with ribosomal s6 kinase (rsk) in the cytoplasm. The PEA15–rsk complex phosphorylates Iκβ, which allows NF-κB (nuclear factor kappa-light-chain-enhancer of activated B cells) to translocate to the nucleus and increase the expression of inflammatory cytokines[48]**(Fig**

1. 3 right). Dysregulation of RhoA-dependent PLCε activation is linked to chronic inflammation, which is involved in cancer progression and formation of tumor microenvironments [49,48,50–54].

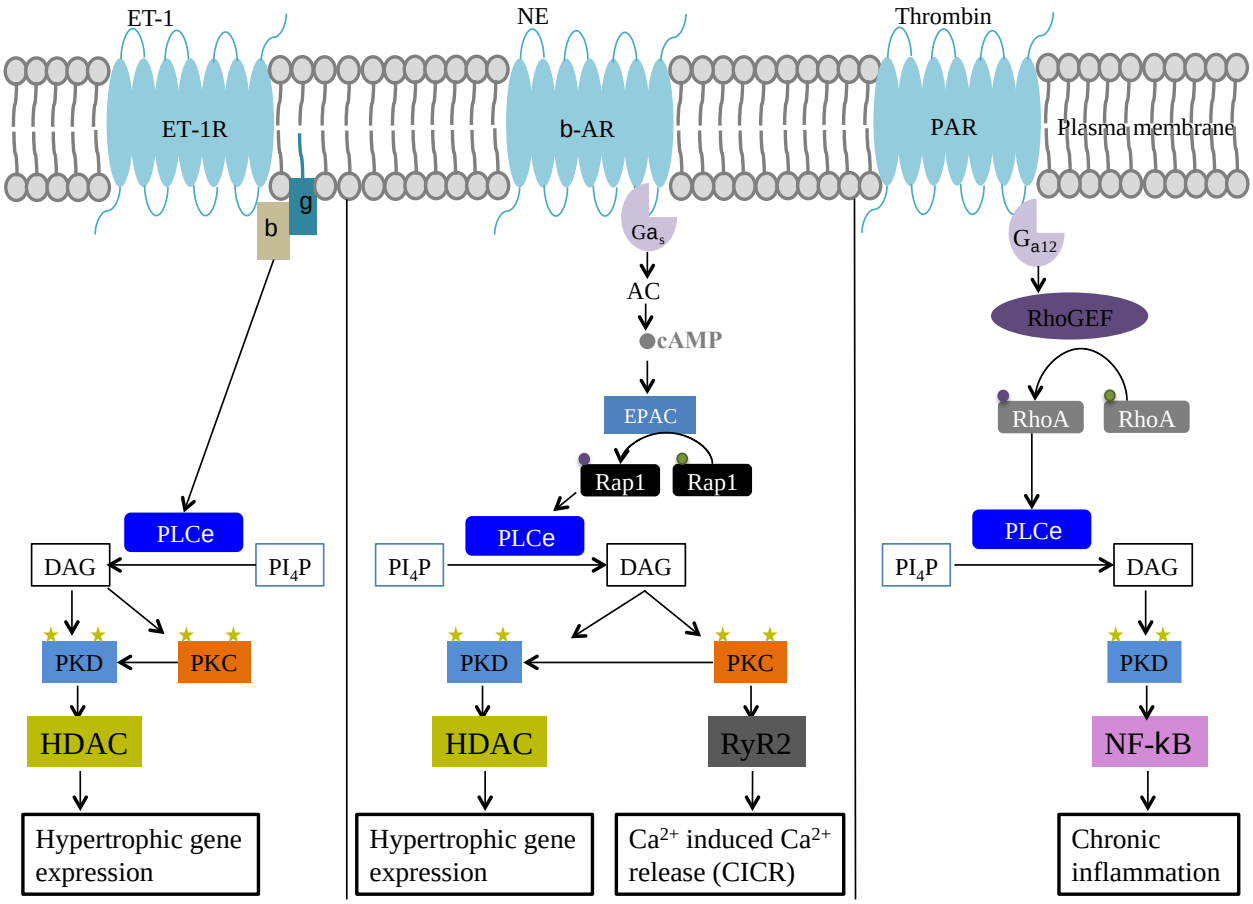

Figure 1.3 GPCR signaling pathways activate PLCε

(**Left**) Stimulation of the endothelin-1 receptor (ET-1R) leads to Gβγ-dependent activation of PLCε. PLCε hydrolyzes phosphatidylinositol-4 phosphate (PI_4P) at the Golgi, activating protein kinase C (PKC) and protein kinase D (PKD), which increase hypertrophy-related gene expression. (**Center**) Stimulation of the β-adrenergic receptor (β-AR) activates adenylyl cyclase (AC), and ultimately Epac (exchange protein directly activated by cAMP), a Rap1A GEF. Rap1A·GTP binds to the RA2 domain of PLCε, and translocates the complex to the perinuclear region. There, PLCε hydrolyzes PI_4P, activating PKC and increasing the expression of hypertrophy related genes and calcium-induced calcium release in the sarcoplasmic reticulum. (**Right**) Stimulation of thrombin receptors leads to RhoA activation. Activated RhoA directly activates PLCε leading to the hydrolysis of PI_4P, and subsequent activating of PKD, which then phosphorylates NF-κB (nuclear factor kappa-light-chain-enhancer of activated B cells) and leading to expression of inflammatory genes.

PLCε is also activated downstream of receptor tyrosine kinases (RTKs), such as the epidermal growth factor receptor (EGFR). EGFR stimulation leads to the activation of the small GTPases Ras and Rap, which bind to the PLCε RA2 domain and translocate the enzyme to the plasma membrane and the Golgi respectively [27,31]. At the plasma membrane, PLCε hydrolyzes PIP_2, increasing intracellular Ca^{2+} and activating PKC. In addition, EGFR stimulation can also activate the GTPase Rap2B through a PLCγ-dependent mechanism [30]. Stimulation of the platelet derived growth factor (PDGF) receptor also activates PLCε through Ras- and Rap1A-dependent mechanisms [55,56].

Two decades have passed since the first reports of PLCε, and despite the importance of this enzyme in cardiovascular function and cancer, little is known about the molecular mechanisms regulating its activity. A major roadblock in understanding this enzyme is the lack of structural information. The only high-resolution structures available are the nuclear magnetic resonance (NMR) solution structures of RA1 and RA2 domains, and a crystal structure of activated H-Ras bound to the RA2 domain [24]. These structures cannot provide insights into the roles of the RA domains in basal activity, nor do they reveal how Ras stimulates lipase activity. Thus, further work is needed to understand the domain architecture of the holoenzyme and provide molecular insights into PLCε function alone and under G protein activating conditions. In this work, I present preliminary work into the characterization of the N-terminal CDC25 domain, interactions between Rap1A and the RA2 domain, and the first high-resolution crystal structure of PLCε.

CHAPTER 2. PRELIMINARY CHARACTERIZATION OF THE PLCε CDC25 DOMAIN

2.1 Introduction

2.1.1 Role of the PLCε CDC25 domain

PLCε and PLCβ have common GPCR activators, but have different temporal regulation [57]. The role of PLCε function downstream of several GPCR agonists, including ET-1, LPA, and thrombin, that are also capable of activating PLCβ, was studied. It was shown that PLCβ was activated acutely but transiently within the first minutes, while PLCε activation was slow but sustained [57]. The presence of the CDC25 and RA domains likely allows PLCε to have this sustained signaling.

The PLCε CDC25 and RA2 domains allow the enzyme to act as both an activator and effector of the Rap1A GTPase through a feed-forward loop (**Fig. 1. 2B**). This mechanism has been studied downstream of GPCR and RTK stimulation. Sustained signaling of PLCε is well understood when cells were stimulated with thrombin or the β-AR agonist isoproterenol. In primary astrocytes, downstream of thrombin activation, PLCε prolonged Rap1A activation. Removal of the CDC25 domain or mutations that disrupt Rap1A binding to the RA2 domain resulted in the loss of sustained Rap1A activation and the Golgi localization of PLCε [40]. Truncations in the CDC25 domain of PLCε resulted in abrogation of Rap1A-dependent sustained activation of extracellular signal-regulated kinases (ERK) [39], protein kinase D activation [40,41] and inflammatory gene expression [40]. Also, in cardiac myocytes it was shown that downstream of β-AR activation, both the RA2 and the CDC25 were required for electrically-evoked Ca^{2+} increase, which was dependent on Rap1A activation [34].

EGF time-dependent activation of Rap1A was monitored, and it was found that in cells transfected with a PLCε variant that lacked the CDC25 domain, Rap1A activation was acute. It was

also found that PLCε translocates to the Golgi where it binds to Rap1A. Removal of the CDC25 domain resulted in transient localization of PLCε at the Golgi [27]. These data suggest a role for the CDC25 and RA2 domain in the prolonged activation of Rap1A and sustained localization of PLCε. This data was supported by another study which showed that when PLCε was activated downstream of PDGF, it resulted in sustained Rap1A activation and phosphatidylinositol hydrolysis. Deletion of the CDC25 domain resulted in transient Rap1A activation and phosphatidylinositol hydrolysis [55]. While the role of the RA2 domain in this process has been extensively studied and residues required for this interaction are known [24,46,55,58] , very little is known about how CDC25 domain interacts with Rap1A.

CDC25 domains are found in several proteins and function to activate small G proteins [59]. Full-length PLCε [55] and an immunoprecipitated fragment spanning residues 1-1200 were shown to have GEF activity for Rap1A [27]. An immunoprecipitated fragment spanning the first 600 residues was able to stimulate extracellular signal-regulated kinase (ERK) phosphorylation, which is a downstream effector of Ras [60]. This suggest that the PLCε CDC25 has directly or indirectly GEF activity for Ras. Though these data inform us on the role of the N-terminus in GEF activity, they do not delineate the domain boundaries nor do they conclusively indicate that the interaction is direct because immunoprecipitated fragments can bind to several other proteins that may have GEF activity towards Rap1A and Ras. In cell-based studies, it was shown that N-terminal truncations of PLCε result in loss of Rap1A activation [39,40,55]. However, these N-terminal truncations may perturb GEF activity by disrupting the rest of the PLCε enzyme and/or compromising its lipase activity. Therefore, it remains of paramount importance to determine how the CDC25 interacts with Rap1A. To this end I have undertaken efforts to purify the PLCε CDC25 domain, with the ultimate goal of determining the crystal structure of the domain in complex with Rap1A.

2.1.2 Comparison of PLCε CDC25 to Other GEF Domains

I wanted to check for sequence similarities between the PLCε CDC25 domain and GEFs used for sequence alignment with Son-of-Sevenless (SOS) in the work that was published elucidating the structure of SOS in complex with Ras [61]. Alignment of the PLCε N-terminus with these GEFs shows significant similarities (**Fig 2. 1**) SOS is the best characterized CDC25-containing GEF which activates Ras [61] (**Fig 2. 2A**). At the SOS-Ras interface there is an α-helix of SOS which contains residues that block the magnesium and nucleotide binding sites; this helix displaces the switch I region of Ras (**Fig. 2 2B**). In addition, there are extensive hydrophobic and electrostatic interactions between Ras and SOS (**Fig. 2 2C**). These interface interactions will be summarized in the following section. The PLCε CDC25 and the SOS CDC25 domains are 24% identical and 43% similar when using the BLAST sequence alignment tool [62]. The structure of the SOS CDC25 domain reveals the presence of two α-helical domains, one that is structural and one that is catalytic (**Fig 2. 2A**). I wanted to check whether predicted secondary structure elements of the PLCε CDC25 domain sequence would match those observed in the structure of SOS. Based on the secondary structure prediction program Jpred [63], PLCε residues 1-305, 364-407, and 495-528 were predicted to be flexible, while residues 529-779 were predicted to contain the well-ordered α-helices analogous to the catalytic domain of SOS (**Fig 2. 3**).

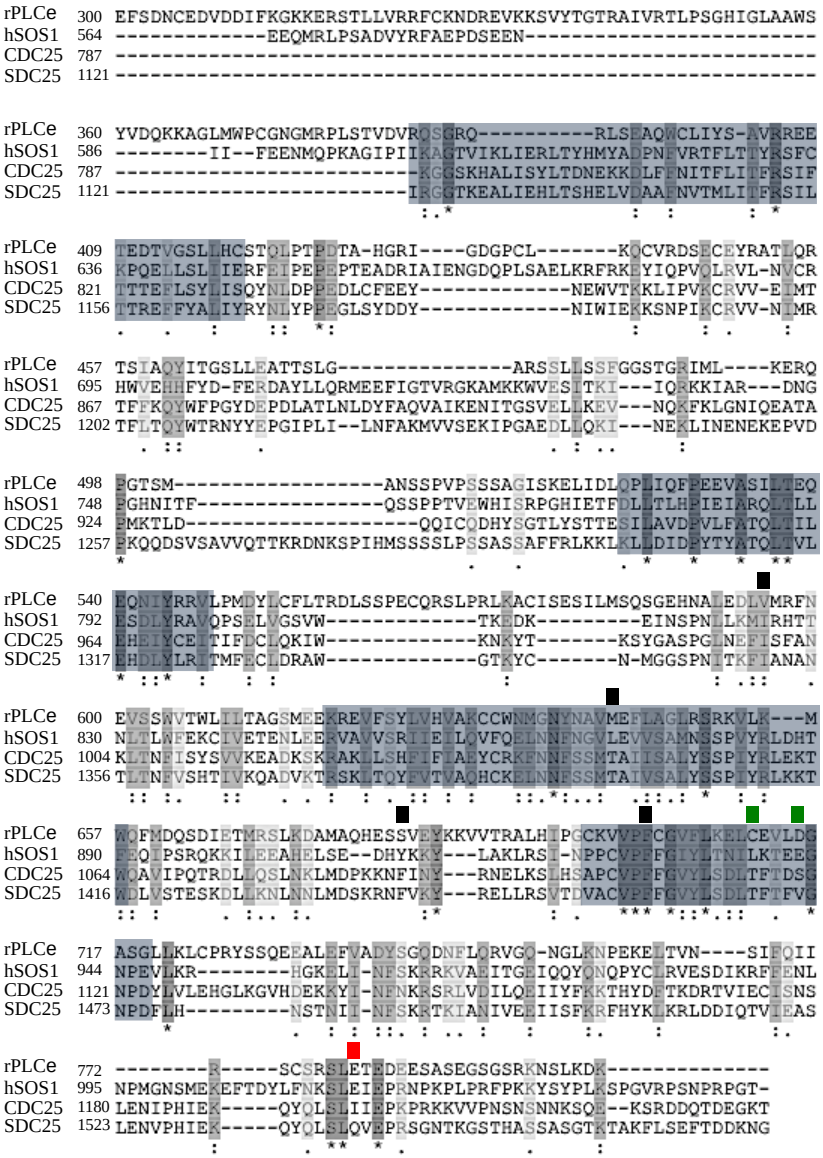

Figure 2.1 Sequence alignment of GEF domains.

Rat PLCε (rPLCε) residues 300-800, human Son of Sevenless 1 (hSOS1) residues 564-1049, *S. cerevisiae* cell division cycle protein 25 (CDC25) residues 1121-1573, and the *S. cerevisiae* CDC25 paralogue SDC25 residues 787-1129 were aligned using Uniprot [64]. Similar sequences are highlighted in grey and regions corresponding to the GEF domain are shaded in dark blue. The crystal structure of SOS–Ras revealed hydrophobic interactions between residues in the switch II of Ras and residues I825, L872, Y912, F929 in SOS. Closed black squares indicate the residues in PLCε that may be involved in the same interface with Rap1A. L938 and E942 of the α-H helix of SOS block the magnesium and nucleotide-binding sites, respectively. Closed green squares indicate the corresponding residues in PLCε. SOS E1002 forms electrostatic interactions with R68 of Ras that promote a conformation that results in disruption of nucleotide binding. Closed red square indicates corresponding residues in PLCε.

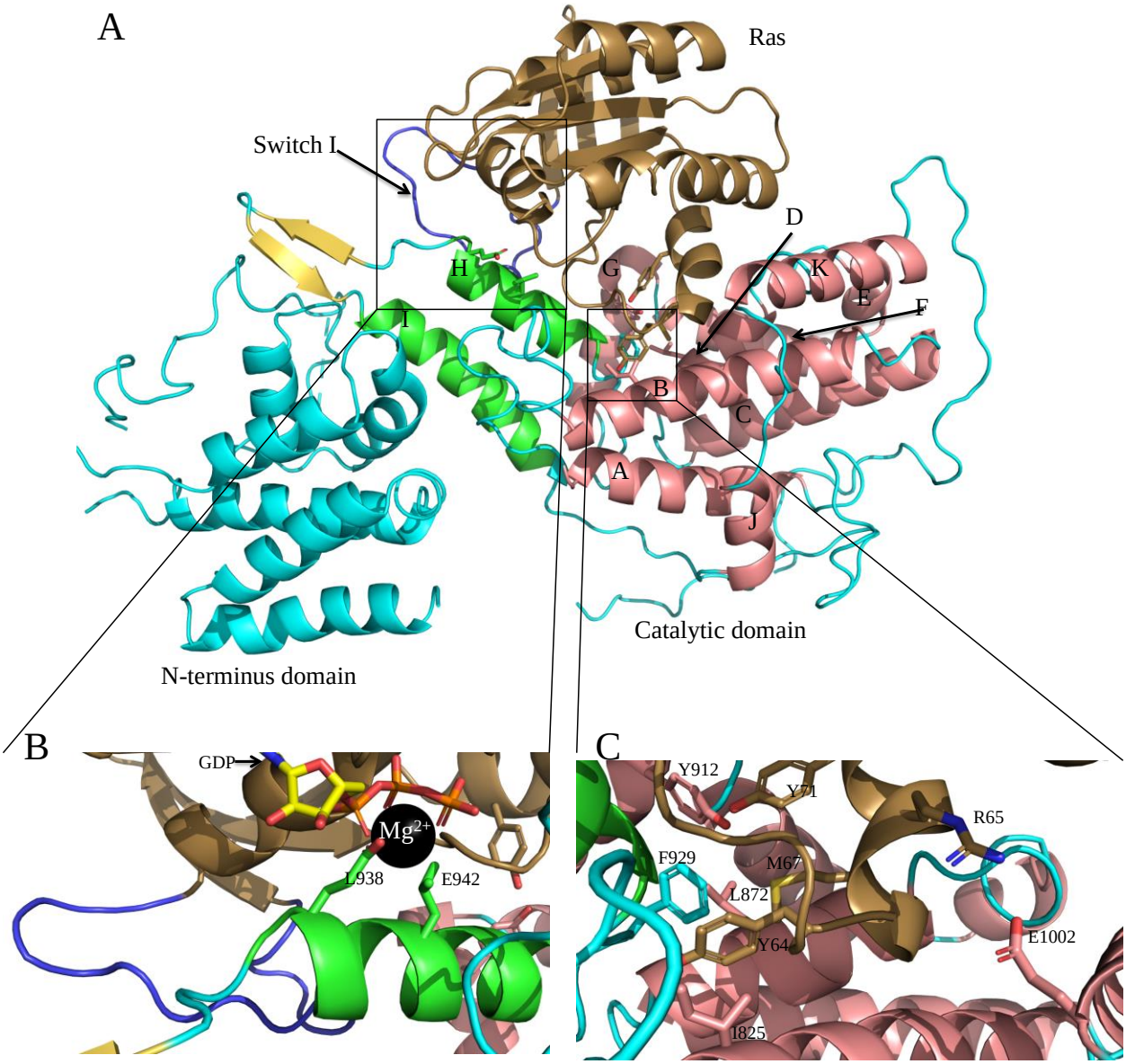

Figure 2.2 Structure of the human SOS (564-1049) in complex with Ras.
A. Human SOS CDC25 (PDB ID: 1BKD) contains an N-terminal α-helical domain (cyan) and a catalytic domain (salmon). The catalytic domain is made up of 11 helices, labeled A through K, and a hairpin loop. The β-hairpin shown in yellow and helices shown in green play a role in displacing the switch regions of Ras and stabilizing its nucelotide free state [61]. Ras is colored in brown. B. The α-helix displaces the switch I region (dark blue) and residues L938 and E942 of the α-H helix of SOS block the magnesium and nucleotide-binding sites, respectively Models of GDP and Mg^{2+} were derived from PDB ID 2C5L [24]. C. Hydrophobic and electrostatic interactions between residues in SOS (cyan and salmon) and Ras (brown). This structure was originally published in *Nature* by Boriack-Sjodin *et al.* 1998, 394 (6691): 337-343.

Figure 2.3 Jpred secondary structure prediction of the PLCε N-terminus.
The secondary structure of PLCε residues 1-800 was predicted using Jpred. Residues 1-305, 364-407, and 495-528 were predicted to be flexible while residues 529-779 were predicted to contain well-ordered secondary structure. Red Hs refer to residues predicted to belong to α helices, and yellow Es refers to residues predicted to belong to β-strands.

The residues in the catalytic domain of SOS CDC25 that are involved in displacing the nucleotide from Ras and stabilizing Ras nucleotide free state appear to be conserved in PLCε (**Fig 2. 1**) There is a hydrophobic pocket at the heart of the SOS-Ras interface. Residues Y64, M67, and Y71 of Ras are accommodated by SOS residues I825, L872, Y912, and F929 [61]. These residues correspond to V595, M642, S682, and F702 in PLCε. In addition, the α-H helix of the SOS CDC25 domain inserts into the nucleotide biding site of Ras by displacing switch 1. This displacement results in SOS CDC25 domain residue L938 and E942 blocking the magnesium and the nucleotide binding sites, respectively [61]. These residues may correspond to PLCε residues C712 and D715, respectively, which have similar charge characteristics. E1002 of the SOS CDC25 domain interacts with R68 of Ras to stabilize a conformation of switch two which also allows disruption of the nucleotide binding. Based on sequence alignment, this residue corresponds to E779 of PLCε . For convenient representation, I generated a PLCε CDC25 homology model using the SOS CDC25 structure (PDB ID 1BKD). I used the SWISS-MODEL repository database [65] and the user template function. PLCε residues 300-780 were used as the target sequence, and SOS residues were used 752-1044 (PDB ID 1BKD) as a template. The resulting PLCε CDC25 domain homology model resembles SOS CDC25 and aligns with an root mean square deviation (r.m.s.d) of 1.7 Å (133 residues **Fig. 2 4 A**). The PLCε CDC25 homology model only contained residues 521-776, suggesting a crucial role of these residues in GEF activity. **Fig. 2.4B** shows residues of the PLCε CDC25 are analogous to those in SOS involved in GEF activity. Based on sequence homology, the PLCε CDC25 domain may interact with Rap1A similarly to how the SOS CDC25 domain interacts with Ras.

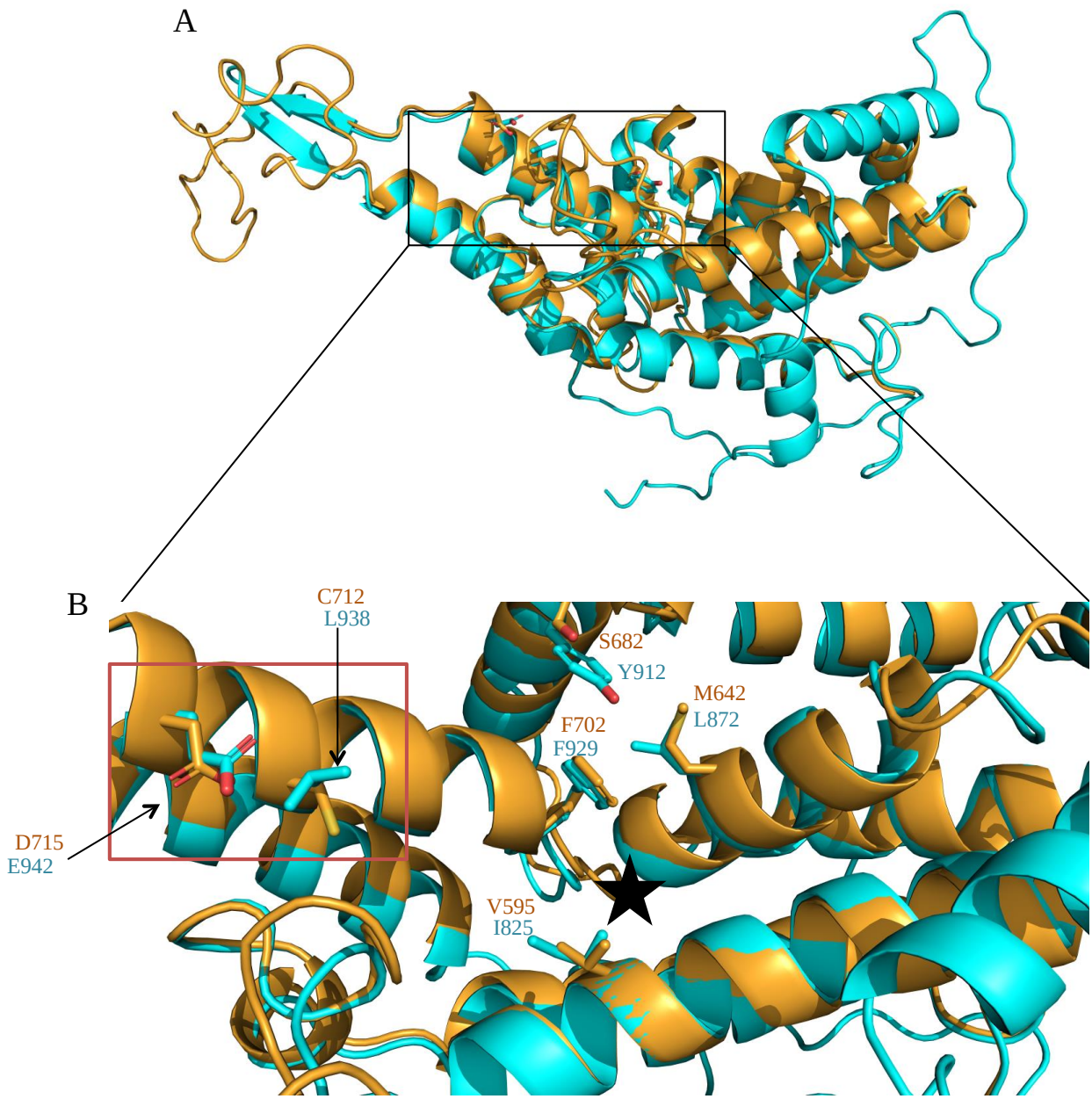

Figure 2.4 Homology model of the PLCε CDC25 domain.
A homology model of residues 300-780 in PLCε (brown) was generated using the SWISS-MODEL webserver 65 and the human SOS1 structure (1BKD residues 752-1044) as a template. The PLC CDC25 homology model includes residues 521-776. The model lacks the SOS α-K helix. Superposition of SOS1 CDC25 (cyan) and PLCε CDC25 homology model shows high structural similarity (r.m.s.d of 1.668 Å, 133 residues). B. Residues involved in hydrophobic interactions at the heart of SOS-Ras interactions (black star) are shown as sticks. Residues predicted to interfere with Mg^{2+} and nucleotide binding are shown in the red box.

Even though much can be inferred from sequence conservation, structural information on PLCe CDC25 domain still lacks. Also, biochemical characterization of PLCε CDC25 has been challenging due to the lack of purified variants of this domain. Therefore, using sequence alignment and secondary structure prediction information as a guide, I hypothesized that six different PLCε CDC25 constructs (**Fig. 2. 5**) would be easily purifiable and tractable to crystallization. To determine their boundaries, the N-terminus of each construct was chosen to begin ~5-10 residues before the first predicted ordered region. To determine the C-termini of the constructs, I used a similar strategy to include the last predicted ordered region. In addition, work in our lab and from others [66–68] suggests that the PLCε PH domain begins at residue 837. Therefore, we also designed a CDC25 variant that ended at residues 822, where sequence alignments are consistent with the presence of a disordered sequence. This work presents experiments that were performed to preliminarily characterize the CDC25 domain of PLCε.

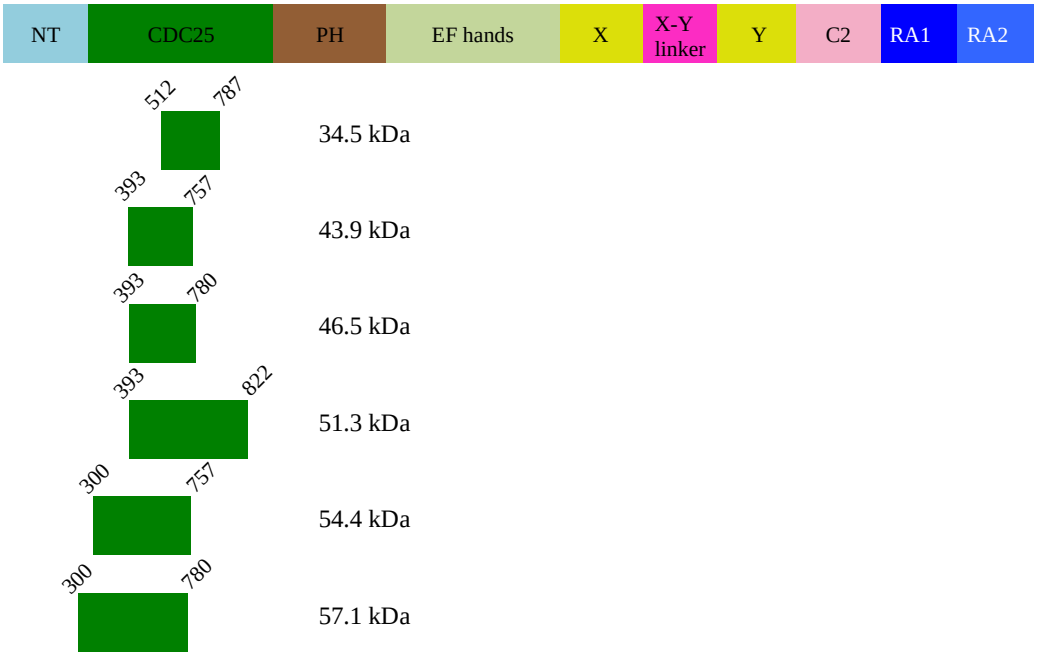

Figure 2.5 PLCε CDC25 domain variants used in this study.
Six CDC25 constructs were tested for expression and GEF activity. The domain boundaries and molecular weights of the variants are listed.

2.2 Methods

2.2.1 PLCε CDC25 Variant Cloning and Expression

Constructs containing PLCε residues 512-787, 393-822, and 393-780 were subcloned into pHis parallel 2, and constructs spanning residues 300-780, 300-757 and 393-757 were subcloned into pETDuet 2.1. Both plasmids were a gift from N. Noinaj (Purdue). The plasmids were transformed into BL21 (DE3) pLysS *Escherichia coli* (*E.coli).* The cells were induced with 0.2 M Isopropyl β-D-1-thiogalactopyranoside (IPTG) when they reached an optical density (O.D) of 0.6-0.8 at 600 nm. Protein expression proceeded for 4 h at 30 °C and cells were harvested by centrifugation at 4,424 x g at 4 °C for 10 min, flash frozen in liquid nitrogen, and stored at -80 °C.

2.2.2 Refolding Trials

All the CDC25 variants expressed as inclusion bodies, therefore the variants were denatured and screened for optimal refolding conditions using the Athena Enzyme Systems QuickFold protocols [69]. Fifteen different buffers were made in-house (**Table 2.1**). Cell pellets containing the different variants were resuspended in lysis buffer, which contained 50 mM Tris-HCl pH 8.5, 200 mM NaCl, 10 mM β-ME, 10% glycerol, 1 mM LL, 1 mM phenylmethylsulfonyl fluoride (PMSF), homogenized by dounce, and lysed by sonication. For sonication the sample was sonicated using a Q55 sonicator (Thermo Fischer) 40 to 50 times in 1-2 second pulses on ice. The lysate was then centrifuged at 100,000 x g at 4 °C for 1 h. The pellet containing the inclusion bodies (IB) was then washed and resuspended twice in wash buffer containing 0.5 M NaCl, 4 M urea, 1 mM EDTA, and 1 mg/ml deoxycholate, at a ratio of 5 mL of wash buffer per 1 g of IB. The mixture was then centrifuged at 20,000 x g for 30 min at 4 °C. The pellet was then resuspended in solubilization buffer, which contained 50 mM Tris-HCl pH 8.5, 8 M urea, and 10 mM DTT at a ratio of 2 mL solubilization buffer per 1 g of IB, and incubated at 50 °C for 15 min. This step ensures the

denaturation of the protein in the IBs. The protein concentration was then adjusted to approximately 1 mg/mL, and diluted if necessary with solubilization buffer. 50 μL of denatured protein was then added dropwise to 950 μL of different buffers as shown in **Table 2.1** and agitated to facilitate mixing and solubilization. The solution was then incubated on a rocker at 4 °C for 1 h followed by centrifugation on a tabletop microfuge. The supernatant should contain soluble, refolded protein. SDS-PAGE was used to confirm the presence of soluble protein in the supernatant. For this, 10 μL of the supernatant was electrophoresed and the gel was analyzed. Appearance of a strong band corresponding to the molecular weight of the CDC25 variant indicated solubility, while the absence of band was consistent with insoluble protein. When the band was faint, the CDC25 variant was deemed slightly soluble. To assess refolding, I then determined whether the soluble CDC25 variant was active in GEF activity assay. This fluorescence polarization (FP) assay monitors the binding of the fluorescein-labeled non-hydrolyzable GTP analog, BODIPY-FL-GTPγS, to Rap1A. This assay will be explained in the next section.

Table 2.1 Composition of Refolding Buffers for the PLCε CDC25 variants.

Buffer 1	50 mM MES pH 6.0, 9.6 mM NaCl, 0.4 mM KCl, 2 mM $MgCl_2$, 2 mM $CaCl_2$, 0.75 M guanidinium HCl, 1 mM dithiothreitol (DTT)
Buffer 2	50 mM MES pH 6.0, 9.6 mM NaCl, 0.4 mM KCl, 2 mM $MgCl_2$, 2 mM $CaCl_2$, 0.5 M arginine, 0.05% polyethylene glycol (PEG) 3,550, 1 mM oxidized glutathione (GSH), 0.1 mM reduced glutathione (GSSH)
Buffer 3	50 mM MES pH 6.0, 9.6 mM NaCl, 0.4 mM KCl, 1 mM ethylenediaminetetraacetic acid (EDTA), 0.4 M sucrose, 0.75 M Guanidine HCl, 0.05% PEG 3,550, 1 mM DTT
Buffer 4	50 mM MES pH 6.0, 240 mM NaCl, 10 mM KCl, 2 mM $MgCl_2$, 2 mM $CaCl_2$, 0.5 M arginine, 1 mM GSH, 0.1 mM GSSH
Buffer 5	50 mM MES pH 6.0, 240 mM NaCl, 10 mM KCl, 1 mM EDTA, 0.4 M sucrose, 0.75 M guanidinium HCl, 1 mM DTT
Buffer 6	50 mM MES pH 6.0, 240 mM NaCl, 10 mM KCl, 1 mM EDTA, 0.5 M arginine, 0.4 M sucrose, 0.05% PEG 3,550, 1 mM GSH, 0.1 mM GSSH
Buffer 7	50 mM MES pH 6.0, 240 mM NaCl, 10 mM KCl, 2 mM $MgCl_2$, 2 mM $CaCl_2$, 0.75 M guanidinium HCl, 0.05% PEG 3,550, 1 mM DTT
Buffer 8	50 mM Tris-Cl pH 8.5, 9.6 mM NaCl, 0.4 mM KCl, 2 mM $MgCl_2$, 2 mM $CaCl_2$, 0.4 M sucrose, 0.05% PEG 3,550, 1 mM GSH, 0.1 mM GSSH
Buffer 9	50 mM Tris-Cl pH 8.5, 9.6 mM NaCl, 0.4 mM KCl, 1 mM EDTA, 0.5 M arginine, 0.75 M guanidinium HCl, 0.05% PEG 3,550, 1 mM DTT
Buffer 10	50 mM Tris-Cl pH 8.5, 9.6 mM NaCl, 0.4 mM KCl, 2 mM $MgCl_2$, 2 mM $CaCl_2$, 0.5 M arginine, 0.4 M sucrose, 0.75 M guanidinium HCl, 1 mM GSH, 0.1 mM GSS
Buffer 11	50 mM Tris-Cl pH 8.5, 9.6 mM NaCl, 0.4 mM KCl, 1 mM EDTA, 1 mM DTT
Buffer 12	50 mM Tris-Cl pH 8.5, 240 mM NaCl, 10 mM KCl, 1 mM EDTA, 0.05% PEG 3,550, 1 mM GSH, 0.1 mM GSSH
Buffer 13	50 mM Tris-Cl pH 8.5, 240 mM NaCl, 10 mM KCl, 1 mM EDTA, 0.5 M arginine, 0.75 M guanidinium HCl, 1 mM DTT
Buffer 14	50 mM Tris-Cl pH 8.5, 240 mM NaCl, 10 mM KCl, 2 mM $MgCl_2$, 2 mM $CaCl_2$, 0.5 M arginine, 0.4 M sucrose, 0.75 M guanidinium HCl, 0.05% PEG 3,550, 1 mM GSH, 0.1 mM GSSH
Buffer 15	50 mM Tris-Cl pH 8.5, 240 mM NaCl, 10 mM KCl, 2 mM $MgCl_2$, 2 mM $CaCl_2$, 0.4 M sucrose, 1 mM DTT

2.2.3 Expression and Purification of Rap1A

Human Rap1A in the pDNR-Dual vector was purchased from Harvard PlasmID and subcloned into pHis parallel 2 using BamHI and SalI restriction sites. The plasmid was transformed into BL21 (DE3) pLysS *E.coli*. Rap1A expressed from BL21 (DE3) pLysS is soluble because these cells lack the machinery to add prenyl group to the C-terminal CaaX motif of Rap1A. The transformed cells were grown overnight at 37 °C on a plate containing carbenicillin and

chloramphenicol. One colony was selected and used to inoculate a 125 mL Luria broth (LB) starter culture. The culture was then incubated overnight at 37 °C and shaking at 225 rpm in a MaxQ 4450 incubator shaker (Thermo Fisher Scientific). The following day, 8 L of LB was inoculated with ~15 mL of the starter culture per L. The cells were then induced with 0.2 M IPTG at an optical density (O.D) of 0.6-1.0 at 600 nm. Protein expression proceeded at 18 °C overnight. Cells were harvested by centrifugation at 8,671 x g for 6 min at 4 °C, flash frozen in liquid nitrogen, and stored at -80 °C.

8L of Rap1A cell pellets were resuspended in 300 mL of lysis buffer containing 20 mM HEPES pH 8.0, 150 mM NaCl, 10 mM β-mercaptoethanol (β-ME), 10% glycerol, 1 mM leupeptin (LL), 50 μM GTP and 1 mM PMSF, and homogenized by dounce. The cells were lysed by sonication. For sonication the sample was sonicated using a Q55 sonicator (Thermo Fischer) 40 to 50 times in 1-2 second pulses on ice. The homogenate was then centrifuged at 4 °C at 100,000 g for 1 h. After centrifugation, the supernatant was filtered with a 40 μm glass fiber filter and loaded onto a Ni-NTA column pre-equilibrated with a buffer containing 20 mM HEPES pH 8.0, 300 mM NaCl, 10 mM β-ME, 40 μM GTP, 5mM $MgCl_2$, 10% glycerol (Buffer A). The column was then washed with ten column volumes (CV) of Buffer A spiked with 20 mM imidazole. The protein was then eluted with buffer A containing 250 mM imidazole (elution buffer). The eluate was concentrated in an Amicon concentrator (EMD Millipore) to 1 mL. The concentrated solution was loaded onto tandem size exclusion columns pre-equilibrated with 20 mM HEPES pH 8.0, 150 mM NaCl, 40 μM GTP, 1 mM $MgCl_2$, and 10 mM DTT (S200 buffer). Fractions corresponding to Rap1A were identified by SDS-PAGE, pooled, and concentrated to at least 3 to 5 mg/mL. The samples were flash frozen in liquid nitrogen and stored at -80°C for future use.

2.2.4 Fluorescence Polarization Guanine Nucleotide Exchange Factor Assay

Fluorescence polarization (FP) was used to measure GEF activity. In this assay, the polarization of a fluorophore is inversely proportional to its molecular rotation (Brownian motion). Its molecular rotation can be altered by binding to another molecule, such as a protein, thereby increasing its mass and slowing its rotation [70,71]. In these experiments, BODIPY-FL-GTPγS, which is fluorescent and smaller than Rap1A, was used to measure the exchange of GDP for this molecule on Rap1A. When BODIPY-FL-GTPγS is free in solution and excited by plane-polarized light, it emits light that is scattered in every direction because of its rapid Brownian motion. However, when BODIPY-FL-GTPγS binds to Rap1A, the molecular mass increases, resulting in slower Brownian motion (tumbling) and the emitted light remains polarized (**Fig 2. 6**) [71]. In these experiments, if the GEF domain is functional, it will catalyze the exchange of GDP for BODIPY-FL-GTP-γ-S on the small G protein.

FP measurements were done using a Synergy H4 plate reader, equipped with 485/20 nm excitation and 528/20 nm emission filters using a previously established protocol [72]. 5 μM purified, soluble Rap1A in 50 mM Tris-HCl pH 8.5, 150 mM NaCl, and 1 mM DTT (exchange buffer), 10 mM $MgCl_2$, and 5 μM BODIPY-FL-GTPγS were mixed in a black 96-well flat-bottomed microplate (Greiner Bio-One) in a volume of 50 μL. The plate was agitated for 1 min, and read for 10 min using a Synergy H4 plate reader. The plate was then removed, and 5 μM of the PLCε CDC25 variant in exchange buffer was added to each well using a multi-channel pipette, for a final reaction volume of 100 μL. Polarization values were measured in units of mP, which are equal to the ratio of the parallel intensity of the polarized light subtracted to the perpendicular intensity of the polarized light and the sum of both values [72].

There are four negative controls: 1) wells containing BODIPY-FL-GTPγS in exchange buffer alone, 2) with Rap1A, 3) with the CDC25 domain, or 4) a combination of all three supplemented with 20 mM EDTA. EDTA chelates Mg^{2+} ions, which are required for GTP binding, and therefore abolishes nucleotide binding [58]. The leukemia-associated RhoGEF (LARG) was used as a positive control to measure BODIPY-FL GTPγS exchange on soluble RhoA [72]. Both LARG and RhoA were gifts from J. Tesmer (Purdue). If the refolded PLCε CDC25 variants have GEF activity, I expected to see an increase in FP from wells containing BODIPY-FL-GTPγS, the CDC25 variant, and Rap1A compared to wells containing only BODIPY-FL GTPγS and Rap1A. I also expected the addition of 20 mM EDTA to result in reduced FP. Wells containing BODIPY-FL-GTPγS and the CDC25 variant alone were used to measure the baseline signal. Finally, the positive control wells containing BODIPY-FL-GTPγS, LARG and RhoA would be expected to have increased FP compared to the ones without LARG. Unexpected results were observed in wells containing EDTA. Spontaneous nucleotide exchange was observed in the first 10 minutes, as shown by an initial increase in the FP, which was then followed by a steady decrease in FP signal.

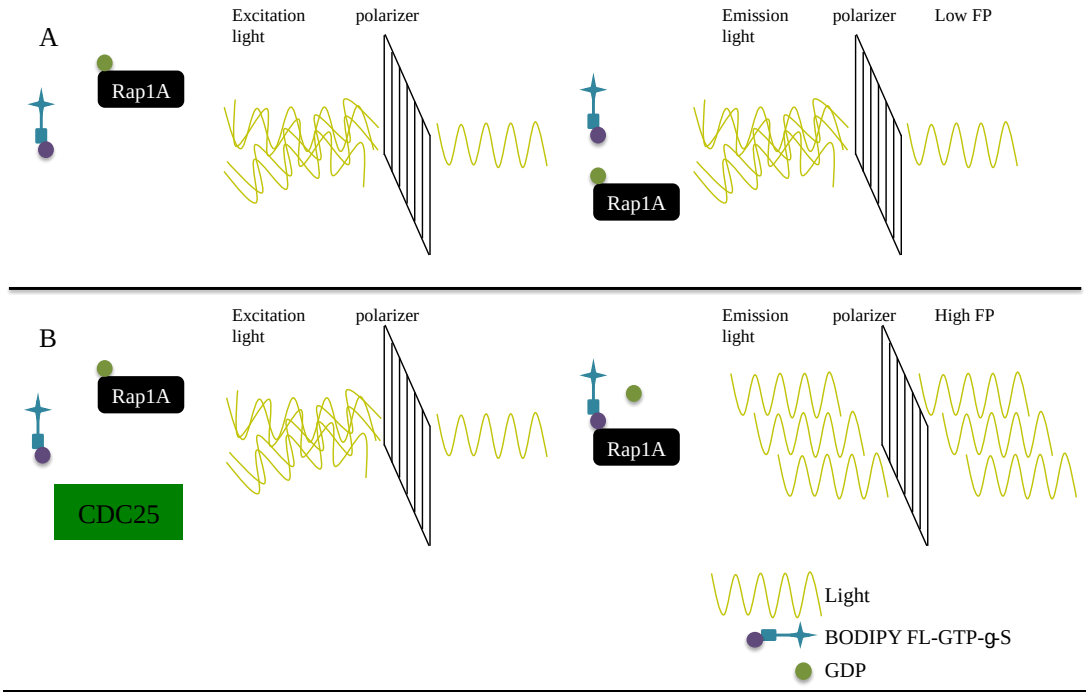

Figure 2.6 Schematic of the fluorescence polarization GEF assay.
Purified Rap1A bound to GDP was mixed with BODIPY-FL-GTPγS in the **A.** absence of CDC25 variant. Free BODIPY-FL-GTPγS tumbles rapidly, as it does not interact with Rap1A, resulting in scattered and a low FP signal or **B.** In the presence of purified CDC25 variants, BODIPY-FL-GTP-γ-S was exchanged onto Rap1A, resulting in slow tumbling and subsequent increase in polarization.

2.2.5 Purification of CDC25_512-787 From Inclusion Bodies

CDC25_512-787 was the smallest of all the variants and contained all residues predicted to be ordered and required for GEF activity based on the Jpred secondary structure prediction, sequence alignment, and homology model. In addition, CDC25_512-787 was soluble and retained GEF activity among all tested variants. Therefore, I proceeded to scale up the refolding protocol for this variant to increase the yield for crystallization efforts. The CDC25_512-787 retained the highest GEF activity after being refolded in buffer containing 50 mM Tris-HCl, pH 8.5, 246 mM NaCl, 10 mM KCl, 1 mM EDTA, 1 mM oxidized glutathione, 1 mM reduced glutathione, and 0.05% PEG 4000. This buffer corresponds to buffer 12 in **Table 2.1**, and was used for scaling up the refolding protocol.

CDC25_512-787 was expressed in BL21 (DE3) pLysS as previously described, and after harvesting, the cells were resuspended in lysis buffer, which contained 50 mM Tris-HCl pH 8.5, 200 mM NaCl, 10 mM β-ME, 10% glycerol, 1 mM LL, 1 mM phenylmethylsulfonyl fluoride (PMSF). The cells were homogenized by dounce and lysed by sonication. For sonication the sample was sonicated using a Q55 sonicator (Thermo Fischer) 40 to 50 times in 1-2 second pulses on ice. The homogenate was then centrifuged at 100,000 x g at 4 °C for one hour. The pellet containing the inclusion bodies (IB) was washed and resuspended twice in wash buffer containing 0.5 M NaCl, 2 M urea, 1 mM EDTA, and 1 mg/ml deoxycholate, at a ratio of 5 mL of wash buffer per 1 g of IB. The mixture was then centrifuged at 20,000 x g for 15 min at 4 °C. The pellet was then resuspended in solubilization buffer, which contained 50 mM Tris-HCl pH 8.5, 8 M urea, and 10 mM DTT at a ratio of 2 mL solubilization buffer per 1 g of IB, and incubated at 50 °C for 15 min. The protein concentration was then adjusted to approximately 6 mg/mL, and diluted as necessary with solubilization buffer. This unfolded protein was then added dropwise to 50 mM Tris-HCl, pH 8.5, 246 mM NaCl, 10 mM KCl, 1 mM EDTA, 1 mM oxidized glutathione, 1 mM reduced glutathione, and 0.05% PEG 4000 (Buffer 12, **Table 2.1**) and agitated to facilitate mixing and refolding. The solution was then incubated on a rocker at 4 °C for 1 h. The refolded protein was then applied to nickel nitrilotriacetic acid (Ni-NTA) resin, and washed with buffer containing 50 mM Tris-HCl pH 8.5, 246 mM NaCl, 10mM KCl, 1mM EDTA, 0.05% PEG 4000, and 1 mM DTT (S200 buffer). The bound protein was eluted using S200 buffer supplemented with 500 mM imidazole (elution buffer), and concentrated to 1 mL using an ULTRA Amicon concentrator (EMD Millipore). The concentrated CDC25_512-787 protein solution was then loaded onto a single Superdex 200 10/300 GL (GE Life Sciences) pre-equilibrated with the S200 buffer. Fractions corresponding to purified protein were concentrated using an Amicon concentrator to ~ 1mg/mL.

Typical yields are ~0.04-0.125 mg of protein per L of culture. The concentrated protein was then aliquoted, flash frozen in liquid nitrogen, and stored at – 80 °C for further studies.

2.3 Results

2.3.1 Refolding of PLCε CDC25 Variants

When protein is expressed in inclusion bodies, denaturants can be used to solubilize the protein in its unfolded state, allowing for refolding [73]. To unfold the CDC25 domain variants, the inclusion bodies were resuspended in the solubilization buffer and then centrifuged. The supernatant, which contained the unfolded CDC25 variants, was removed and added dropwise to the refolding buffers listed in **Table 2.1**. The refolded protein was centrifuged again to remove aggregates, and the refolded protein remained in the supernatant. Refolding trials in buffers 2, 4, 6, 8, 10, 12, and 14 were performed. These buffers were first tested because they contain oxidized glutathione (GSH) and reduced glutathione (GSSH). Aggregated proteins in inclusion bodies often contain non-native disulfide bonds [74]. 8 M urea and 10 mM of the reducing agent DTT in the solubilization buffer are used to disrupt these bonds [74,75]. The use of GSH and GSSH facilitates formation of naturally occurring disulfide bonds for proper refolding of the protein [76]. I used SDS-PAGE to confirm the solubility of the protein in the tested buffers and fluorescence polarization to determine whether the soluble protein was active.

2.3.1.1 CDC25_512-787 Refolding Trials

The CDC25_512-787 variant was first tested because it was the smallest of all variants. After unfolding CDC25_512-787 in the solubilization buffer, 50 μL aliquots were refolded in buffers 2, 4, 6, 8, 10, 12, and 14 (**Table 2.1**). The solutions were then centrifuged to remove aggregates. The resulting supernatants contained refolded protein. 10 μL of the supernatant from each refolding condition was electrophoresed to determine solubility. As shown by the SDS-PAGE gel, CDC25_512-787 was soluble in buffers 2, 4, 6, and 12, and slightly soluble in buffers 8, 14, and 10 (**Fig 2. 7**).

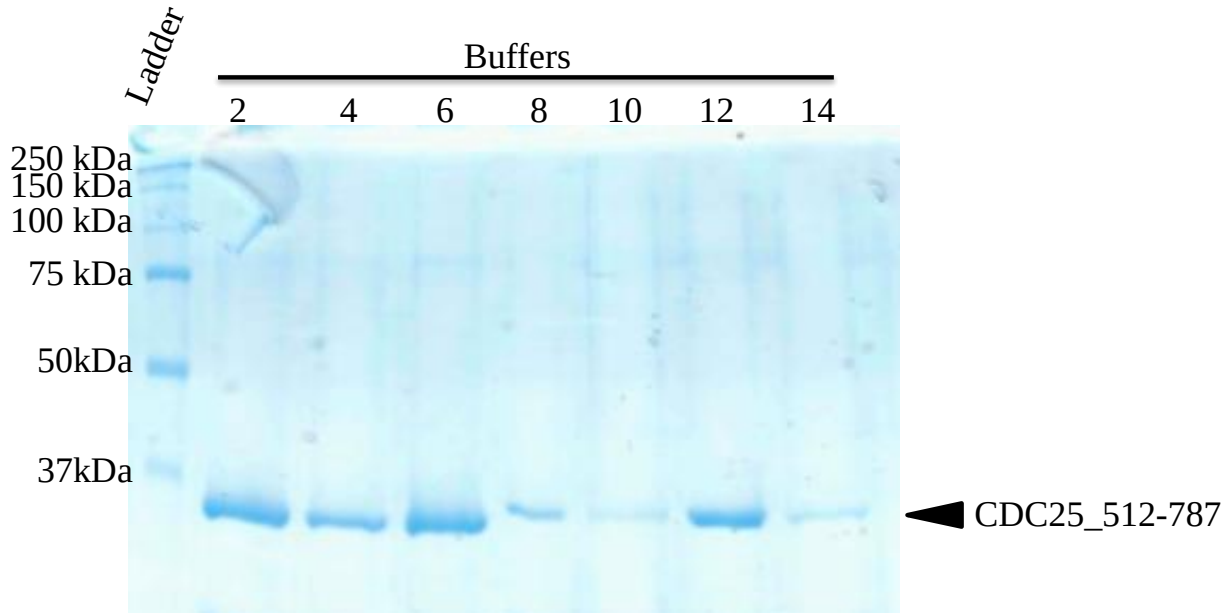

Figure 2.7 Solubility of CDC25_512-787 variant after refolding experiments.
The CDC25_512-787 variant was refolded in buffers described in **Table 2.1**. The numbers at the top of the gel correspond to the buffer listed in Table 2.1. CDC25_512-787 was soluble in buffers 2, 4, 6, and 12, and slightly soluble in buffers 8, 10, and 14.

Since the CDC25_512-787 was soluble in all the buffers tested, I wanted to confirm the protein was correctly folded by determining the activity of the soluble protein. To do this, I measured the GEF activity of the CDC25_512-787 for Rap1A using the fluorescence polarization (FP) assay. The CDC25_512-787 variant showed two times increased in GEF activity for Rap1A in refolding buffers 8 and 12 upon GEF addition. This is shown by the increase in FP in the presence of the CDC25_512-787 (Rap1A+ Buffer # CDC25 + BODIPY, where **#** means buffer number) compared to the negative control, which lacked CDC25_512-787 (Rap1A + Buffer # + BODIPY) (**Fig 2. 8D, F**). In buffers 2, 4, 6, 10, and 14, the FP signal remained the same in the presence or absence of the CDC25_512-787 (**Fig 2. 8A, B, C, E, G**). The positive control LARG had GEF activity for RhoA as shown in **Fig. 2. 8H.** This is shown by a ten times increase in FP signal when LARG was added (RhoA + LARG + BODIPY), compared to negative control, which lacked LARG (RhoA + BODIPY).

The FP signal from the wells containing EDTA was initially elevated and then decreased steadily. The signal from these samples was still higher than wells containing only Rap1A or RhoA in the absence of their respective GEFs. We do not know the reason for this EDTA-dependent spontaneous induction of nucleotide exchange. However, it has been shown that EDTA increases BODIPY-FL-GTPγS with the GTPase Cdc42 [77]. Negative FP signals were observed in the wells containing only BODIPY-FL-GTPγS (Bodipy). This may just be the value at background because it is observed in all our experiments.

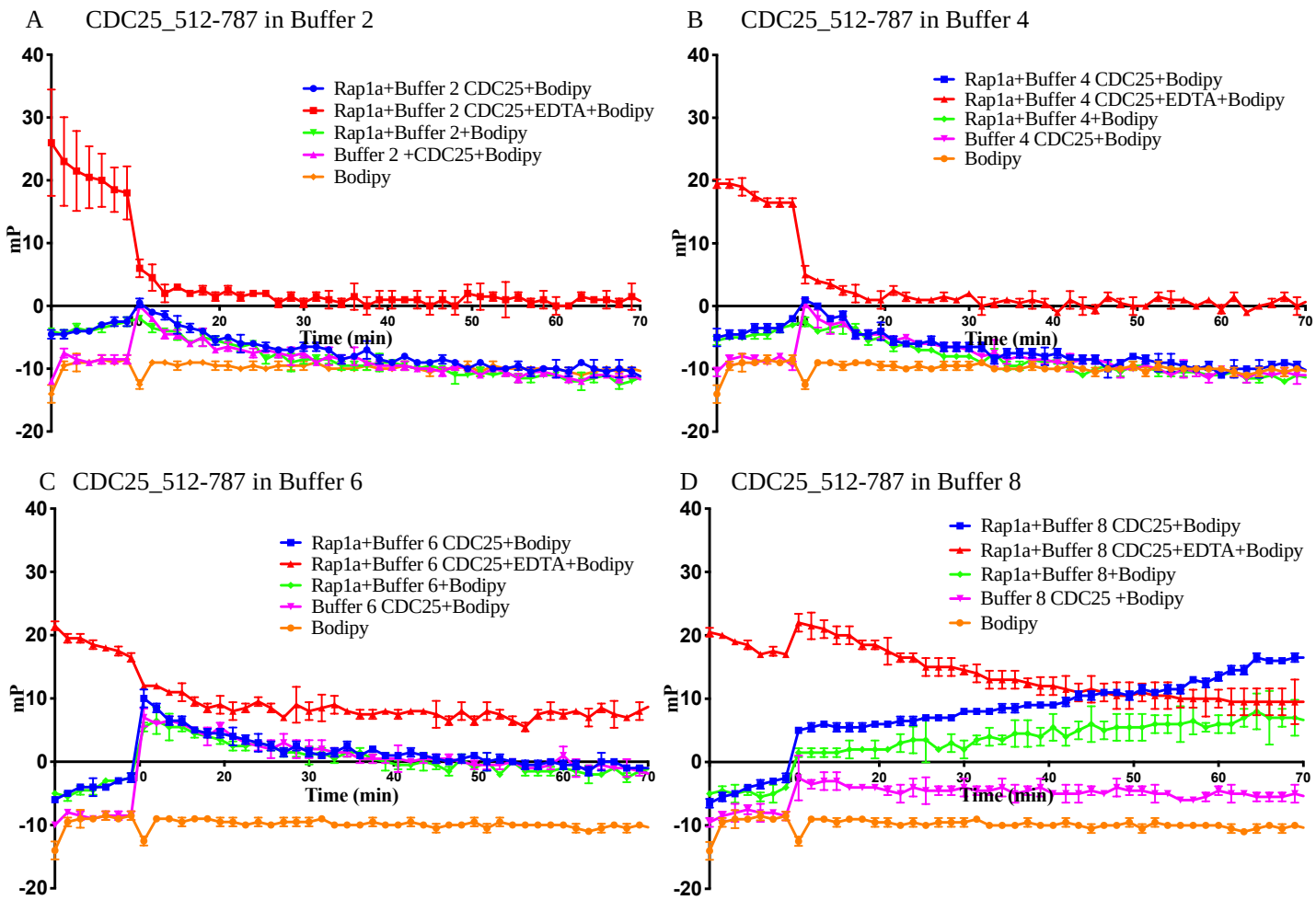

Figure 2.8 GEF activity of PLCε CDC25_512-787 in different buffer compositions.

(A-G) The GEF activity of CDC25_512-787 for Rap1A was measured in various refolding buffers. CDC25_512-787 retained GEF activity only in buffers 8 and 12. There are four negative controls: BODIPY-FL-GTPγS (orange), Rap1A (green), or the CDC25_512-787 (purple), in exchange buffer alone and all three combined in a buffer supplemented with 20 mM EDTA (red). (**H**). LARG-dependent GEF activity for RhoA was used as a positive control. Polarization values (mP) were measured as a function of time.

Figure 2.8 Continued

E CDC25_512-787 in Buffer 10

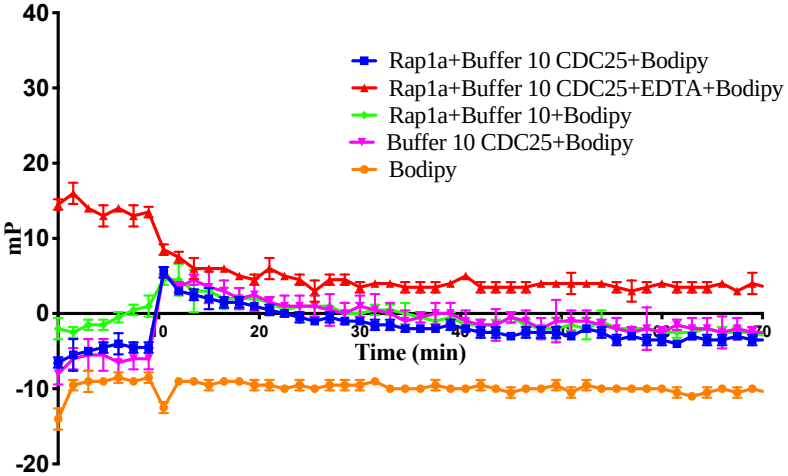

F CDC25_512-787 in Buffer 12

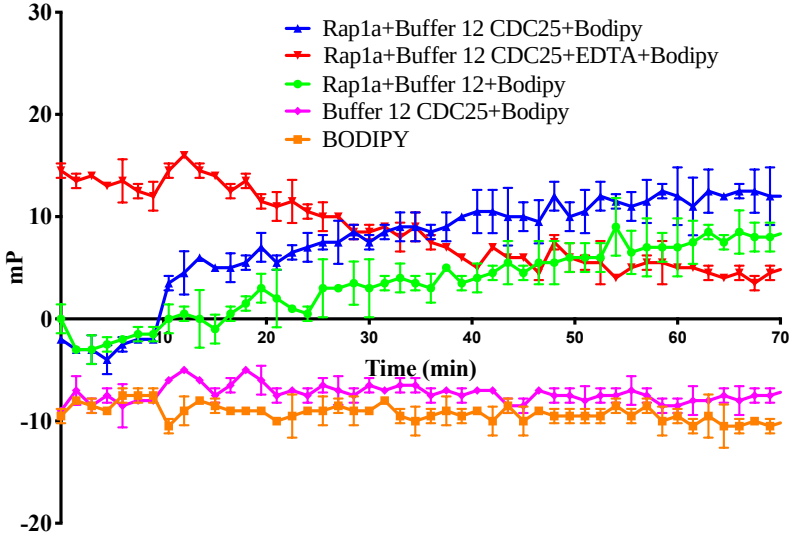

G CDC25_512-787 in Buffer 14

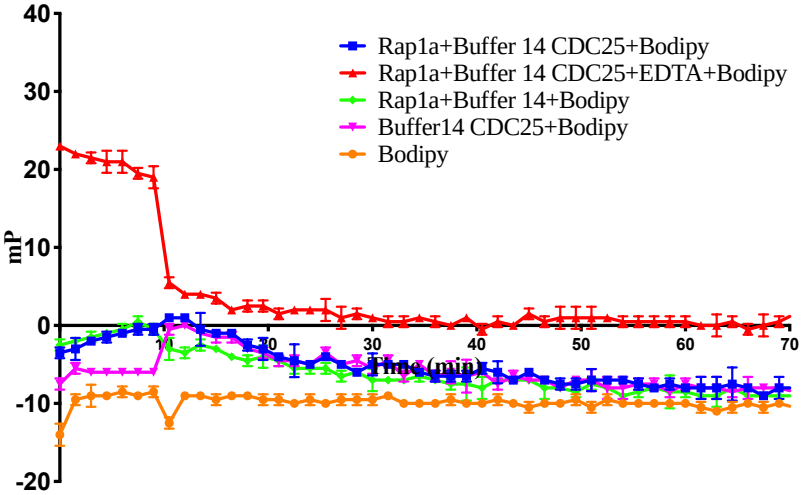

H LARG+RhoA

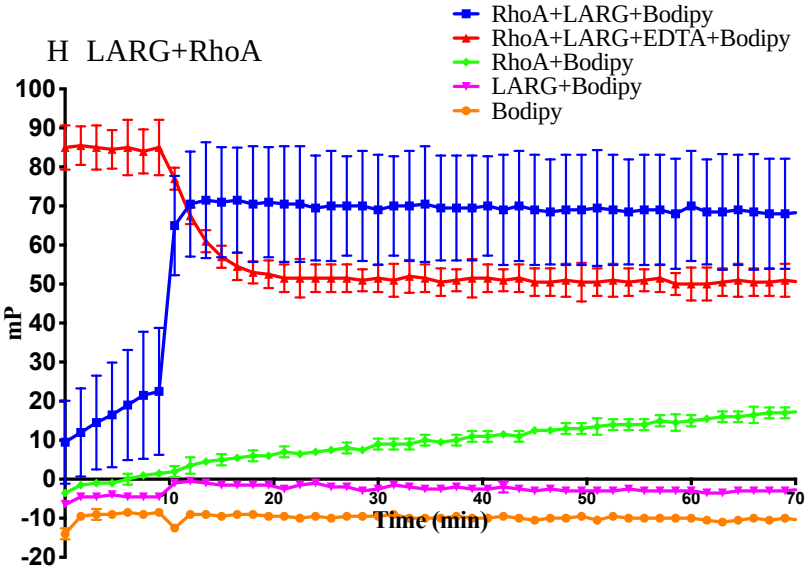

2.3.1.2 CDC25_300-780 Refolding Trials

CDC25_300-780 variant was tested second because it was the largest of all variants. After unfolding CDC25_300-780 in the solubilization buffer, 50 μL aliquots were refolded in buffers 2, 4, 6, 8, 10, 12, and 14. The solution was then centrifuged to remove aggregates. The resulting supernatant solution contained refolded protein. 10 μL of the supernatant was electrophoresed to monitor solubility. As shown by the SDS-PAGE gel, CDC25_300-780 was soluble in buffers 2, 4, 6, 10, and 14 but was insoluble in buffers 8 and 12 (**Fig 2. 9**).

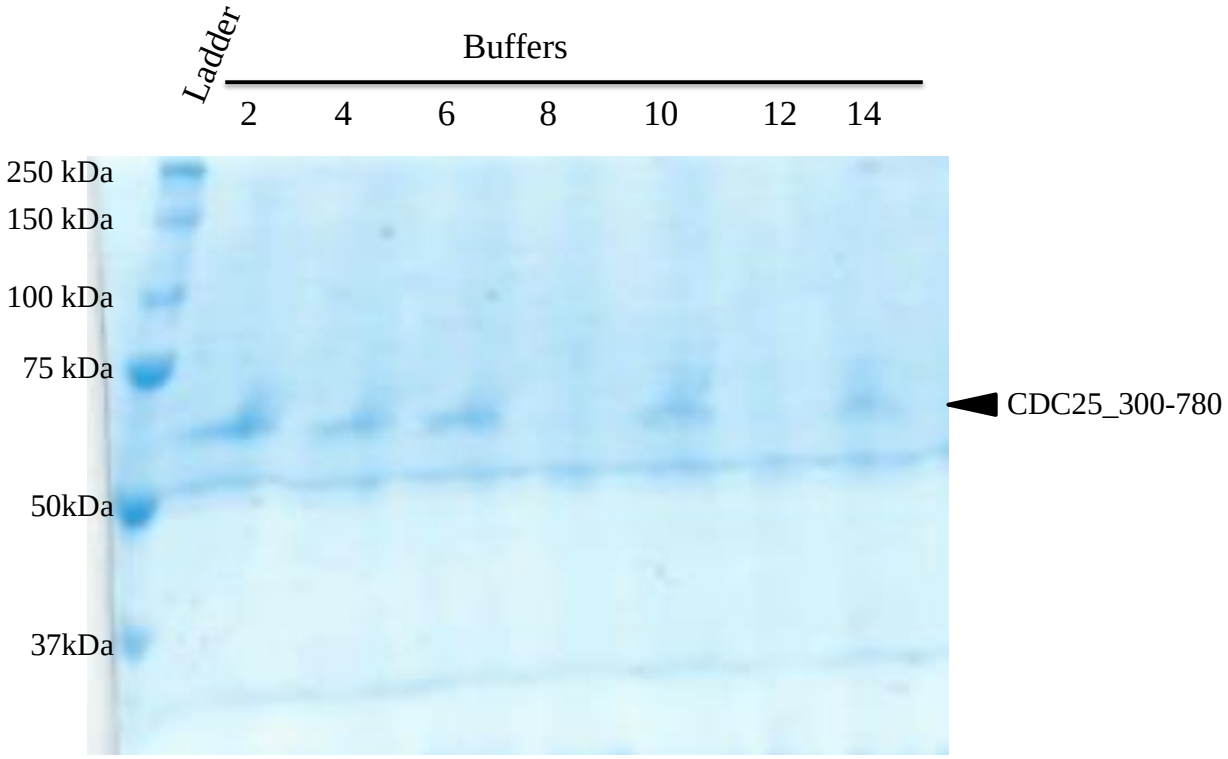

Figure 2.9 Solubility of CDC25_300-780 variant after refolding experiments. CDC25_300-780 variant was refolded in buffers described in **Table 2.1**. SDS-PAGE gel of CDC25_300-780 refolded in various buffers. The numbers at the top of the gel correspond to the buffer listed in Table 2.1. CDC25_300-780 was soluble in buffers 2, 4, 6, 10 and 14 and insoluble in buffers 8 and 12.

I wanted to confirm that the CDC25_300-780 variant was correctly refolded in buffers 2, 4, 6, 10, and 14 by determining if the soluble protein had GEF activity. To do this, I measured the GEF activity of the CDC25_300-780 for Rap1A using the FP assay. The CDC25_300-780 variant did not retain GEF activity for Rap1A in any of the tested buffers. This is shown by the fact that the FP signal from wells containing CDC25_300-780 (Rap1A + Buffer # CDC25 + BODIPY) was similar to wells that lacked the CDC25 domain (Rap1A + Buffer # + BODIPY**, Fig. 2. 10 A, B, C, D, E**). Similar to the CDC25_512-787 experiments, the positive control (LARG + RhoA) had a threefold increase in FP compared to RhoA alone, while negative FP signals were observed in the wells containing only BODIPY-FL-GTPγS in exchange buffer (Bodipy) or GEF (CDC25-300-80 or LARG) alone **Fig. 2. 10F**.

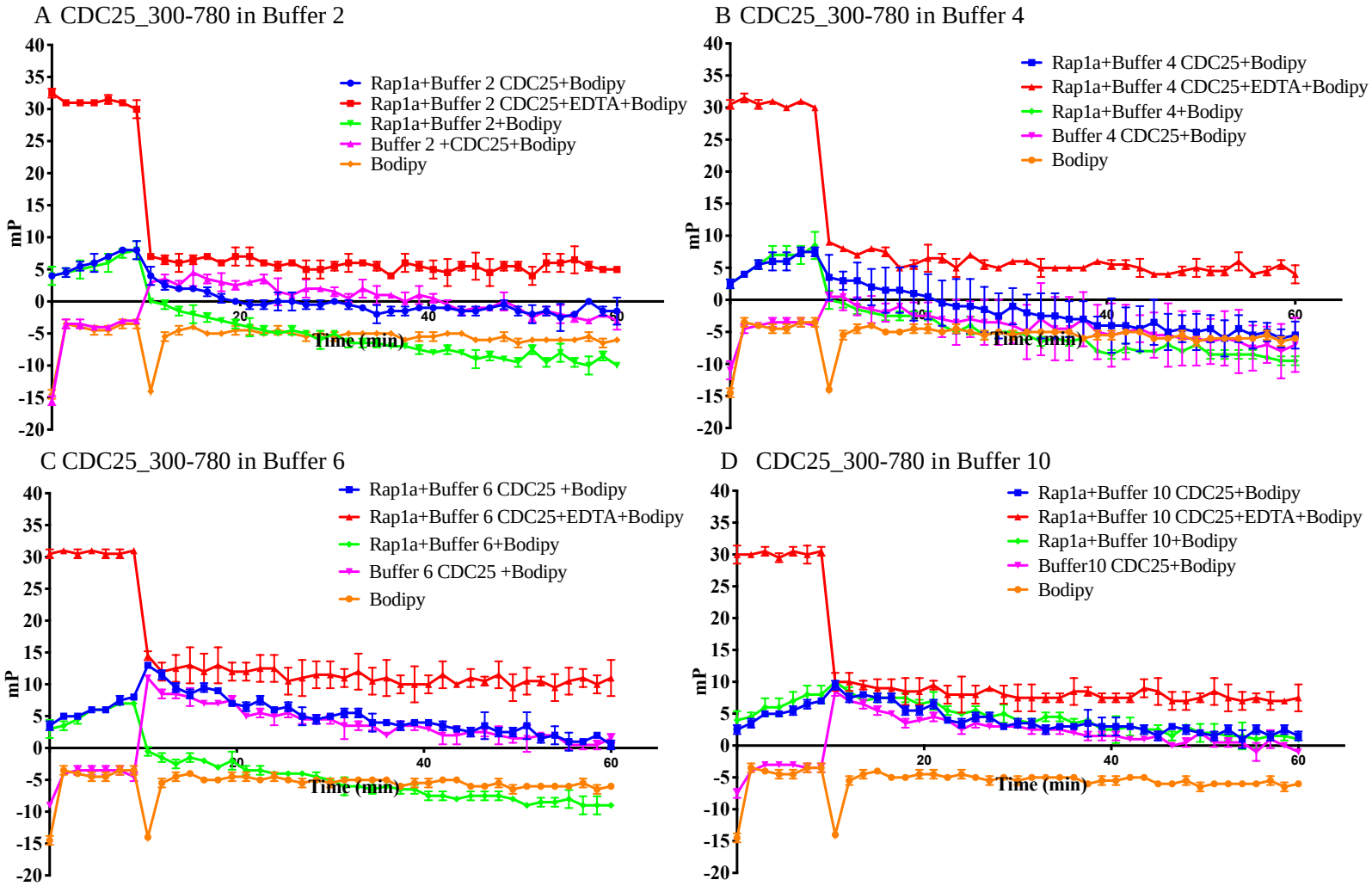

Figure 2.10 GEF activity of PLCε CDC25_300-780 in different buffer compositions.
The GEF activity of CDC25_300-780 for Rap1A was measured in refolding buffers **A**. 2, **B**. 4, **C**. 6, **D**. 10, and **E**. 14. EDTA was included as a negative control. CDC25_300-780 did not retain GEF activity in any buffers. (**F**). LARG-dependent GEF activity for RhoA was used as a positive control. Polarization values (mP) were measured as a function of time.

Figure 2.10 Continued

E CDC25_300-780 in Buffer 14

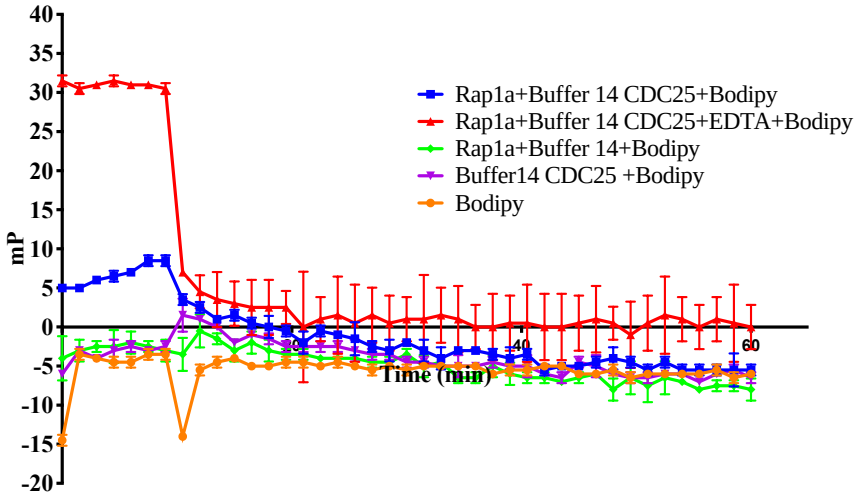

F LARG+RhoA

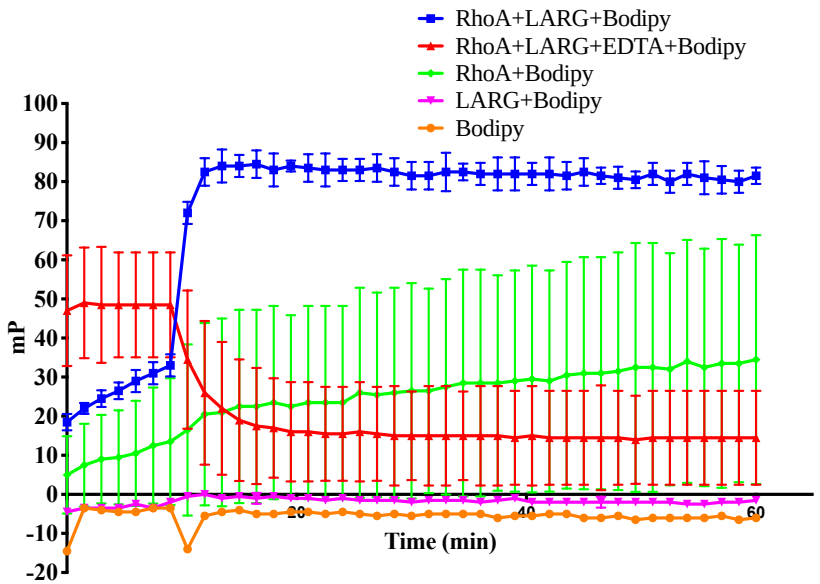

2.3.1.3 CDC25_300-757, CDC25_393-757, and CDC25_393-780 Refolding Trials

Since I successfully refolded CDC25_512-787 in buffers 8 and 12, I focused the refolding trials of CDC25_300-757, CDC25_393-757, and CDC25_393-780 with these buffers. Interestingly, these buffers are slightly alkaline, a feature that has been shown to be important for proper refolding of some proteins in inclusion bodies in the presence of oxidized and reduced glutathione [74,76]. After unfolding CDC25_300-757, CDC25_393-757, and CDC25_393-780 in the solubilization buffer, 50 μL of each solution was refolded in buffers 8 and 12. The solution was then centrifuged to remove aggregates. The resulting supernatant solution contained refolded protein. 10 μL of the supernatant was electrophoresed to determine solubility. As shown by the SDS-PAGE gel, CDC25_300-757 was insoluble and CDC25_-393-757 was soluble in both buffers. CDC25_393-780 was soluble in buffer 8, but not buffer 12 (**Fig 2.11**).

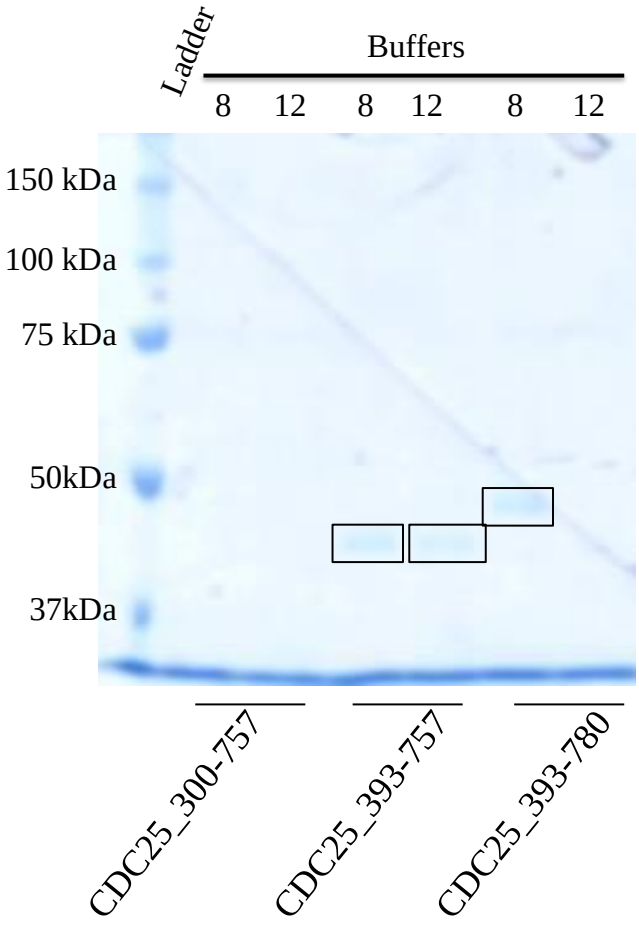

Figure 2.11 Solubility of CDC25_300-757, CDC25_393-757, and CDC25_393-780 variants after refolding.
SDS-PAGE gel of CDC25_300-757, CDC25_393-757, and CDC25_393-780 refolded in buffers 8 and 12. The numbers at the top of the gel correspond to the buffer listed in Table 2.1. CDC25_300-757 was insoluble in all tested buffers, CDC25_393-757 was soluble in both buffers, and CDC25_393-780 was only soluble in buffer 8.

We wanted to confirm that soluble CDC25_393-757 and CDC25_393-780 had GEF activity. To do this, we measured the GEF activity of CDC25_393-757 and CDC25_393-780 for Rap1A using the FP assay. The CDC25_393-757 variant had no GEF activity in either buffer (**Fig. 12A, B**). CDC25_393-780 GEF activity for Rap1A in buffer 8 was insignificant according to the t-test analysis (**Fig. 12C**).

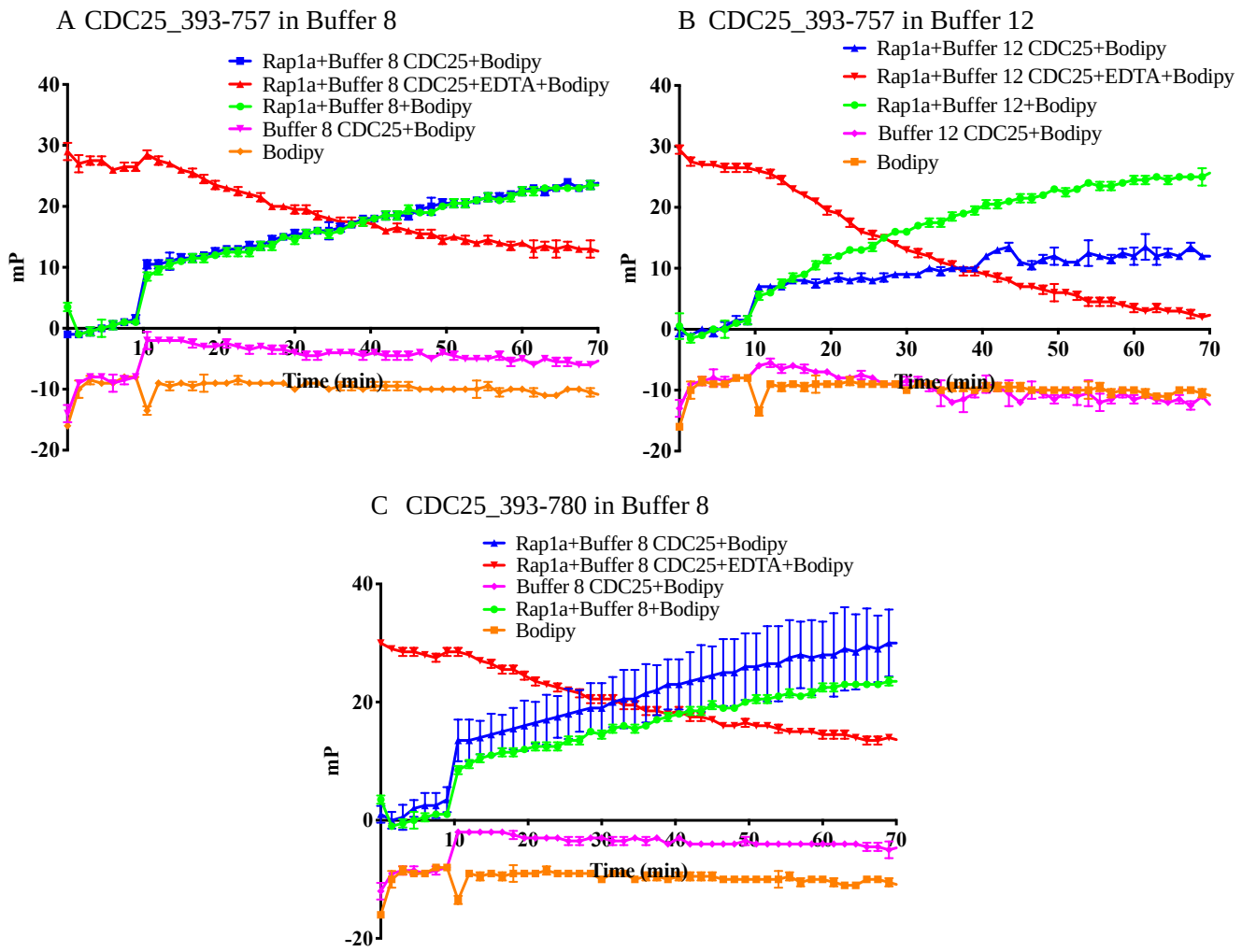

Figure 2.12 GEF activity of CDC25_393-757, and CDC25_393-780 in different buffer compositions.
The GEF activity of CDC25_393-757 for Rap1A was measured in refolding buffers **A**. 8, **B**. 12. CDC25_393-757 did not retain GEF activity in any buffers and CDC25_393-780 retained GEF activity in buffer 8. **C.** The GEF activity of CDC25_393-780 for Rap1A was measured in refolding buffer 8. EDTA was included as a negative control. Polarization values (mP) were measured as a function of time.

2.3.2 Expression, Purification, and Characterization of PLCε CDC25_512-787

As CDC25_512-787 appeared to retain some GEF activity, I began large-scale expression and refolding trials. As shown in **Figure 2.13A**, CDC25_512-787 was refolded in Buffer 12, centrifuged, and loaded on a Ni-NTA column. The refolded domain remained bound to the column in the presence of 20 mM imidazole solution, and was eluted with Buffer 12 spiked with 500 mM imidazole. The eluted protein was then concentrated to volume of 1 mL and subjected to further purification by size exclusion chromatography using a single Superdex 200 10/300 GL column. Some of the CDC25_512-787 was aggregated, as shown by a peak in the void volume (6-10 mL) of the size exclusion chromatogram (**Fig. 2.13B**). A second peak was observed at the predicted volume corresponding to the molecular weight of CDC25_512-787 (**Fig. 2.13B**). This is also consistent with the CDC25_512-787 being monomeric in solution. To further confirm that the protein in the second peak was functional, its GEF activity was measured using the FP assay previously described. As shown in **Fig 2. 14**, addition of the CDC25_512-787 appeared to increase the exchange of GDP for BODIPY-FL-GTPγS on Rap1A.

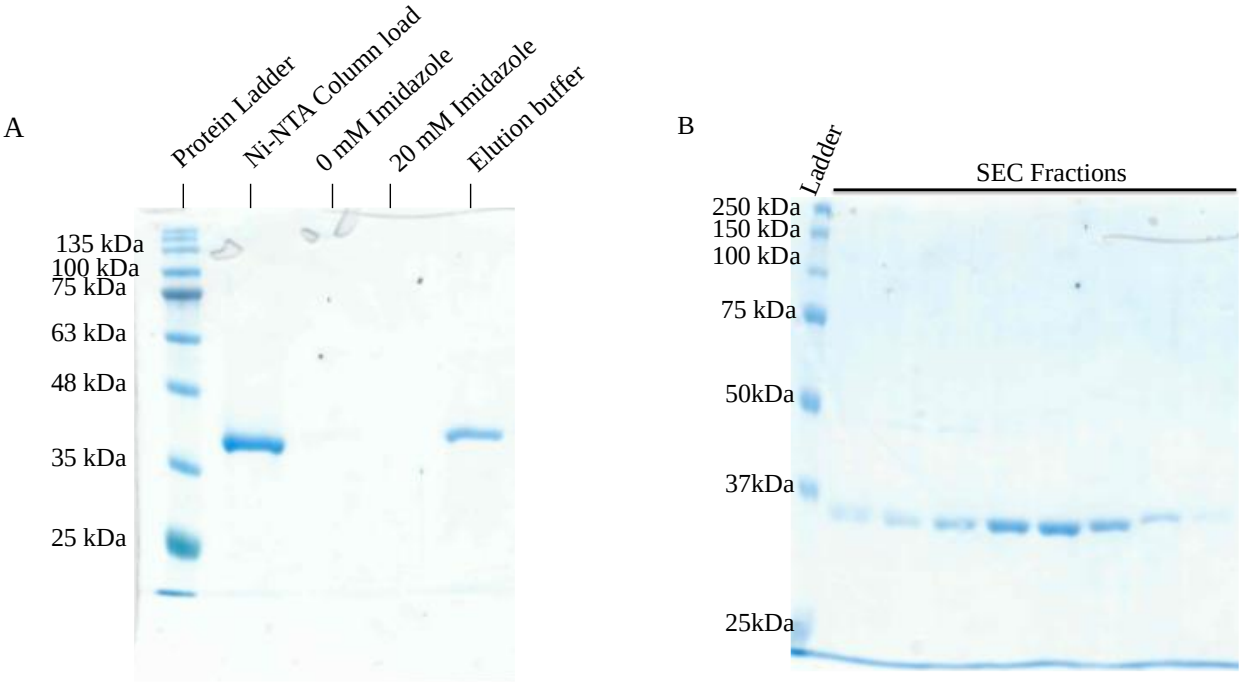

Figure 2.13 Purification of CDC25_512-787.

A. The refolded CDC25_512-787 protein was first purified using Ni-NTA affinity chromatography. The refolded protein before Ni-NTA column load (Ni-NTA column load), flow-through, wash, and elution fractions were analyzed by SDS-PAGE. After loading, the column the resin was washed with S200 buffer, and then S200 buffer spiked with 20 mM imidazole (20 mM imidazole). The protein was eluted with S200 supplemented with 500 mM imidazole (elution buffer). **B.** Pooled fractions corresponding to the second peak in C were electrophoresed on an SDS-PAGE gel. Fractions 26-32 were concentrated, and the purified protein tested for GEF activity by FP. **C.** Representative size exclusion chromatogram of CDC25_512-787. Part of the refolded CDC25_512-787 was aggregated and eluted in the void volume. The second peak at higher volume is consistent with the molecular weight of the CDC25_512-787 protein.

Figure 2.13 continued

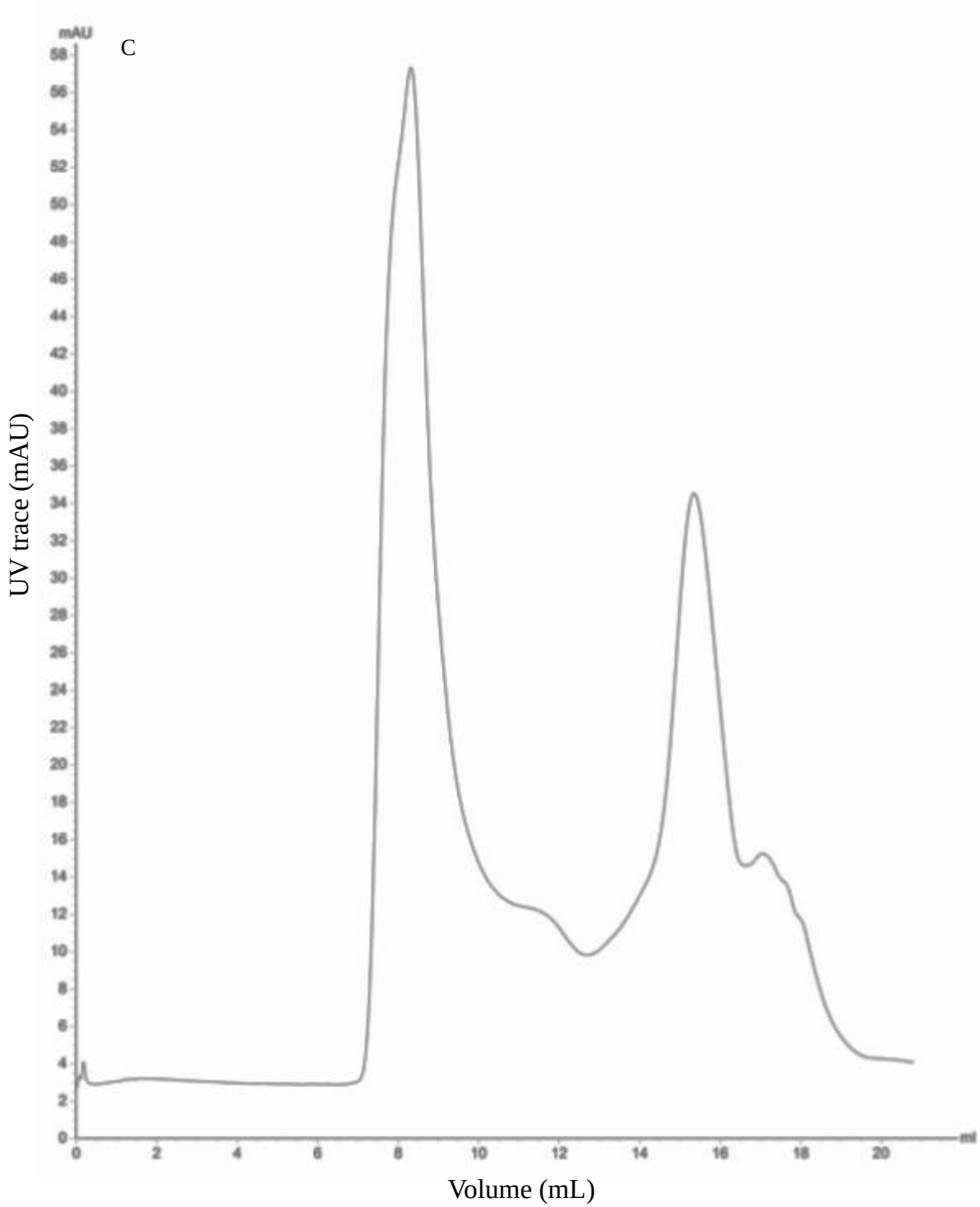

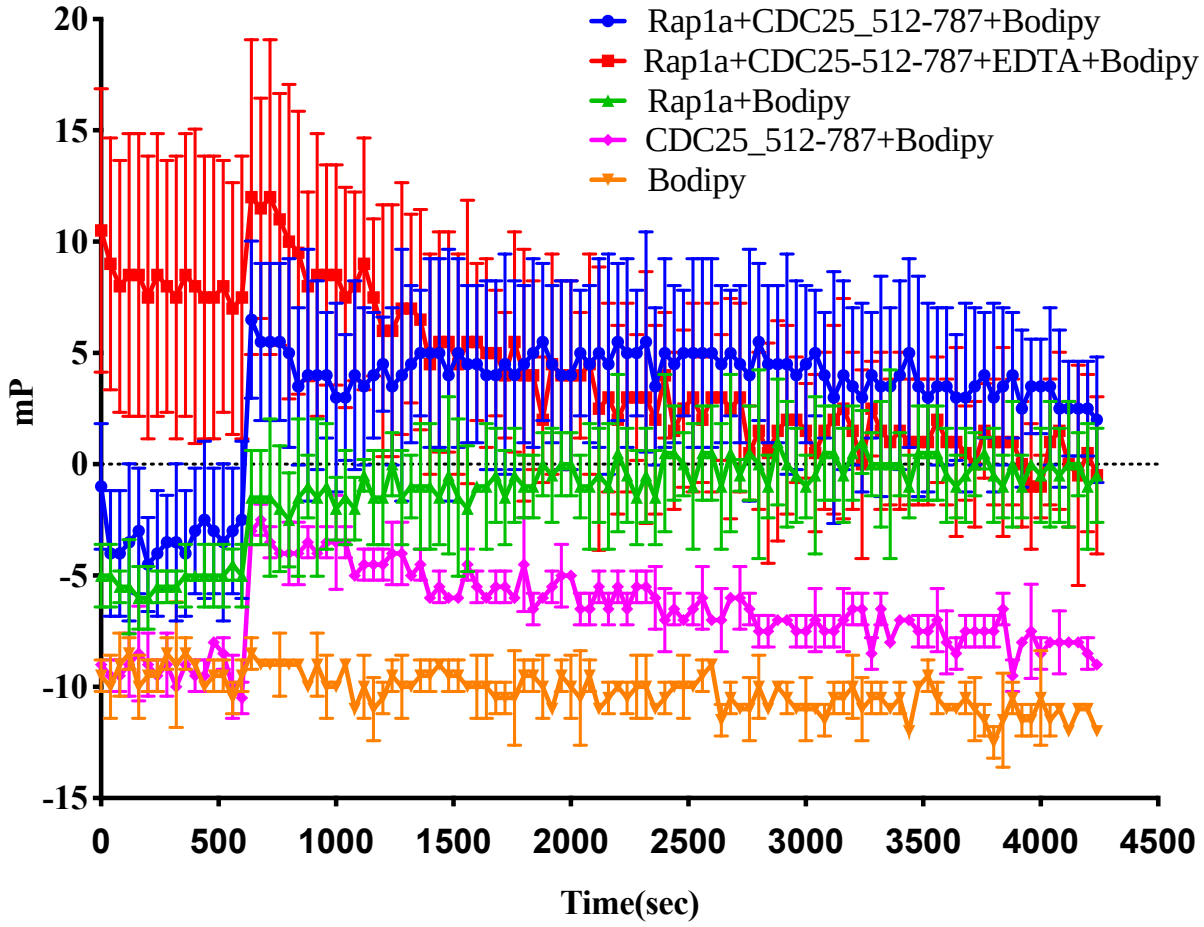

Figure 2.14 CDC25_512-787 GEF activity.
The GEF activity of the CDC25_512-787 domain from a larger refolding experiment was measured using FP.

2.3.3 Discussion and Future Directions

The CDC25 domain is required for PLCε-dependent Rap1A activation [27]. However, the preliminary data presented here demonstrates significant challenges in the expression and purification of this domain. While several constructs varying at the N- and C-termini were tested, all variants were expressed as inclusion bodies. However, some useful information was still obtained. The greatest success in refolding was seen with variants that contained residues 512-780, which aligns with the GEF site of SOS. This is supported by a study that showed an immunopurified fragments of PLCε spanning residues 532-775 had GEF activity [27]. We also

observed high sequence similarities between residues of the SOS CDC25 domain that engage Ras and analogous residues in PLCε CDC25. Most of the studies done trying to understand the role of CDC25 have used N-terminal truncations, which may perturb GEF activity by disrupting the rest of the PLCε enzyme and/or compromising its lipase activity. I propose that mutations of residues V595, M642, S682, and F702, which correspond to SOS residues forming a hydrophobic pocket with Ras, C712 and D715, which correspond to SOS residues involved in nucleotide and magnesium displacement, and E779 which correspond to SOS residues that stabilize the nucleotide free states of Ras will give more direct insight into the function of PLC CDC25 domain. In addition, since residue 780 seems to be the consensus C-terminal residue in sequence alignment, Jpred secondary structure prediction and PLCε CDC25 homology models I propose that we design a construct that spans residues 1 through 780 which will comprise the CDC25 but also residues N-terminal of it. A similar strategy was used to in the published work elucidating the crystals structure of SOS CDC25 in complex with Ras [61]. The authors mentioned that recombinant fragment that includes the CDC25 catalytic domain alone expressed poorly and had low solubility and showed that the N terminal domain was required for the structural stability of the catalytic domain [61]. Additional biochemical and structural studies will be required to understand how the CDC25 domain interacts with Rap1A, and the role of the CDC25 domain in PLCε basal activity.

CHAPTER 3. THE CRYSTAL STRUCTURE OF PLCε

3.1 Introduction

3.1.1 Previous Efforts to Characterize the Structure of PLCε

Expression and purification of full-length PLCε has proven difficult. The first published attempt came from work in the Smrcka laboratory, who isolated full-length rat PLCε from Sf9 cells using Ni-NTA affinity purification [78]. Another group was able to purify a fragment of rat PLCε encompassing EF3-RA1 (residues 1258-2215) from High5 cells. The authors showed that this fragment could hydrolyze the membrane lipids PIP_2 and PI_4P [66,67]. This data suggests that the CDC25, PH domain and part of the EF hands were not required for lipase activity. However, the authors mentioned they attempted to purify full length but the yield was consistently too low [67].

Given the challenges in purifying PLCε, it is not surprising that structural information is also limited. The only information available are the solution structures of the two RA domains and a crystal structure of constitutively active H-Ras·GTP with a mutant of the RA2 domain [24]. The NMR 2D HSQC (heteronuclear single quantum coherence) spectra of tandem RA1-RA2 domains showed that they are flexibly connected to each other. NMR experiments revealed that H-Ras·GTP–RA2 complex does not interact with RA1. Biochemical assays also showed that the RA2 domain was not required for activity, but that removal of the RA1 domain decreased the specific activity of PLCε [24]. While this work showed how the H-Ras G protein binds to RA2, it does not show how G protein binding regulates lipase activity. In addition, these structures do not reveal how the RA domains or other regulatory domains contribute to the basal lipase activity in the context of the full-length protein. Therefore, a need for the structure of full-length or a catalytically active variant of PLCε is required to determine essential intradomain interactions for function.

3.1.2 Contribution of Regulatory Domains to the Stability of PLCε

Published work has shown that the CDC25 domain is dispensable for lipase activity [66,67], and purification of the full-length PLCε is extremely challenging [58,67,79]. Therefore, domain deletion variants were generated to identify fragments of PLCε that retained activity and could be used for structural analysis. Ongoing work in the Lyon lab has identified a number of PLCε domain deletion variants that can be expressed and purified from insect cells [79]. The largest PLCε variant that has been expressed and characterized to date is PLCε PH-COOH, which contains the four conserved core domains (**Fig. 3. 1**) and the two C-terminal RA domains. Additional N- and C-terminal truncations that have been characterized are PH-C2 (lacks the C-terminal RA domains), EF-COOH (lacks the PH domain) [79], PH-COOH ΔRA1 (lacks RA1), PH-COOH ΔRA2 (lacks RA2) [80], and EF-RA1 (lacks the PH and RA2 domains) (**Fig 3. 1**). To test the thermal stability of these variants we used differential scanning fluorimetry (DSF). Briefly, the PLCε variant and a hydrophobic dye are mixed and incubated at increasing temperatures. This leads to unfolding of the protein, resulting in the exposure of hydrophobic regions of the protein. The dye then binds the exposed regions and fluoresces. As the protein aggregates at higher temperatures, the hydrophobic regions are buried, and the dye can no longer bind to the protein. From the thermal shift curve one can infer the melting temperature of the PLCε variant [81]. When the thermostability of the PLCε variants was measured, it was shown that PH-COOH, PH-COOH ΔRA2, EF-COOH, and EF-RA1 had similar melting temperatures (T_m) (**Fig 3. 1**). This suggests the PH and RA2 domains are dispensable for the thermal stability of the enzyme. However, the deletion of the C-terminal RA domains in the PH-C2 variant [79] or the RA1 domain in PH-COOH ΔRA1 [80] resulted in a significant decrease in the thermostability (**Fig. 3. 1**). These data are consistent with the RA1 domain stably interacting with the core of the enzyme.

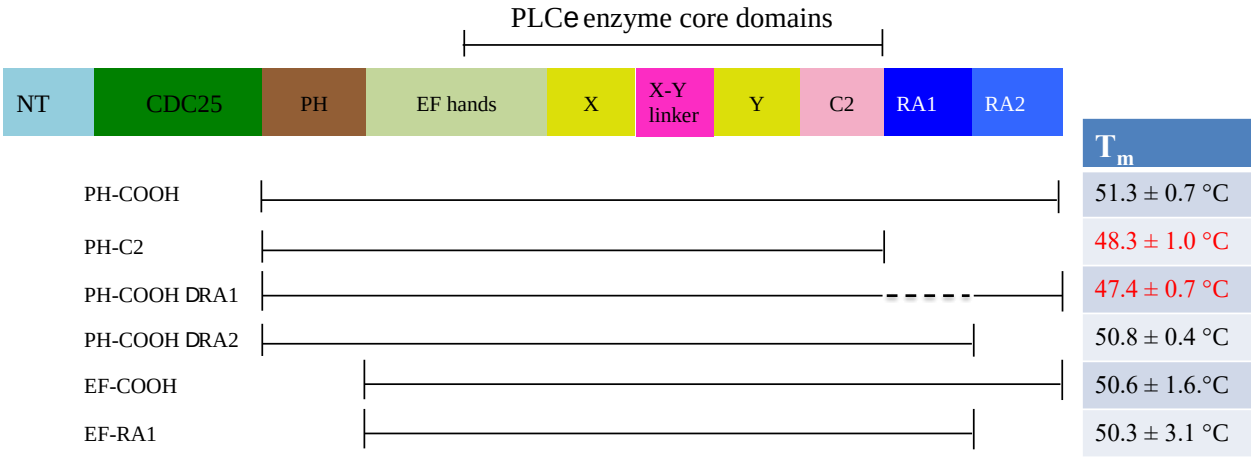

Figure 3.1 Thermal stability of PLCε variants.
(Left) Domain architecture of PLC□ domain deletion variants under study. (Right) Thermal stability of PLCε variants was measured using differential scanning fluorimetry (DSF). The melting temperature (Tm) of each variant is reported as the average of at least three experiments performed in duplicate ± SD. Thermostability measurements of PH-COOH, PH-C2, and EF-COOH were done and published by E. Garland-Kuntz & M. Sieng 79 while Thermostability measurements of PH-COOH ΔRA1 and PH-COOH ΔRA2 were perform by M.Sieng and have been submitted to the Journal of Biological Chemistry (JBC) [80]

3.1.3 Solution Architecture of PLCε variants

From NMR studies, it was shown that the RA2 domain is flexibly tethered to the RA1 domain [24]. However, whether or how the PH domain interacts with the PLCε core is still unclear. In the Lyon Lab, E. Garland-Kuntz and M. Sieng used small angle x-ray scattering studies to characterize the domain architecture of PLCε in solution using three different variants. In these Guinier plots, fit of the points on the linear regression lines shows that all the three purified variants are monodispersed in solution (**Fig. 3. 2A, B, C**). The pair-distance distribution plot, which represents all possible intramolecular vectors of the protein indicate that the PH-COOH is consistent with a predominantly compact shape with some extended features (shown by the tail on the curve at higher r values, **Fig. 3. 2A**) [79]. To determine which domain was responsible for this feature, E. Garland-Kuntz removed the C terminal RA domains of PLCε. Removal of the C terminal RA domains in PH-C2 fragment did not result in abrogation of the extended feature

suggesting they are not responsible for the observed extended features. Because the PH-COOH and PH-C2 variants both share a PH domain, we thought this feature might correspond to that domain. To determine whether the PH domain was responsible for this feature, the PH domain was deleted. Deletion of the PH domain resulted in a pair distribution that still had the extended feature, but was less pronounced than in the first two variants. It was speculated that the presence of an elongated tail in the pair distribution of the EF-COOH correspond to the first two EF hands of PLCε, which do not form interdomain contacts with the rest of the enzyme core in related PLCβ crystal structures [10,12,14,15]. This is also consistent with the fact that there are no observable electron density in the crystal structures of PLCδ [17] the first two EF hands because they are disordered. To confirm these data, M. Vancamp used crosslinking studies of PLCβ3 to show that protrusions in the PLCβ3 SAXS envelope could be diminished when the PH domain was crosslinked to the EF-hands [79]. These data, along with our DSF and SAXS studies of PLCε indicate that the PH domain of PLCε and PLCβ are likely both mobile in solution.

Putting this data together, we hypothesized that the PLCε variant EF3-RA1, which lacks the PH domain and EF1/2 hands and the flexibly tethered RA2 domain, would retain activity and be tractable for crystallization. Indeed, the PLCε EF3-RA1 variant was purifiable, monomeric in solution, retained basal activity and was crystallizable (elucidated in the following section).

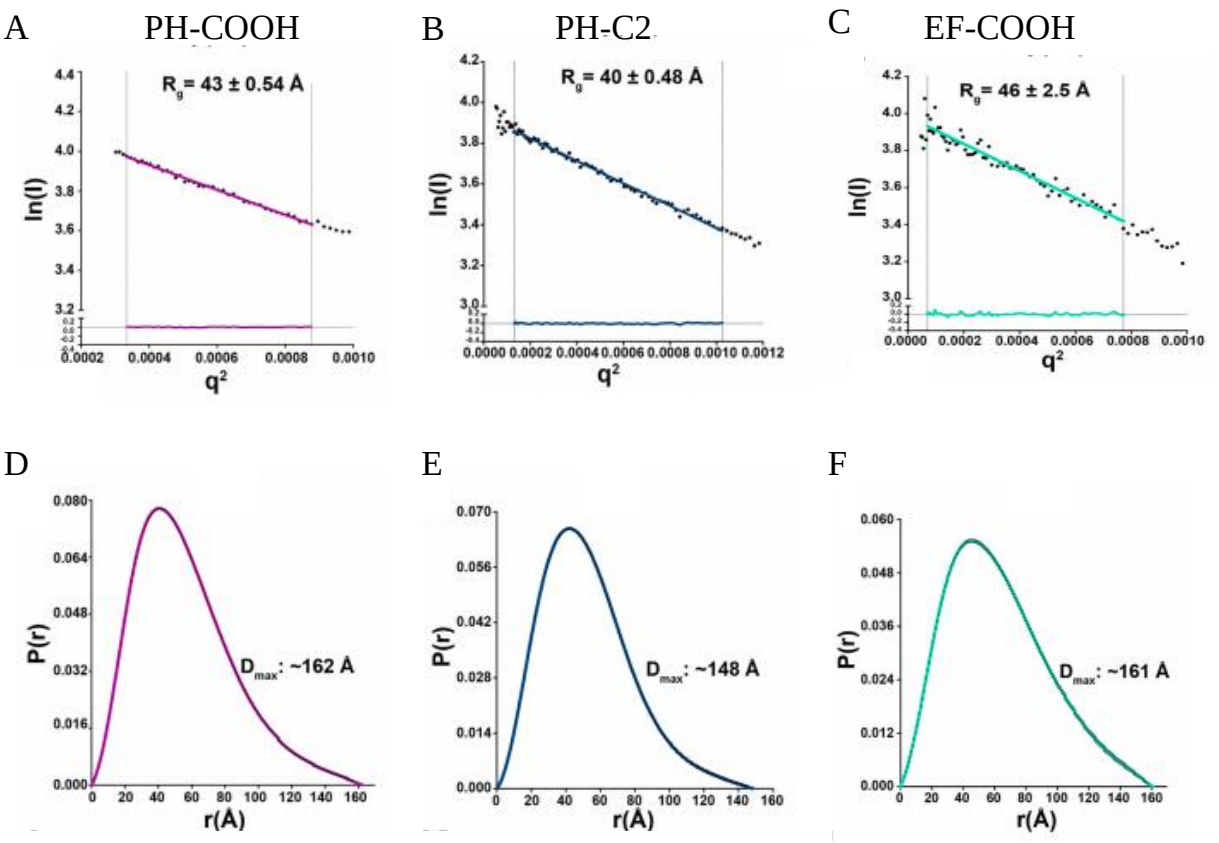

Figure 3.2 The PH domain of PLCε is conformationally dynamic in solution
Small angle X-ray scattering (SAXS) studies of the PLCε domain deletions variants. Refer to Fig 3.1 for domain boundaries of the domain deletion variant. In the Guinier plots (**A-C**) fit of the points on the linear regression lines indicate that the PH-COOH, PH-C2, and EF-COOH, are monodispersed in solution. Pair distance distribution functions of **D.** PH-COOH **E.** PH-C2, and **F.** EF-COOH indicate variants have compact shape with some extended features. The maximum diameters (D_{max}) in the variants are 162Å, 148Å, and 161Å, respectively. This figure is adapted from an article originally published in the *Journal of Biological Chemistry*. Garland-Kuntz, E. *et al.* Direct observation of conformational dynamics of the PH domain in phospholipases Cε and β may contribute to subfamily-specific roles in regulation. J. Biol. Chem; 293(45): 17477-17490 © the American Society for Biochemistry and Molecular Biology.

3.2 Methods

3.2.1 Cloning, Bacmid Generation, and P_0 Generation

The PLCε EF3-RA1 plasmid was generated from a plasmid containing PLCε EF-RA1 (residues 1035-2098) subcloned into pFastBac-HTA vector (Invitrogen). The pFastBac-HTA vector incorporates a hexahistidine tag and a tobacco etch virus (TEV) protease site at the 5’ end

of the multiple cloning site. To generate the PLCε EF3-RA1 in pFastBac-HTA, I deleted residues 1035-1283 with primers 5'-AGCATTGGATTGGAAGTACAG-3' (antisense) and 5'-GCTGCTGCAAGCATTGTG-3' (sense) using the Q5 site directed mutagenesis Kit (New England Biolabs. NEB). To generate baculovirus for protein expression, the pFastBac vector encoding PLCε EF3-RA1 was transformed into DH10Bac cells using a modified version of the Invitrogen Bac-to-Bac protocol. Briefly, 5 μL of 0.2 ng/μL of the EF3-RA vector were incubated with 100 μL DH10Bac cells on ice for 30 min. The transformation reaction was heat shocked for 45 sec at 42 °C, and incubated on ice for 2 min. The reaction was then transferred to a sterile 15 mL tube containing 900 μL of SOC medium (NEB) warmed to 37 °C, and incubated at 225 rpm for 4 h at 37 °C. 100 μL of the transformation reaction was plated onto TKG plates, which contained 10 μg/mL tetracycline, 50 μg/mL kanamycin, and 7 μg/mL gentamicin supplemented with 0.1 μg/mL X-gal and 0.32 mM IPTG. Plates were incubated at 37 °C for 48 h. X-gal is a lactose analog that can be hydrolyzed by β-galactosidase, an enzyme found in most bacteria, including the DH10Bac cell line. X-gal itself is colorless, but when cleaved by β-galactosidase, one of the products is blue. This allows identification of an active β-galactosidase enzyme in blue/white screening assays. I used blue/white screening for colony selection from TKG plates. When the DH10Bac cells are transformed with pFastBac DNA, a recombination event can occur in the β-galactosidase gene. If the recombination does not occur, the colonies are blue, indicating an intact β-galactosidase gene. When the recombination occurs, the β-galactosidase gene is disrupted, and the colonies appear white [82,83]**.** White colonies containing the PLCε EF3-RA1 insertion were confirmed by restreaking. From the second plate, a single white colony was selected and used to inoculate 4 mL of LB supplemented with 10 μg/mL tetracycline, 50 μg/mL kanamycin, and 7 μg/mL gentamicin and grown at 37 °C at 225 RPM over night. The cells were then harvested

by centrifugation, and the pellet resuspended in 300 μL of resuspension buffer (Qiagen) followed by addition of 300 μL of P2 lysis buffer (20 mM NaOH, 10% w/v Sodium dodecyl sulfate), and incubated at room temperature for 5 min. 300 μL of P3 neutralization buffer (3 mM Potassium acetate pH 5.5) was then added, and incubated on ice for 10 min, followed by centrifugation for 10 min at 14,000 x g. The supernatant was transferred into a clean 1.5 mL microfuge tube and centrifuged again for 5 min at 14,000 x g. The supernatant was then added to 800 μL of isopropanol, mixed, and incubated on ice for 10 min. The slurry was centrifuged for 15 min at 14,000 x g, the supernatant removed, and the pellet was washed with 500 μL of 70% ethanol. To remove the ethanol, the sample was centrifuged twice for 5 min at 14,000 x g. The bacmid was air-dried to remove residual ethanol, and resuspended in TE buffer (10 mM Tris-Cl and 1mM EDTA) by gentle agitation.

3.2.2 Baculovirus Production

In a sterile 24-well round-bottom block, 150 μL of insect media (Corning Insectagro) and 9 μL Fugene (Promega) were added to each well, followed by 10 μL of the PLCε EF3-RA1 bacmid at ~1,000-5,000 ng/μL. The reaction was incubated in a cell culture hood for 30 min. at room temperature. 850 μL of Sf9 cells at $2x10^6$ cells/mL confluency were then added to each well. The block was sealed with a sterile, breathable membrane (Aeraseals) and incubated for 5 hours in a 27 °C incubator shaking at 120 rpm. Then, 3 mL of Insectagro media supplemented with 10% fetal bovine serum (FBS) were added to each well, the block was resealed, and the transfections incubated at 27 °C at 300 rpm for 1 week. Control wells contained cells and media, or cells, media and Fugene. The viruses were harvested by centrifugation for 12 min at 2,000 x g, and the P_0 virus in the supernatant was transferred to a sterile tube, wrapped in foil, and stored at 4 °C.

3.2.3 P_1 and P_2 virus generation

Protein expression in insect cells is performed by infecting Sf9 or High5 cells with P_2 virus stock. The P_0 seed stock is first amplified to make a P_1, followed by a second amplification to make the P_2 virus. To produce the P_1 viruses, 50 μL of P_0 was transferred in a 1 L flask containing 50 mL of Sf9 cells at $2x10^6$ cells/mL and incubated at 27 °C at 120 rpm for 72 hours. The infection was monitored through the appearance of larger cells that double in population no more than one time. The P_1 virus was harvested by centrifugation for 10 min at 2,000 x g and the supernatant filtered through a sterile 0.2 μm filter. P_1 viruses were wrapped in foil and stored at 4 °C. To make the P2 viruses for protein expression, 200 μL of the P_1 virus was used to infect 200 mL of Sf9 cells at $2x10^6$ cells/mL for 72 hours at 27 °C at 120 rpm. The P_2 virus was harvested and stored as described for the P_1 virus.

3.2.4 PLCε EF3-RA1 expression and purification

Six liters of Sf9 cells at $2.5x10^6$ cells/mL were infected with the P_2 virus, with 25 mL P_2 used to infect 750 mL cells. The cells were harvested 40-48 hours post-infection by centrifugation at 2,000 x g for 10 min, flash frozen in liquid nitrogen, and stored at -80 °C. Cell pellets were then resuspended 300 mL of lysis buffer containing 50 mM Tris-Cl pH 7.5, 50 mM NaCl, 10 mM β-mercaptoethanol (β-ME), 2 EDTA-free protease tablets, 0.1 mM EDTA, 0.1 mM ethylene glycol-bis β-aminoethyl ether (EGTA), and lysed by douncing on ice. The lysate was then centrifuged at 100,000 x g at 4 °C for 1 hour. After centrifugation, the supernatant was filtered through a 40 μm glass fiber filter, and loaded onto a 4 mL Ni-NTA column equilibrated with 10 column volumes (CV) of buffer containing 50 mM Tris-Cl pH 7.5, 100 mM NaCl, 10 mM β-ME, 0.1 mM EDTA, and 0.1 mM EGTA (buffer A). The resin was washed with 5 CVs of Buffer A spiked with 20 mM imidazole and 40 mM imidazole. The protein was eluted with 5 CVs of buffer A containing 100

mM imidazole, and then 15 CVs of buffer A supplemented with 200 mM imidazole. The resulting elution solution was then concentrated to a final volume of 15-20 mL. The hexahistidine tag was cleaved by the addition of 4% (w/w) tobacco etch virus (TEV) protease and dialyzed overnight at 4 ℃ against 1.5-2 L of Buffer A. The dialysate was then reapplied to the Ni-NTA column equilibrated with Buffer A, the flow-through containing the cleaved protein was collected, and passed over the column two more times. The flow-through was then concentrated to 1 mL and loaded onto a MonoQ anion exchange (Mono Q 5/50 GL, GE Life Sciences) column equilibrated with one CV of buffer containing 50 mM Tris-Cl pH 7.5, 50 mM NaCl, 2 mM DTT, 0.1 mM EDTA, and 0.1 mM EGTA (start buffer). The protein was eluted by gradient elution using the start buffer and a buffer containing 50 mM Tris-Cl pH 7.5, 500 mM NaCl, 2 mM DTT, 0.1 mM EDTA, and 0.1 mM EGTA (high salt buffer). Fractions corresponding to the protein of interest were identified by SDS-PAGE, concentrated to 1 mL, and loaded onto tandem size exclusion columns (SEC, Superdex 200 10/300 GL) equilibrated with once CV of 50 mM Tris-Cl pH 7.5, 200 mM NaCl, 2 mM DTT, 0.1 mM EDTA, and 0.1 mM EGTA (S200 buffer). Fractions corresponding to the desired protein were identified by SDS-PAGE, pooled, and concentrated to at least 7 mg/mL. The protein was aliquoted, flash frozen in liquid nitrogen, and stored at -80 °C.

3.2.5 Measuring the Thermostability of PLCε EF3-RA1

Differential scanning fluorimetry (DSF) was used to measure the thermostability of the PLCε EF3-RA1 variant. In a MicroAmp optical 96-well reaction plate (Applied Biosystems), 0.5 mg/mL PLCε EF3-RA1 was incubated with 5 mM SYPRO Orange, and 5mM $CaCl_2$ dihydrate in a final reaction volume of 20 μL diluted in the S200 buffer. The plate was then sealed with MicroAmp optical adhesive film (Applied Biosystems) and centrifuged for 1 min at 1000 x g. The plate was then heated incrementally in an Applied Biosystems ViiA 7 Real-Time polymerase chain

reaction (PCR) instrument. As the protein denatures, SYPRO Orange binds to the newly exposed hydrophobic regions and fluoresces. The data was then fit to a Boltzmann distribution, where the inflection point of the denaturation curve can be used to calculate the melting temperature (T_m) of the protein.

3.2.6 Measuring the Basal Activity of PLCε EF3-RA1

To measure the basal activity of PLCε EF3-RA1, a modified version of the CisBio IP-One assay was used. We used a phosphatidylinositol (PI) liposome-based assay combined with the Cisbio fluorescence resonance energy transfer (FRET)-based IP-One G_q kit, which detects myo-inositol-1-phosphate (IP_1) accumulation. This assay required four stock solutions: 1) The 2x incubation buffer contained 100 mM HEPES pH 7, 6 mM EGTA, 2 mM EDTA, 200 mM NaCl, and 10 mM $MgCl_2$, 2) the 2x assay buffer contained 100 mM HEPES pH 7, 6 mM EGTA, 160 mM KCl, 3) the liposome solution contained 300 μM phosphatidylethanolamine (PE) and 750 μM PI diluted in 1x assay buffer spiked with 1 mM DTT, and 3) the protein stock solution contained 3 ng/μL of PLCε EF3-RA1, 1 mM DTT, and 3 mg/mL bovine serum albumin (BSA). 5 μL of the 1x incubation buffer supplemented with 0.1 M DTT, 5 μL of the 1x assay buffer supplemented with 1mM DTT, and 13.6 μM Ca^{2+} were added to Eppendorff tubes on ice. Negative controls contained 5 μL 1x incubation buffer supplemented with 0.1 M DTT and 5 μL of the 1x assay buffer spiked with 1 mM DTT were added. Immediately, 10 μL of the 3 ng/μL PLCε EF3-RA1 stock solution was added to the reactions. The samples were then centrifuged using a tabletop centrifuge at full speed for 1 min. The liposome solution was mixed by gentle vortexing and incubated at room temperature (RT) for 5 min, followed by two 30 sec. bursts of sonication in a water bath, separated by 10 sec. incubations on ice. To start the reactions, 10 μL of the sonicated liposome solution was added to the samples, and the mixture was then incubated at 37 °C for 2, 4, 6, 8, and

10 min. After incubation,5 μL of the quench buffer containing 1x assay buffer, 1mM DTT, and 210 mM EGTA was added to stop the reaction. The tubes were then centrifuged on a tabletop microfuge for one min at room temperature. 14 μL of the resulting mixture was transferred to the wells of a 384-well plate. Then, 3 μL of 0.2 μm filtered 1x d2-labelled IP_1 (acceptor fluorophore) and 3 μL of filtered reconstituted 1x anti-IP_1 cryptate (donor fluorophore) were added to the plate at room temperature (**Fig 3. 3**). The 384-well plate was then centrifuged at 1,000 x g for 1 min at and incubated for one hour at room temperature. Fluorescence resonance energy transfer (FRET) was then measured using the Synergy H4 plate reader using the Gen 11.1 software. The samples were excited at 380 nm, and the emissions at 620 and 665 nm were measured. The acceptor/donor ratio of fluorescence at 665/620nm was then used to calculate the IP_1 concentration. A standard curve was plotted using a non-linear least-squares fit of the ratio of fluorescence 665/620 versus known IP_1 concentrations. The IP_1 concentration in the reactions was then calculated from standard curve.

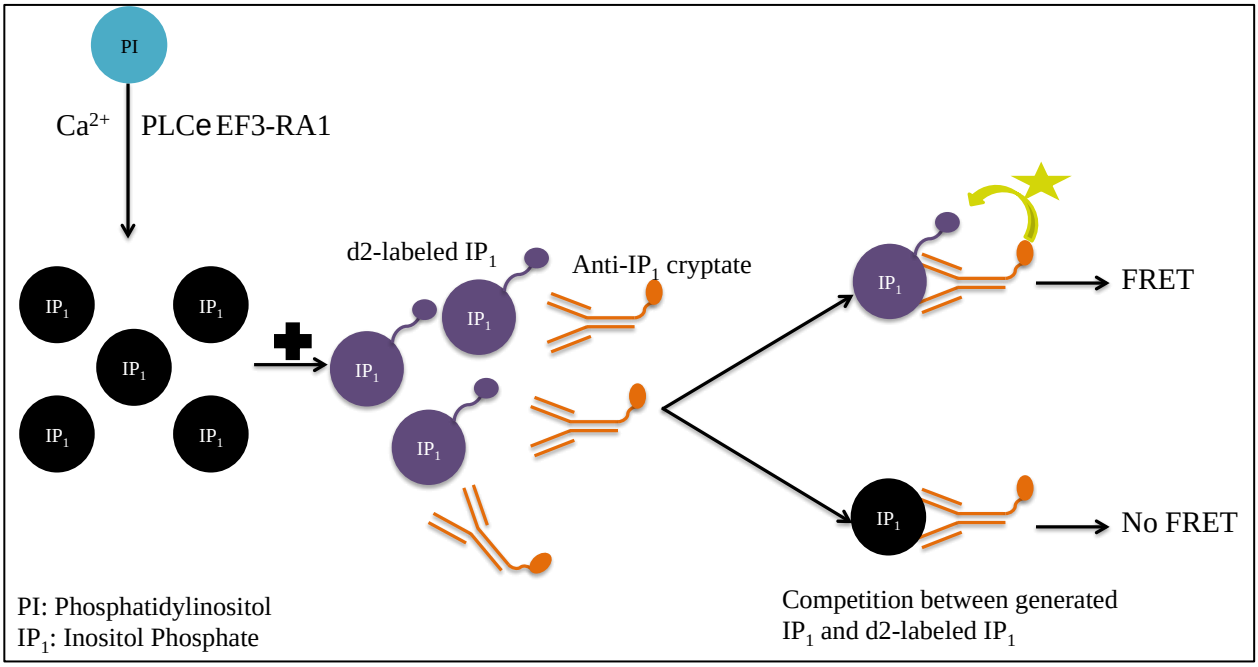

Figure 3.3 Schematic of the IP-One Assay.

In the presence of PLCε EF3-RA1 and Ca^{2+}, phosphatidylinositol (PI) is hydrolyzed from liposomes to produce inositol 1-phosphate (IP_1). The reaction is then mixed with d2-labeled IP_1 and anti-IP_1 cryptate (shown by the black addition sign). The IP_1 generated from the PLCε EF3-RA1 reaction competes with the d2-labeled IP_1, the FRET acceptor, for binding to anti-IP_1-cryptate (the FRET donor). If no IP_1 has been produced, the anti-IP_1 cryptate binds d2-labeled IP_1, resulting in FRET (top). If IP_1 is generated, then anti-IP_1 cryptate binds to the IP_1 and there is no FRET (bottom). The yellow arrow and star indicate FRET. Increasing concentrations of IP_1 from the PLCε EF3-RA1 reactions are inversely proportional to the FRET signal.

3.2.7 Crystallization of PLCε EF3-RA1

As PLCβ has been crystallized in conditions containing polyethylene glycol (PEG) [10,12,14,15], I wanted to screen for crystallization conditions of PLCε EF3-RA1 using crystallization screens containing PEGs. Using the Mosquito HTS liquid handling robot (TTP LabTech), commercially available PEG-based crystallization sparse matrix screens were screened at 4 °C and 12 °C. Hanging drop vapor diffusion was used for crystallization, and drops contained 0.2 μL of the PLCε EF3-RA1 stock solution and 0.2 μL of the well solution. The PLCε EF3-RA1 concentration ranged from 3-10.6 mg/mL (**Table 3. 1**). In the protein stock solution, PLCε EF3-RA1 was adjusted to the desired concentration using the S200 buffer and spiked with 10 mM $CaCl_2$ dihydrate such that the molar ratio of protein to Ca^{2+} was 1:1

Table 3.1 Optimal crystallization conditions screening for PLCε EF3-RA1

VENDOR	SCREEN	Temperature	protein concentration
Hampton Researc	PEG-Ion	4 °C, 12 °C	3 mg/mL, 4.03 mg/mL, 6.4 mg/mL, 10.6 mg/mL
Hampton Researc	index	4 °C, 12 °C	3 mg/mL, 4.03 mg/mL, 6.4 mg/mL, 10.6 mg/mL
Hampton Researc	MembFac	4 °C	4.03 mg/mL, 10.6 mg/mL
Jena Bioscience	PACT++HTS	4 °C	4.03 mg/mL, 10.6 mg/mL
Jena Bioscience	JCSG++HTS	4 °C	4.03 mg/mL, 10.6 mg/mL
Jena Bioscience	Classic HTSI	4 °C	4.03 mg/mL, 10.6 mg/mL
Jena Bioscience	Membrane HTS	12 °C	3 mg/mL, 6.4 mg/mL
Molecular Dimen	Morpheus&Midasplus MD1-107	4 °C, 12 °C	3 mg/mL, 4.03 mg/mL, 6.4 mg/mL, 10.6 mg/mL
Molecular Dimen	Proplex	4 °C, 12 °C	3 mg/mL, 4.03 mg/mL, 6.4 mg/mL, 10.6 mg/mL
Molecular Dimen	Stura FootprintCombination/ Ecoscreen-BN 012-1-43	4 °C, 12 °C	3 mg/mL, 4.03 mg/mL, 6.4 mg/mL, 10.6 mg/mL

From these screens, crystal showers were obtained from the Membrane HTS screen in conditions containing 10% (w/v) PEG 4000, 50 mM TRIS pH 8.5, and 500 mM NaCl at a protein concentration of 6.4 mg/mL (**Fig 3. 4A**). I followed up with refined screens in a 24-well Greiner pre-greased flat bottom tray with solutions covering the pH range 7.5-9.0 and PEG concentrations 7.5-20% w/v. After several rounds of refinement, crystal clusters were generated. These are not

favorable for diffraction data collection because of the presence of multiple lattices (**Fig 3. 4B**). To obtain larger and single crystals, I screened other buffers and PEG species. MES buffer and PEG 8000 were found to generate small single crystals that diffracted to ~9 Å. I then proceeded to microseeding in order to obtain even larger, highly ordered, single crystals for better diffraction.

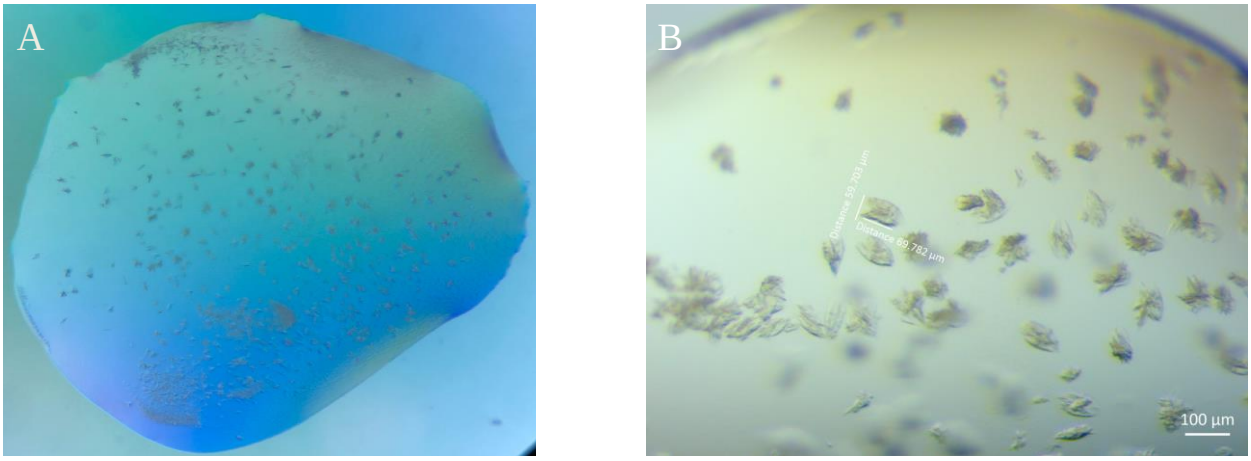

Figure 3.4 Initial screening of optimal crystallization conditions of PLCε EF3-RA1. **A.** PLCε EF3-RA1 crystal showers were present in conditions containing 10 % w/v PEG 4,000, 50 mM TRIS pH 8.5, and 500 mM NaCl. **B.** From initial rounds of refinement, PLCε EF3-RA1 crystallized as larger clusters. The scale bar is 100 µm. The photographs were taken using a Carl Zeiss microscope.

The concentration of PLCε EF3-RA1 was adjusted to approximately 5 mg/mL and spiked with 10 mM $CaCl_2$ dihydrate such that the molar ratio of protein to $Ca^{2+}$was 1:1. Diffracting crystals of PLCε EF3-RA1 were obtained by hanging drop vapor diffusion. The hanging drops contained 0.8 µL of protein stock solution spiked with $CaCl_2$ dihydrate and 0.8 µL of well solution. The well solution contained 100 mM MES pH 5.8, 0.2 M NaCl, and 6.5% (w/v) PEG 8000. The hanging drop was then streak seeded using a cat whisker dipped in a seed stock generated the same day. To generate the seed stock, a drop containing crystals was added to 4 µL of reservoir solution. The crystal drop was streakseeded with crystals grown in 6.25% PEG 4,000, 100 mM MES pH 6.00, and 0.2M NaCl at 12 °C using a protein concentration of 6.1 mg/mL. The seed stock was crushed using a pipette tip and pipetted up and down to generate microcrystals. A diluted seed

stock was also generated by adding 2 μL of the concentrated stock to 18 μL of the reservoir solution.

Crystals were harvested in a cryoprotectant solution containing 50 mM Tris-Cl pH 7.5, 2 M NaCl, 2 mM DTT, 0.1 mM EDTA, 0.1 mM EGTA, 0.1 mM $CaCl_2$ dihyrate, 0.2 M MES pH 5.8, 0.4 M NaCl, and 29% PEG 8,000. Crystals were flash frozen in liquid nitrogen. Diffraction data was collected at the Advanced Photon Source on the GM/CA 23ID-D beamline using a Pilatus3 6M detector. All data was collected at 110 K and a wavelength of 1.03 Å.

3.2.8 Model building and refinement

Diffraction data was indexed, integrated, and scaled using the automated data reduction software package autoPROC [84]. Initial diffraction to 1.96 Å was observed, but due to radiation damage and anisotropy, the data was truncated to 2.7 Å. Initial phases were determined by molecular replacement using the structure of PLCβ3 (domains EF3-C2, PDB ID 3OHM)[15] as a search model. The NMR structure of the RA1 domain (PDB ID 2BYE) [24] was generated using SWISS-Model [65], and fit within the electron density. The model of the structure was built using alternating rounds of manual building in COOT [85] and non-crystallographic restrains (NCS) using the refinement tool in PHENIX [86] and Refmac5 [87] in CCP4 [88]. Stereochemical correctness of the structure was analyzed using Molprobity [89].

3.3 Results

3.3.1 PLCε EF3-RA1 Expression and Purification

PLCε EF3-RA1 was expressed and purified from Sf9 cells. After lysis and centrifugation, the supernatant containing PLCε EF3-RA1 was first applied to a Ni-NTA affinity column. As shown in **Fig 3. 5A**, PLCε EF3-RA1 has a molecular weight of 95 kDa, and was eluted from the column

by addition of buffers containing 100-250 mM imidazole. The N-terminal His-tag was cleaved using the TEV protease, reducing the size of PLCε EF3-RA1 to 92 kDa. The untagged PLCε EF3-RA1 was then loaded onto a MonoQ column and eluted with high salt (**Fig 3. 5A**). Fractions containing PLCε EF3-RA1 were identified by SDS-PAGE, pooled, and concentrated for purification by size exclusion chromatography (SEC). The SEC chromatogram (**Fig. 3. 5C**) and SDS-PAGE analysis (**Fig. 3. 5B)** of fractions corresponding to PLCε EF3-RA1 reveals that the protein is monomeric and homogeneous, and eluted at the predicted molecular weight (25-30 mL, **Fig 3. 5C**). Typical yields are between 0.4 mg and 1.3 mg per liter of culture.

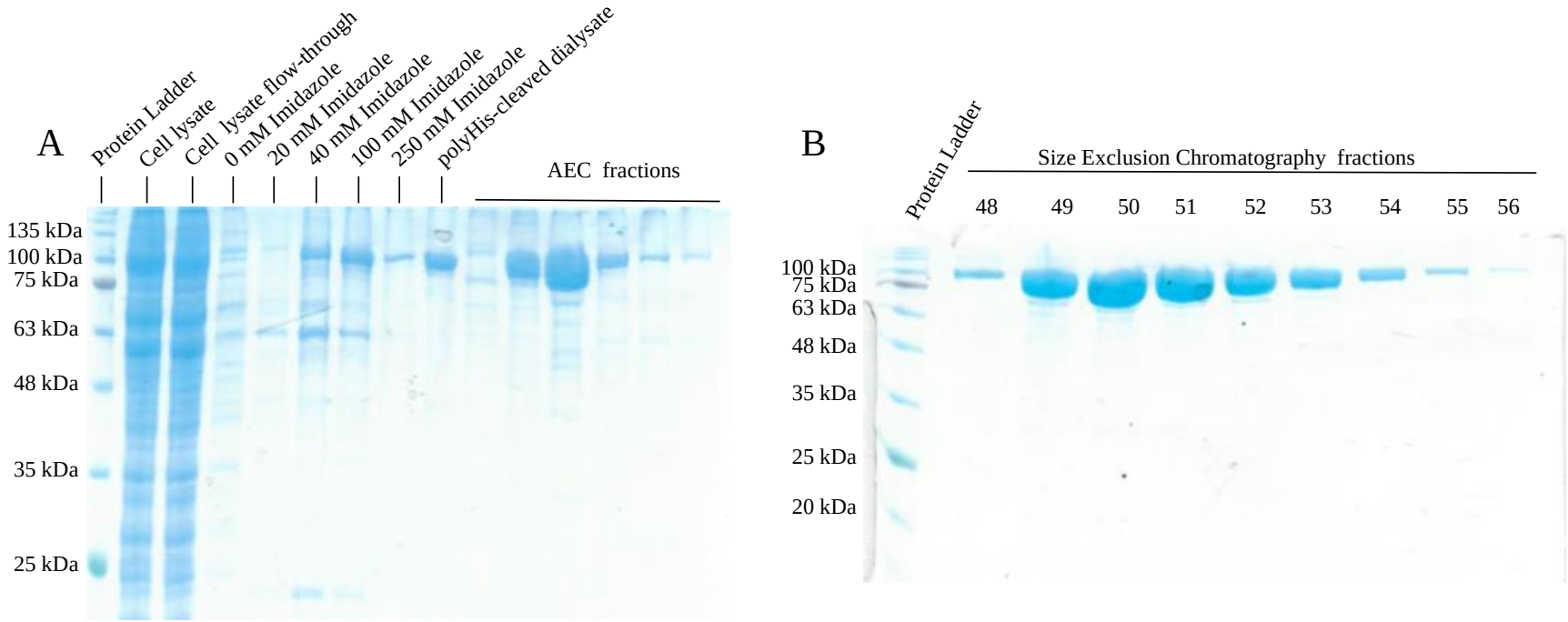

Figure 3.5 Optimization of PLCε EF3-RA1 Purification.

A. A representative SDS-PAGE gel of the PLCε EF3-RA1 purified by Ni-NTA gradient elution and anion exchange chromatography (AEC). The molecular weight standard (protein ladder), the PLCε EF3-RA1 load (cell lysate), flow-through (cell lysate flow-through), wash, and elution fractions were analyzed by SDS-PAGE. After loading, the column was washed with buffer A (0 mM imidazole), buffer A spiked with 20 mM imidazole (20 mM imidazole), and buffer A spiked with 40 mM imidazole (40 mM imidazole). The protein was eluted with buffer A supplemented with 100 or 250 mM imidazole (elution buffer). Fractions containing EF3-RA1 were pooled for AEC and analyzed by SDS-PAGE. **B** A representative SDS-PAGE gel of PLCε EF3-RA1 after SEC. Fractions 48-56 were analyzed by SDS PAGE gel. The fraction numbers are indicated at the top of the gel. **C.** A representative SEC chromatogram of PLCε EF3-RA1.

Figure 3.5 continued

C

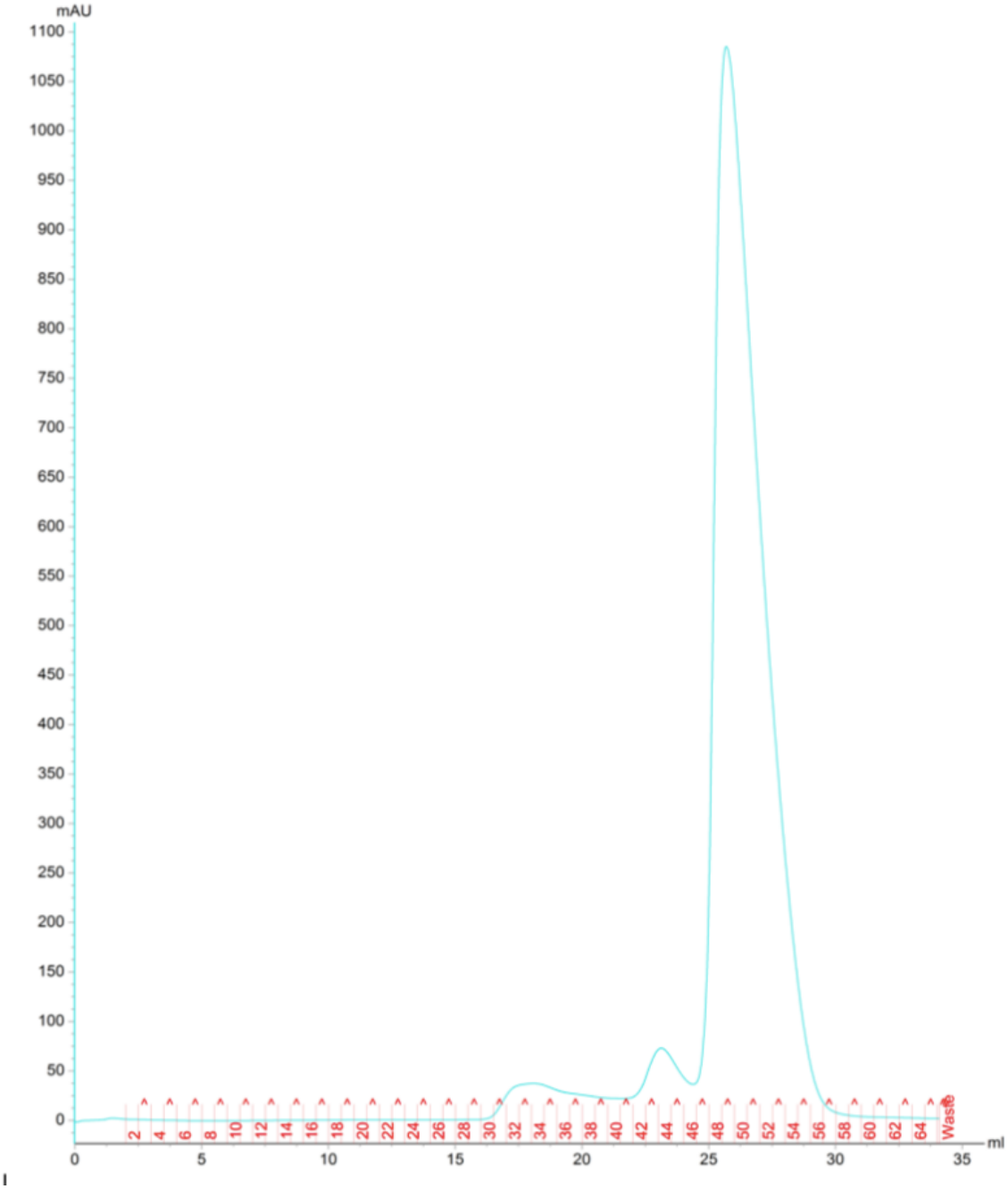

3.3.2 PLCε EF3-RA1 Thermostability and Basal Specific Activity

To test whether removal of the EF1/2 hands impacted the stability of PLCε EF3-RA1, its melting temperature was determined by DSF. The melting temperature of PLCε EF3-RA1 is 51.6 ± 0.8°C, which is similar to other PLCε variants lacking the PH domain and/or the RA2 domain (**Fig 3. 6**) [79,80]. This data suggests the EF1/2 hands are not required for thermostability and may not stably associate with the core of the enzyme.

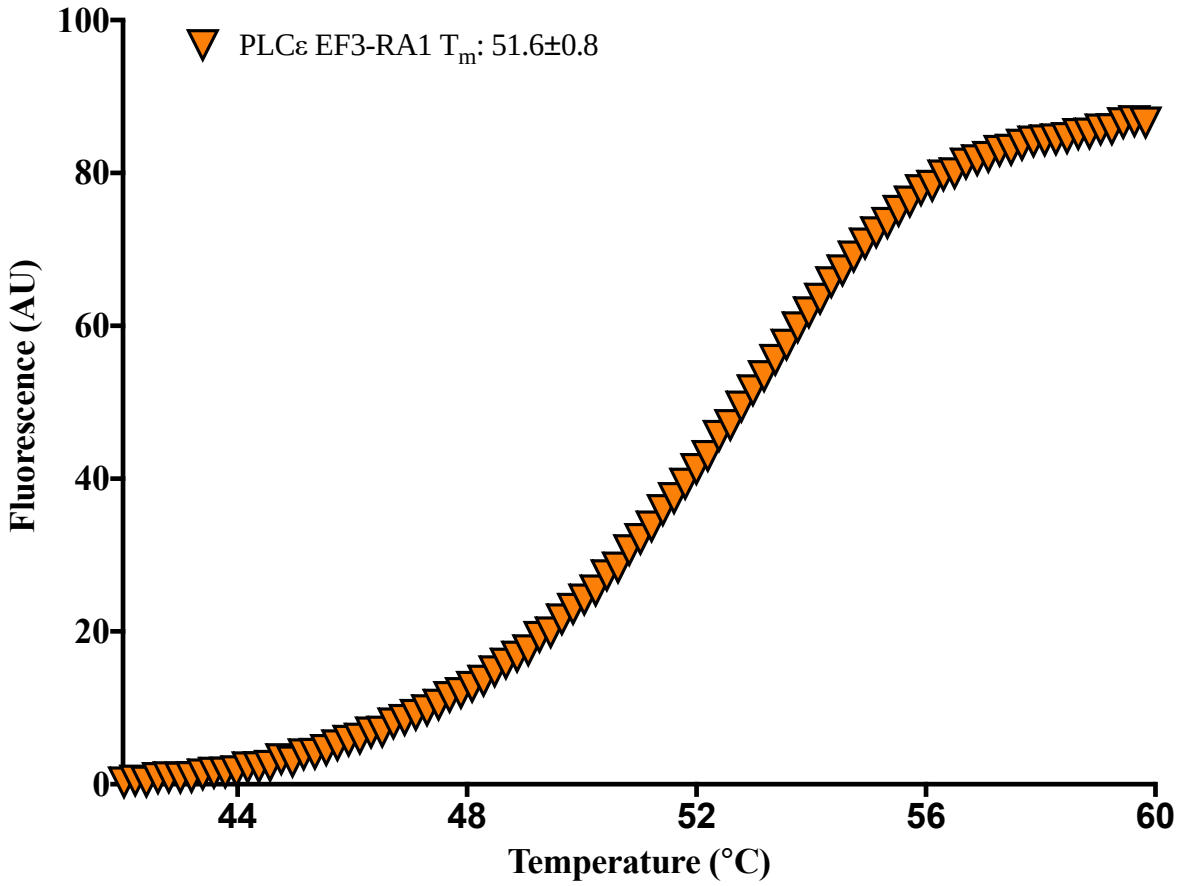

Figure 3.6 Thermostability measurements of PLCε EF3-RA1.
Representative thermal denaturation curve of PLCε EF3-RA1 is shown. The melting temperature (Tm) is 51.6 ± 0.8 °C. Data represent at least three experiments performed in duplicate ± SD.

I next determined the basal activity of PLCε EF3-RA1 using a modified version of the CisBio's IP-One assay. As shown in **Fig. 3. 7**, I observed a time-dependent increase in IP_1 accumulation, and found that PLCe EF3-RA1 had a specific activity of 47.5 ± 19.5 nmol IP_1/min/nmol PLCε EF3-RA1. PLCε enzymes are calcium dependent enzymes [58,66,67], therefore, as a negative control, PLCε EF3-RA1 was incubated in a buffer lacking Ca^{2+} and assayed for PI hydrolysis (**Fig. 3. 7**).

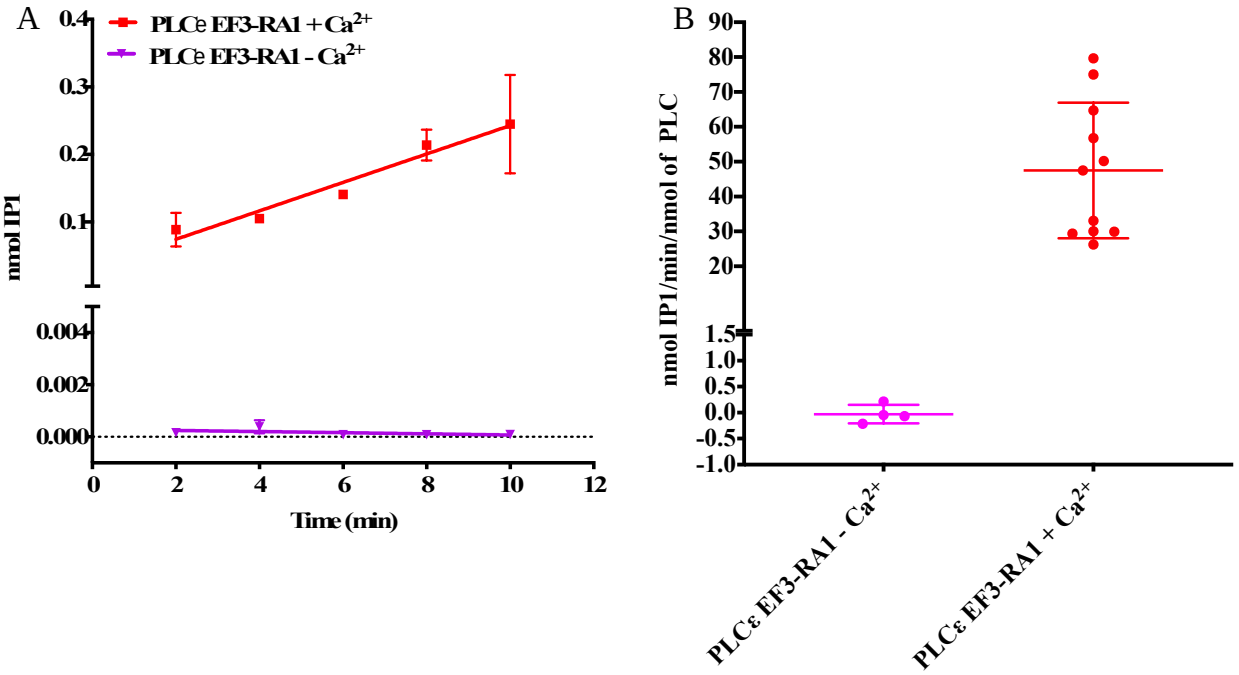

Figure 3.7 Basal activity of PLCε EF3-RA1 in vitro.
A. Representative time courses for PI hydrolysis by PLCε EF3-RA1 without (-Ca^{2+}) and withCa2+ (+Ca^{2+}) showing time-dependent production of IP1. The final protein concentration used in the assay was 1 ng/mL PLCε EF3-RA1 B. The basal specific activity of PLCε EF3-RA1, with and without Ca^{2+}. The data shown here represent ≥ 3 independent experiments performed in duplicate ± SD.

3.3.3 PLCε EF3-RA1 Crystallization and Structure Determination

PLCε EF3-RA1 crystallized as thin shark tooth-like crystals, ~50-70 μm in length and ~30 μm in width (**Fig 3. 8A**). These crystals diffracted to 2.7 Å (**Fig 3. 8B**).

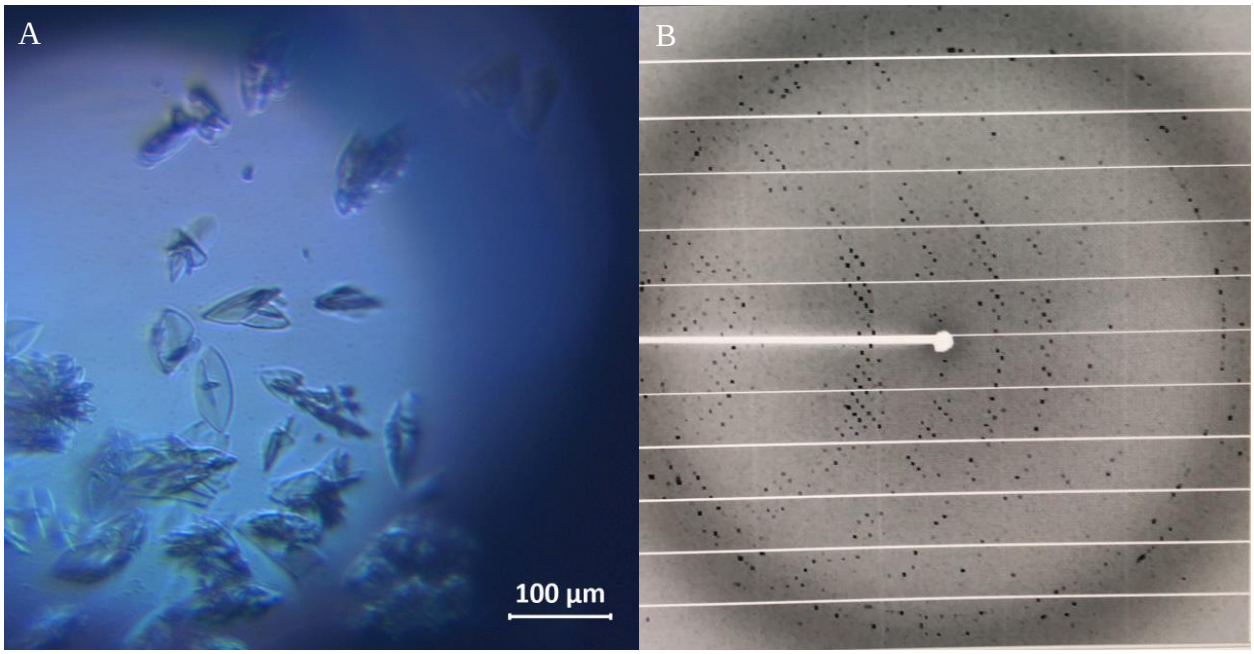

Figure 3.8 Crystals and diffraction of PLCε EF3-RA1
A. Crystals of PLCε EF3-RA1 that (**B**) diffract to better than 2.7 Å. Diffraction data was collected at GM/CA 23-ID-D beamline at the Advanced Photon Source (APS). The scale bar is 100 μm.

Four molecules of PLCε EF3-RA1 were observed in the asymmetric unit (ASU). The protein crystallized as a dimer of dimers, where one dimer is formed by chains A and B, and the second dimer by chain C and Chain D (**Fig 3. 9B**). Even though PLCε EF3-RA1 contained residues 1284- 2098 (**Fig. 3. 9A**), these residues were not all visible in the final model. Chain A, B, C, and D span residues 1303-2093, 1303-2096, 1303-2090, and 1304-2089, respectively. In the final model, 95.4 % of residues are found in the favored region of the Ramachandran plot, 4.9 % of residues are allowed regions and 0.17 % in disallowed regions (**Table 3. 2**).

Table 3.2 Data Collection and Refinement Statistics for PLCε EF3-RA1

Data Collection	
X-ray source	GM/CA 23-ID-D
Wavelength (Å)	1.03 Å
Resolution (Å)	136.72-2.73 (2.83-2.73)
Space group	P1 2_1 1
Cell dimensions	
a, b, c (Å)	93.572, 127.75, 139.34
a, b, c (°)	90, 101.12, 90
Total reflections	288367 (29634)
Unique reflections	84800 (8445)
R_{sym}	0.2678 (2.057)
Completeness (%)	99.45 (99.72)
(I/s_I)	5.08 (1.07)
Redundancy	3.4 (3.5)
($CC_{1/2}$)	0.971 (0.312)
Refinement	
Refinement resolution (Å)	29.9–2.73
Total reflections used	84779 (8445)
RMSD bond lengths (Å)	0.019
RMSD bond angles (°)	2.09
Estimated coordinate error (Å)	0.48
Ramachandran plot	
Favored (%)	95.44
Outliers (%)	0.17
R_{work}/R_{free} (%)	0.2015 (0.3165)/ 0.2782 (0.3823)
Protein atoms	2446
Solvent molecules	233
Average B-factor (Å^2)	
Protein	51.54
Solvent	38.3

Values in parentheses are for highest-resolution shell.

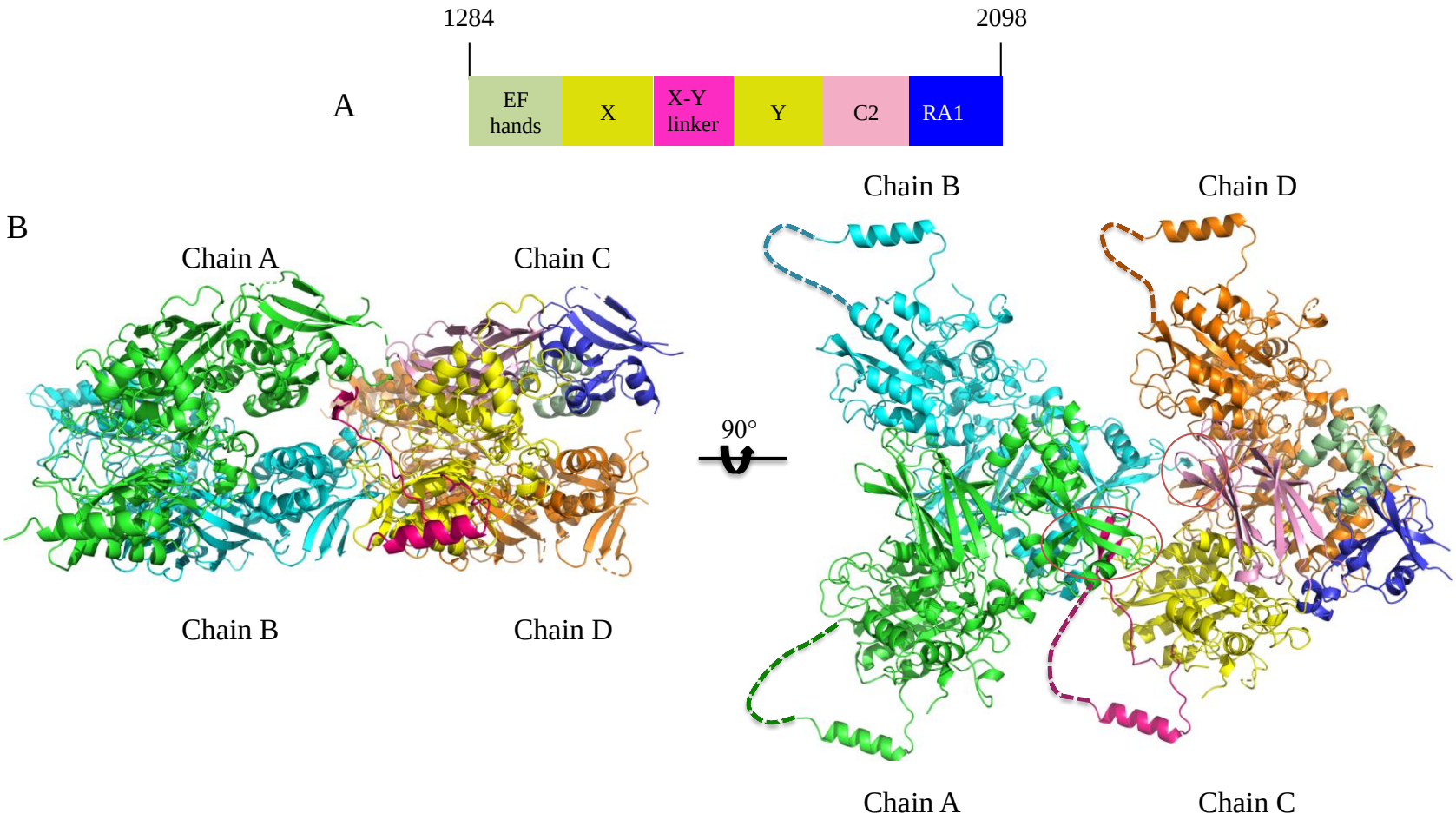

Figure 3.9 PLCε EF3-RA1 crystallizes as dimer of dimers in the ASU.

A. Domain diagram of PLCε EF3-RA1. **B.** The structure was solved by molecular replacement using PLCβ3 as a search model (46% identity to PLCβ3 EF3-C2, PDB ID 3OHM)[15]. The NMR structure of the RA1 domain (PDB ID 2BYE)[24] was fit in the ensuing density. Representation of EF3-RA1 molecule in the ASU shows a dimer formed by chain A and B and another one by chain C and Chain D. Crystal contacts are formed between the β-hairpin loop of the X-Y linker of Chain C and the RA1 domain of Chain A. A C-terminal β-strand of the RA1 domain of Chain B contacts the C2 domain of Chain D. An N-terminal helix of the X-Y linker in each molecule contacts the EF hands of a symmetry-related molecule. These contacts are circled in red. Domains are colored as in **A.**

Comparison of the EF3-C2 regions of PLCε and the well-characterized PLCδ1 (PDB ID 2ISD) [17] reveals that this region is structurally well conserved with an r.m.s.d. of 1.248 Å over 333 residues. There are, however, subtle differences between the loops in the C2 domain. Namely the first and second β-strands (cβ1-cβ2) and cβ5-cβ6 loops, which are shorter in PLCε. These loops contain the Ca^{2+} binding site in PLCδ1 (**Fig 3. 10**).

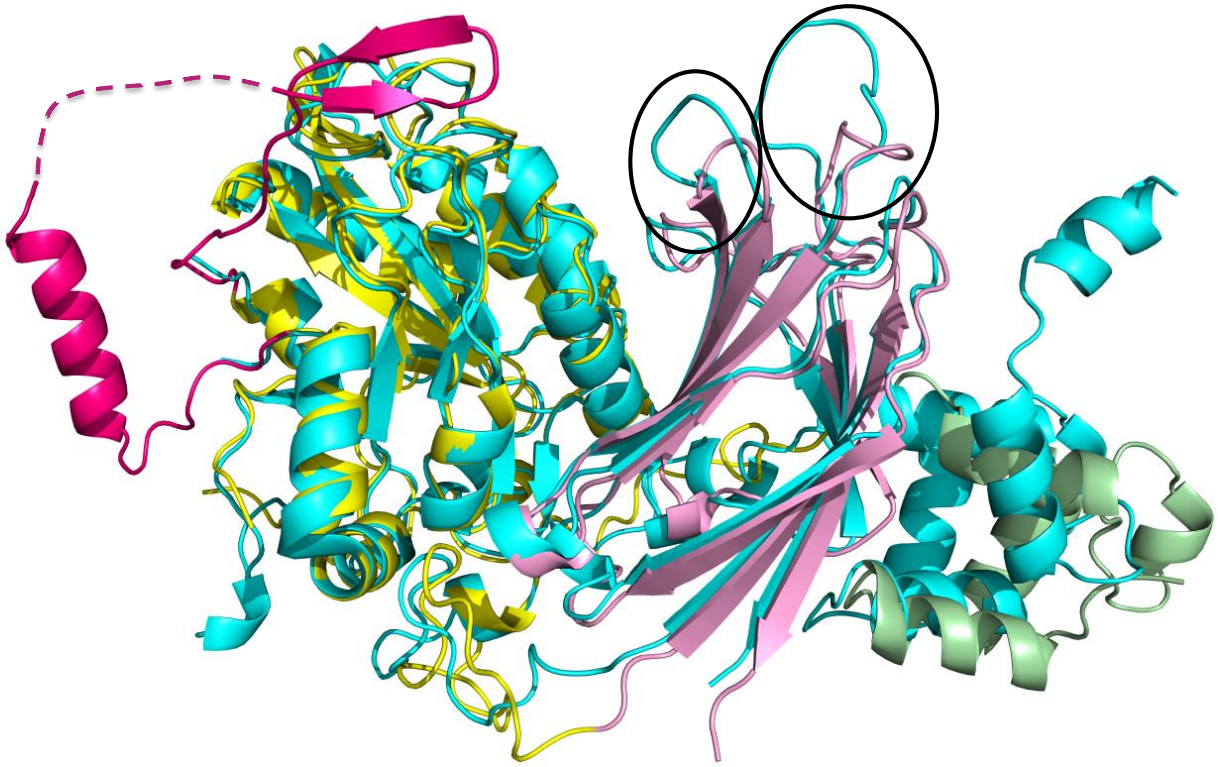

Figure 3.10 Comparison of the EF3-C2 (core) of PLCε and PLCδ
The structures of PLCε and PLCδ were superimposed using PYMOL with an RMSD of 1.248 Å over 333 residues spanning the EF3-C2 and excluding the X-Y linker. The core of both enzymes are structurally similar with subtle differences in cβ5-cβ6 (left) and cβ1-cβ2 (right) loops (circled in black), respectively.

Two very important features of PLCε are observed in the structure. The structure shows that the RA1 domain makes extensive contacts with the third and fourth EF (EF3/4) hands and the C2 domain. The structure also reveals ordered regions of the X-Y linker: an N-terminal α-helix, a β-hairpin loop, and a C-terminal extended run that covers the active site (**Fig 3. 11**).

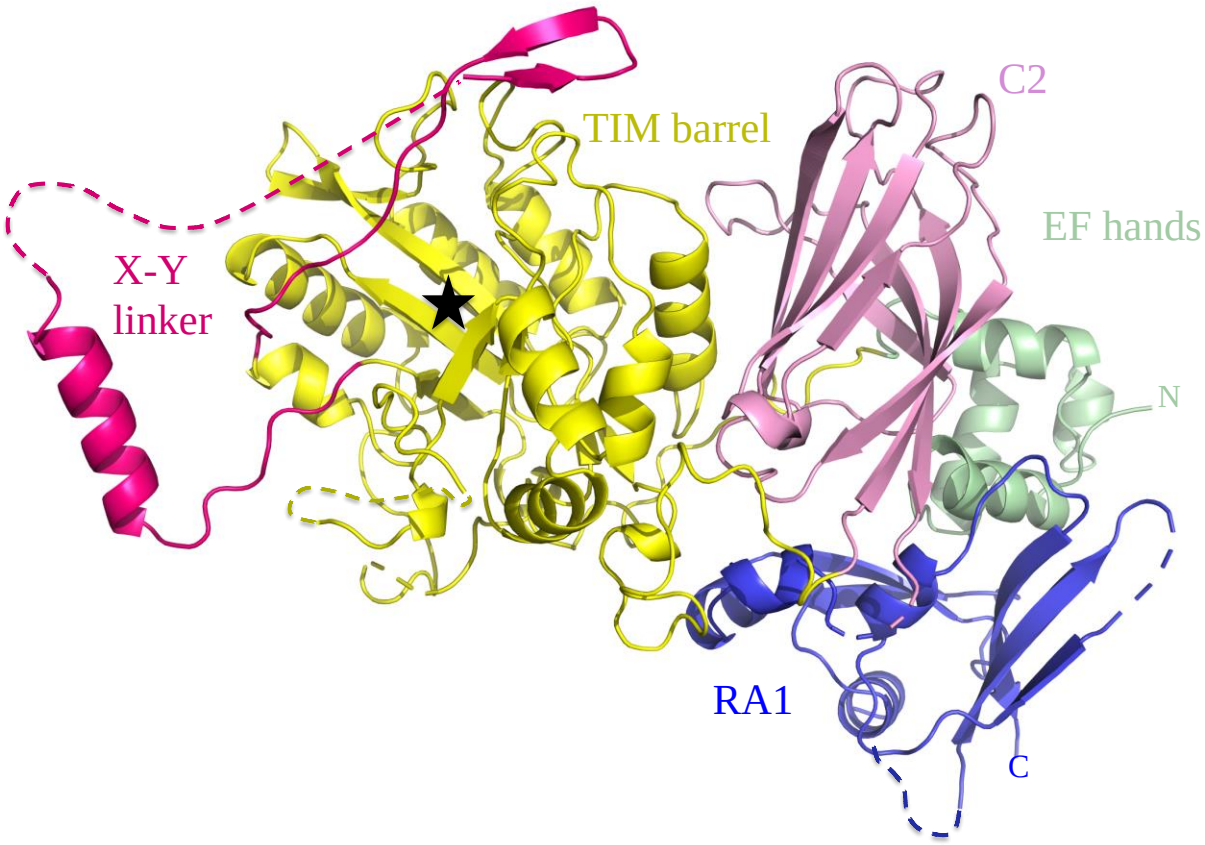

Figure 3.11 Crystal structure of PLCε EF3-RA1.
Domains are colored as in Figure 3.9A. Disordered regions are shown as dashed lines, and the N- and C-termini of the protein are labeled N and C. The RA1 domain interacts with EF hands 3/4 and the C2 domain. The N- and C-termini are ordered in X-Y linker. The location of the active site is shown by a black star.

3.3.4 The PLCε EF3-RA1 X-Y linker is partially ordered

All PLC enzymes must interact with the cell membrane to hydrolyze their substrate. Therefore, recruitment to the membrane is a crucial step in activation. The X-Y linker has been shown to play an autoinhibitory role in some PLC subfamilies, including PLCε [13]. The X-Y linker is poorly conserved, but in most cases contains a highly conserved acidic stretch reported to be essential for activation. Removal of the X-Y linker increases PLC basal activity [13,90], but its mechanism of regulation remains unclear as it is largely disordered in all published structures [13–15,17,90]. PLCε has the largest X-Y linker, comprising 124 residues. In the PLCε EF3-RA1 crystal structure, there is clear density for 44 residues. The linker contains an ordered N-terminal α-helix, followed by a disordered region that contains the acidic stretch, then a β–hairpin loop and an extended region over the active site (**Fig. 3. 12A**). The N-terminal α-helix is amphipathic. As shown in **Fig. 3. 12B,** blue residues are polar and located on one side of the helix, while hydrophobic residues are colored pink and are on the opposite side of the helix. The β-hairpin interacts with the TIM barrel through hydrophobic and ionic interactions, followed by a long extended run of amino acids that cover the active site (**Fig. 3. 12C, D**). It appears the interaction stabilizes the extend run.

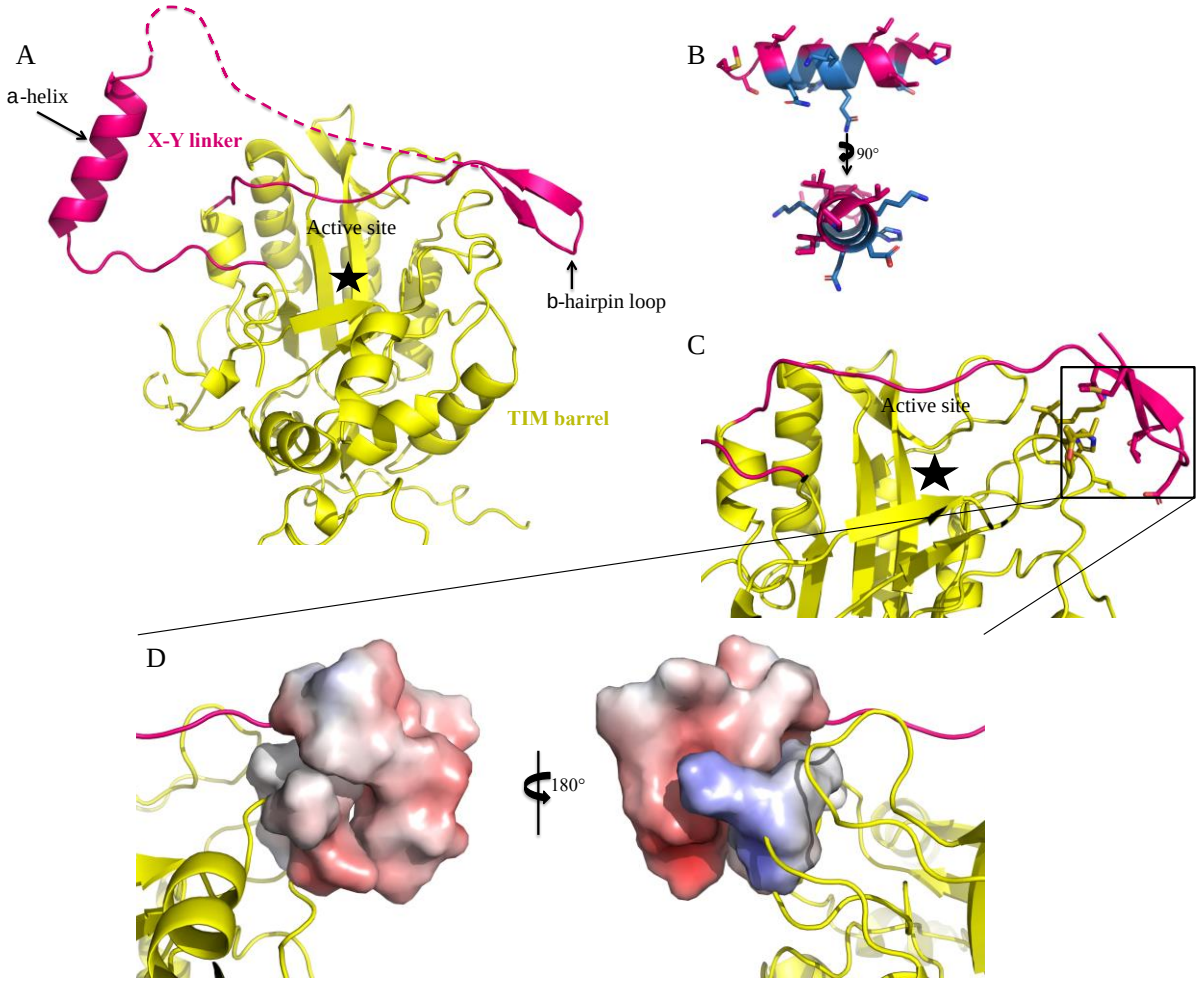

Figure 3.12 The structure of PLCε EF3-RA1 reveals portions of the regulatory X–Y linker. **A.** The N-terminus of the X–Y linker forms a well-ordered amphipathic α-helix, followed by a disordered region, a β-hairpin loop, and an extended run at the C-terminus. **B.** The α-helix is amphipathic with basic residues (blue) and hydrophobic residues (pink) on opposite sides of the helix. **C.** The extended region of the X–Y linker covers the active site, and is **D.** stabilized through hydrophobic and electrostatic interactions between the β-hairpin and the TIM barrel.

3.3.5 The PLCε Active Site is Conserved

PLCs are Ca^{2+}-dependent enzymes, and all published structures of these enzymes have contained strong density corresponding to Ca^{2+} in the active sites [10,13–15,90]. While the PLCε EF3-RA1 crystallization conditions contained Ca^{2+}, there was no electron density in the active site associated for this ion (**Fig. 3. 13A**). A comparison between the PLCε and PLCβ3 (PDB ID 4QJ4) [90] active sites (r.m.s.d. of 0.436 Å, 199 Cα atoms) shows that the positions of the residues required for Ca^{2+} coordination are highly conserved (**Fig. 3. 13A, B**). In PLCβ3, residues N333, Y335, D364, and E413 are involved in Ca^{2+} coordination, H332 and E362 are involved in both catalysis and Ca^{2+} coordination, while H376 and S619 are solely involved in catalysis [90] (**Fig. 3. 13B**). Analogous residues are similarly positioned in PLCε (**Fig. 3. 13A**). Comparison of the relative position of these residues in both structures, as shown in **Figure 3. 13C** reveals that the geometric arrangement is similar between both enzymes despite the absence of Ca^{2+} in the active site of PLCε.

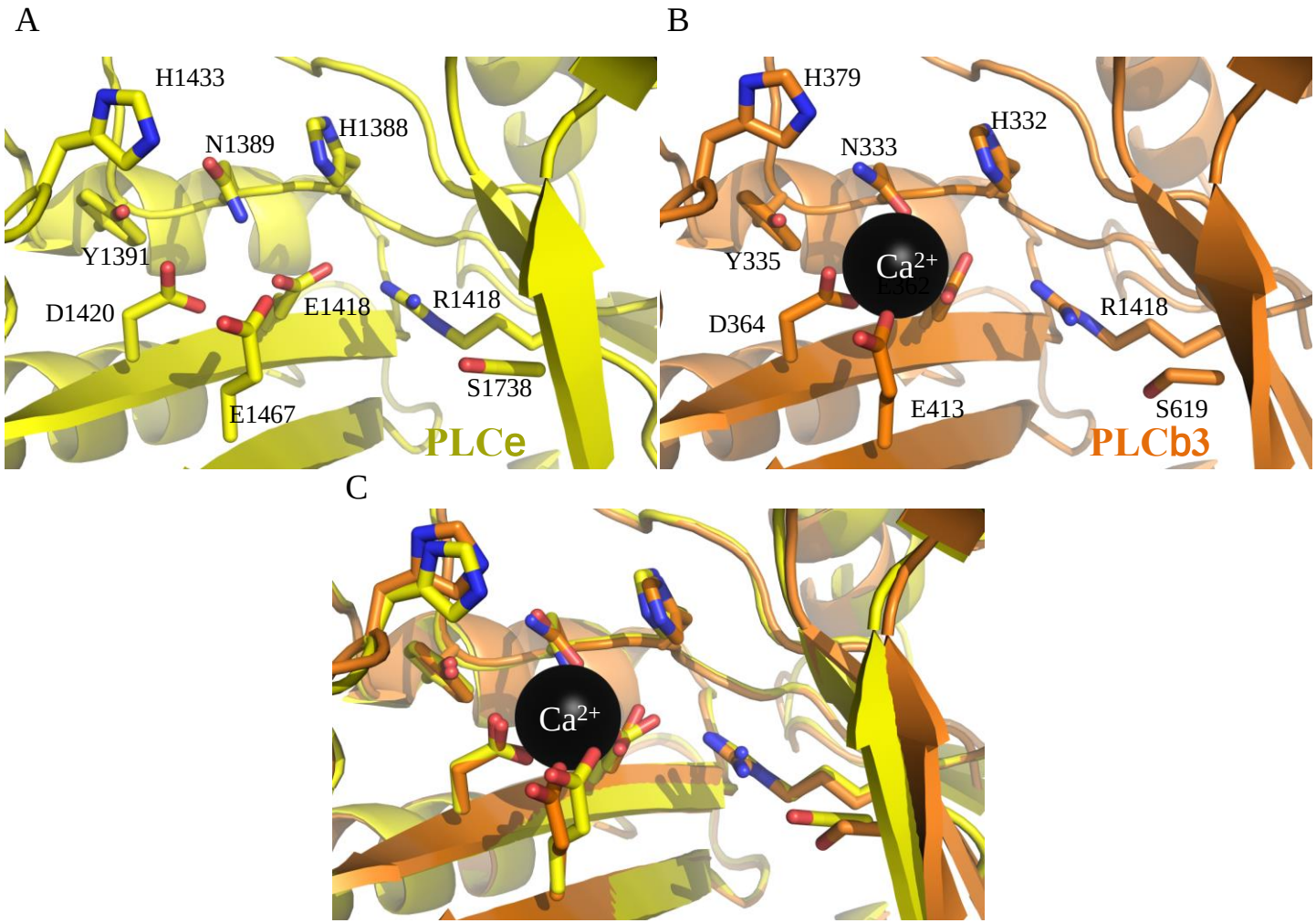

Figure 3.13 The PLC active site is conserved across subfamilies**.**

A. The active site residues of PLCε, which are analogous to those in PLCβ3, predicted to be involved in Ca^{2+} coordination and catalysis **B.** Active site of PLCβ3 (PDB ID 4QJ4). N333, Y335, D364, and E413 are involved in Ca^{2+} coordination; H332 and E362 are involved in both catalysis and Ca^{2+} coordination; and H376 and S619 are involved in catalysis The Ca^{2+} ion is shown as a black sphere. **C.** Superposition of the active sites of PLCε and PLCβ3 (r.m.s.d. of 0.436 Å, 199 residues).

3.3.6 The RA1 Domain Interacts with EF Hands 3/4 and the C2 Domain

The PLCε RA1 domain is also clearly resolved in our structure. This domain makes contacts with the EF3/4 hands, the C2 domain, and the TIM barrel-C2 linker. Approximately 1,600Å^2 surface area is buried at the interface (**Fig. 3. 14**).

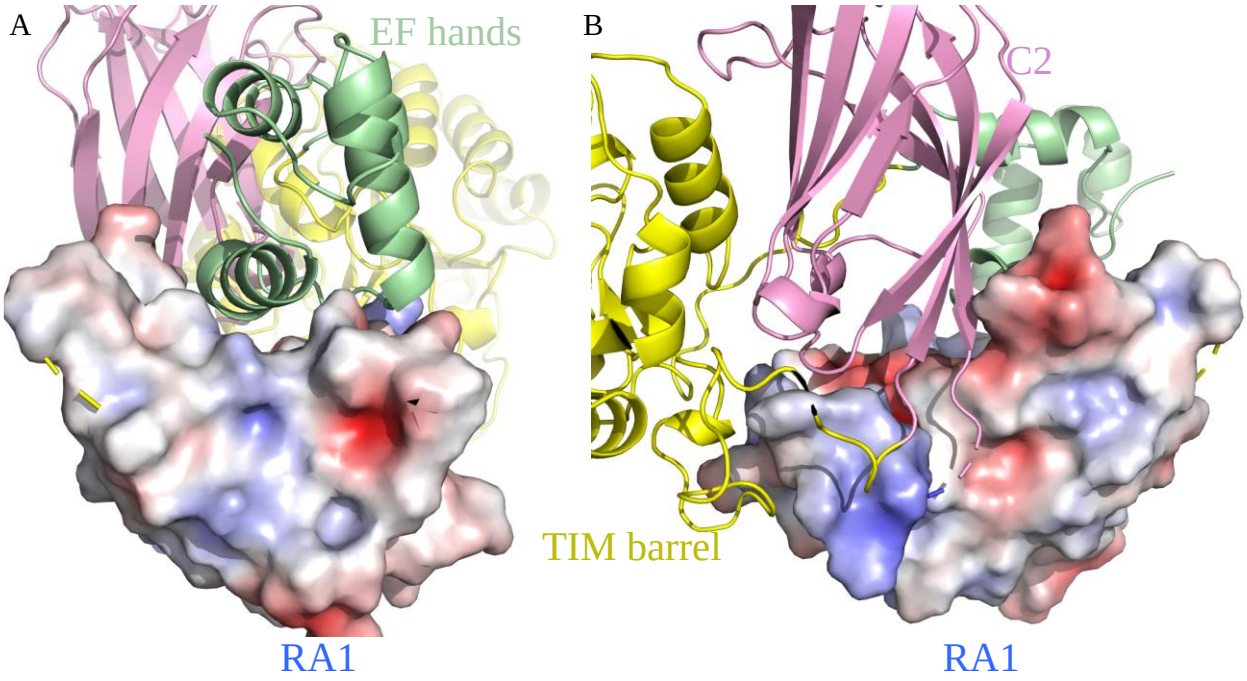

Figure 3.14 The RA1 domain interacts with EF hands and the C2 domain.
The RA1, shown as a surface with positive regions in blue, hydrophobic regions in white, and acidic regions in red [91] interacts with **A.** the first α-helix of the of the EF3 hands and the loop between the first and second α-helices of the EF3 hand. **B.** The RA1 domain also interacts with the C2 domain and the linker between the C2 and the TIM barrel.

Important interactions are seen at the EF3/4-RA1 interface. Residue N1316 in the EF3 hand makes hydrogen bonds with the main chain of G2084 in the RA1 domain. The structure also reveals ionic interactions between D1312 located in the EF3 hands, and R2085 of the RA1 domain (**Fig. 3. 15A**). Residue F2006 of the RA1 domain inserts into a hydrophobic pocket formed by I1307, L1308, Y1324 and I1327 of the EF3 hand (**Fig. 3. 15B**).

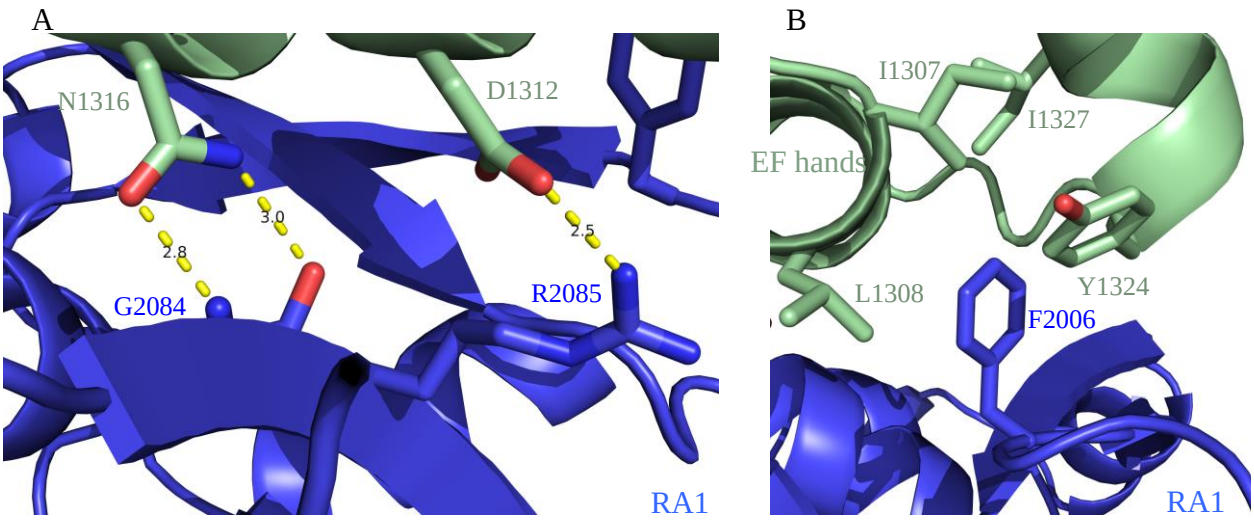

Figure 3.15 The EF3/4 hands interact with the RA1 domain.
Residues at the interface of the RA1 domain and the EF3/4 hands **A.** the main chain amide nitrogen of G2084 and the side chain carboxyl group of N1316 are 2.8 Å. the main chain carboxyl group of G2084 and the side chain amide nitrogen of N1316 are 3.0 Å apart and form hydrogen bonds. R2085 and D1312 are 2.5 Å apart and form electrostatic interactions**. B.** F2006 from the RA1 domain interacts with the EF3/4 through a hydrophobic pocket.

Additional cation-π stacking is observed between residues R1965 of the C2 domain and F2077 of RA1 (**Fig. 3. 16A**). There are also interactions between the linker connecting the C2-RA1 domains with the C2 domain and the TIM barrel-C2 linker. D1911 of the C2 domain interacts with R1987 located in the C2-RA1 linker (**Fig. 3. 16B**). F1982 in the C2-RA1 linker inserts into a hydrophobic pocket formed by F1909 of the C2 domain, and V1823, M1831 and F1835 of the TIM barrel-C2 linker (**Fig. 3. 16B**). Efforts to analyze the functional validity of the interface between EF3/4, the C2 domain, and the RA1 domain are ongoing.

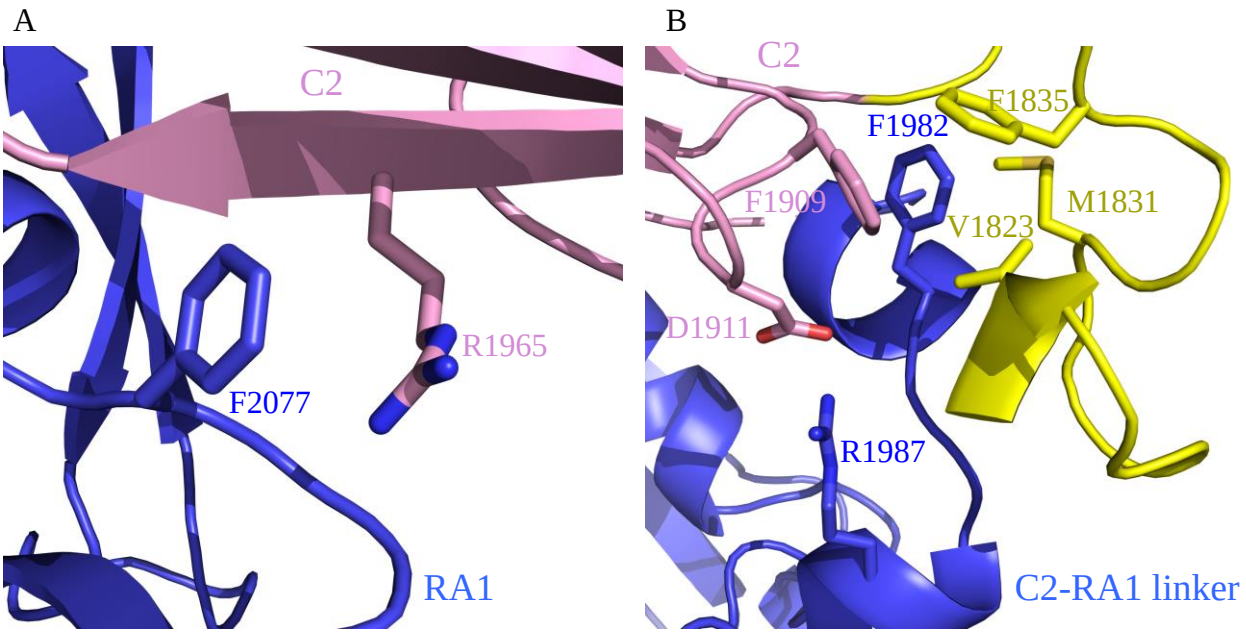

Figure 3.16 Residues at the interface of the RA1 and C2 domains.
A. Cation-π stacking between F2077 in the RA1 domain and R1965 from the C2 domain. B. Electrostatic interactions are formed between R1987 in the C2-RA1 linker and D1911 from the C2 domain, along with hydrophobic interactions between F1982 in the RA1 domain, a pocket formed by V1823, M1831 and F1835 from the TIM barrel-C2 loop, and F1909 of the C2 domain.

The RA1 domain is similar to RA2 domain [24] (r.m.s.d. 0.857 Å over 57 residues, **Fig 3. 17A**) with 25 % identity and 42 % sequence similarity. Experimentally, it has been shown that RA1 binds small G protein with lower affinity compared to RA2 [58] but both bind mAKAP scaffolding protein similarly [25]. Structurally, it is not known why PLCε is comprised of two evolutionary related RA domains with different functions with regards to small G proteins interactions. A look at the structure of RA1 in the context of PLCε reveals that the EF3/4 and C2 domains obstruct the G protein binding site on the RA1 domain (**Fig 3. 17B**). It would require major conformational changes to accommodate the G proteins. This suggest that PLCε has evolved a mechanism whereby it repurposed a thermodynamically stable and naturally occurring domain for different function.

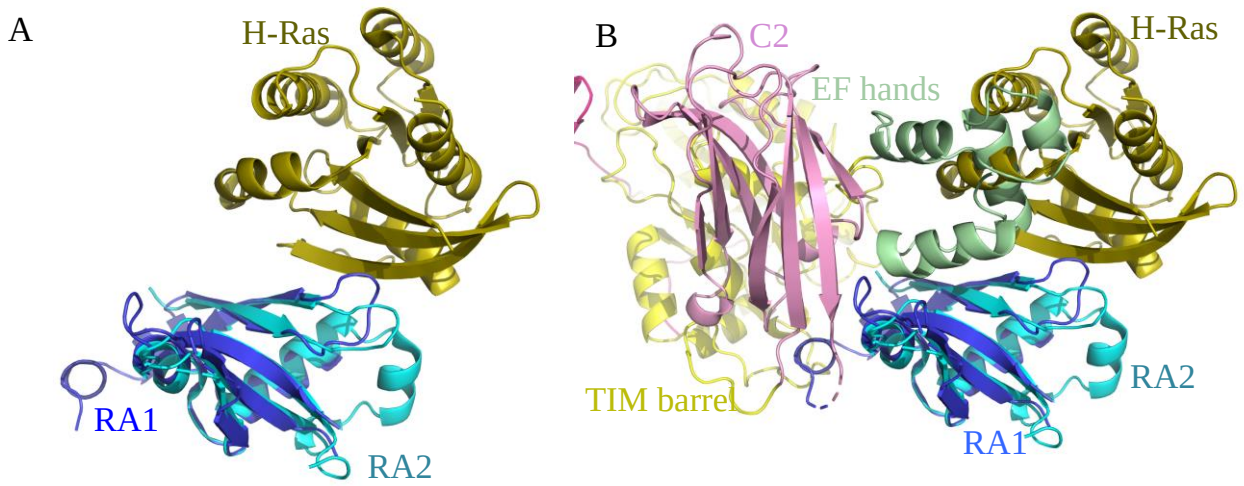

Figure 3.17 The orientation of the RA1 domain prevents G protein binding. The structure reveals extensive contacts between RA1 and the EF hands and the C2 domain. **A.** The RA1 domain and the RA2 domain (PDB ID 2C5L) [24] superimpose with an r.m.s.d of 0.857 Å (57 residues). Rat RA1 (1991-2098) and RA2 (2114-2222) domains are 25% identical and 42% similar **B.** Superimposing the RA2 domain bound to H-Ras with the RA1 domain in the PLCε EF3-RA1 structure reveals steric clashes between the G protein and the EF3/4 hands.

3.4 Discussion and Future Directions

I have determined the first crystal structure of PLCε. This structure reveals unique ordered regions in the X-Y linker and how the RA1 domain interacts with the PLCε core domains. The N-terminus of the X-Y linker features a well-ordered N-terminal amphipathic helix with hydrophobic and basic residues on opposite sides of the helix. The amphipathic helix of each chain within the ASU interacts with a symmetry-related molecule in the structure. From the SEC chromatogram, together with SAXS and negative stain electron microscopy reconstructions (Garland-Kuntz, E.E.*et al*, data not shown), PLCε EF3-RA1 is monomeric and monodispersed in solution. Therefore, I hypothesize that the amphipathic α-helix plays a role in the autoinhibition mechanism by potentially participating in ionic interactions and hydrophobic contacts with the membrane. Introduction of a cysteine mutation in this linker would disrupt the helix and would therefore, inform us about the functional relevant of this ordered part. The extended region of the linker

covers the active site, and appears to be stabilized by the interactions between the β-hairpin and loops in the TIM barrel. In PLCβ3 structures, a similar ordered feature has been shown [14,92]. PLCβ3 X–Y linker residues 575–586 block PIP_2 binding site in the enzyme active site. In PLCε these residues correspond to 1632-1643. This suggests that the observed extended run is physiologically relevant. We are currently using internal deletions of the ordered regions of the X-Y linker to validate the functional importance of these elements in the autoinhibition of PLCε**.**

In our structure we do not observe the RhoA insert spanning residues 1662-1729. However it has been shown this insert is not required for RhoA interaction with PLCε [93]. Therefore, I propose that a complex between RhoA and PLCe EF3-RA1 will form and tractable for crystallization. This complex would give us structural insight into how RhoA engages the RhoA insert for PLCε lipase activity.

The interactions between the RA1 domain and the EF hands and C2 domain are quite extensive. As work from M. Sieng *et al* found, deletion of the RA1 domain decreases stability and activity, suggesting this interaction is functionally important (submitted to *J. Biol. Chem.*) [80]. We are currently validating the interfaces using site-directed mutagenesis to determine if some or all of the residues are important for the interactions between the RA1 domain and the EF3/4 hands and the C2 domain. In the PLCε EF3-RA1 structure, RA1 is composed of numerous solvent exposed hydrophobic residues. There is a cluster of hydrophobic residues (L2021, I2024-L2029, A2034, A2035, and F2038-M2040, **Fig 3. 18**), which I propose interact with mAKAP. In fact, two hydrophobic residues (W793 and W867) of mAKAP located in the first spectrin repeat have been shown to play a crucial role in the mAKAP-RA1 interaction required for subcellular localization [25,26]. Maybe this clustered solvent-exposed hydrophobic residues form a hydrophobic interaction with these two tryptophan residues. In the future, we would like to determine the crystal structure

of PLCε EF3-RA1 and the scaffolding protein mAKAP. An understanding of the interface between the RA1 domain and mAKAP would help develop heart failure therapies without interfering with PLCε function in other subcellular locations.

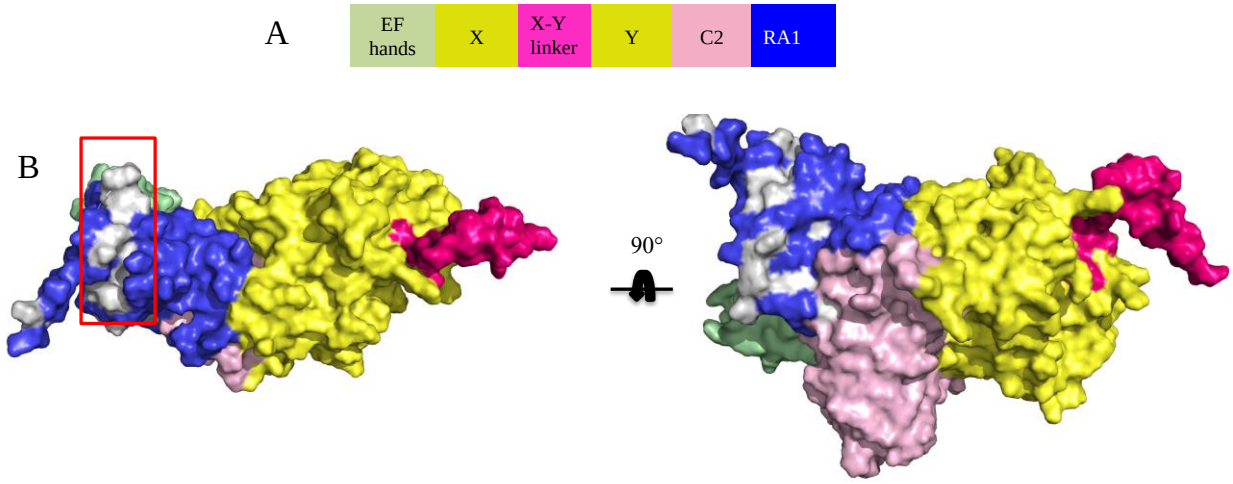

Figure 3.18 Solvent exposed hydrophobic residues in RA1
A. Domain diagram of the PLCε EF-RA1 B. Surface representation of PLCε EF3-RA1. Solvent exposed hydrophobic residues in RA1 are shown in white. Solvent exposed hydrophobic residues proposed to interact with mAKAP are contained in the red box. The domains are colored as in A. The surface representation of the PLCe EF3-RA1 model was done in PYMOL.

CHAPTER 4. PURIFICATION OF THE RAP1A^{G12V}-PLCε RA2 COMPLEX

4.1 Introduction

RA domains are found in many different proteins[94] and bind to activated Ras or Rap. Even though RA domains have sequences that are not conserved, they retain the same overall fold [24]. The RA2 domain of PLCε (RA2) structurally resembles RA domains of other proteins and binds active H-Ras [24] , leading to an increase in PLCε activity [31]. Ras activation of PLCε leads to plasma membrane translocation and PIP_2 hydrolysis [31]. On the other hand, Rap1A also activates PLCε by binding to the RA2 domain, and leads to translocation to the Golgi and hydrolysis of PI_4P [26,27]. Interactions between Rap1A and the RA2 domain play a crucial role in sustained PLCε lipase activity. Rap1A is also the only G protein activated by the PLCε CDC25 domain [27,40,55]. In addition, Rap1A binding to the RA2 domain is required for βAR-induced cardiac hypertrophy [34]. The crystal structure of the PLCε RA2 bound to activated H-Ras has been solved [24], but there is no structural information for the complex between Rap1A and the RA2 domain. Ras and Rap1A are 56% identical, but it was shown that Rap1A binds the RA2 domain with lower affinity compared to Ras [24] (**Fig. 4.1**). The difference in binding may be due to poor conservation of the G protein residues that interact with the RA2 domain. For example, E31 and E63 of H-Ras, are substituted by K31 and Q63 in Rap1A, and may decrease the affinity of Rap1A for the RA2 domain [24]. Therefore, it is important to determine the structure of the Rap1A–RA2 complex. To this end I have begun efforts to isolate a stable complex between a constitutively active form of Rap1A, Rap1A^{G12V}, and the PLCε RA2 domain for crystallization studies.

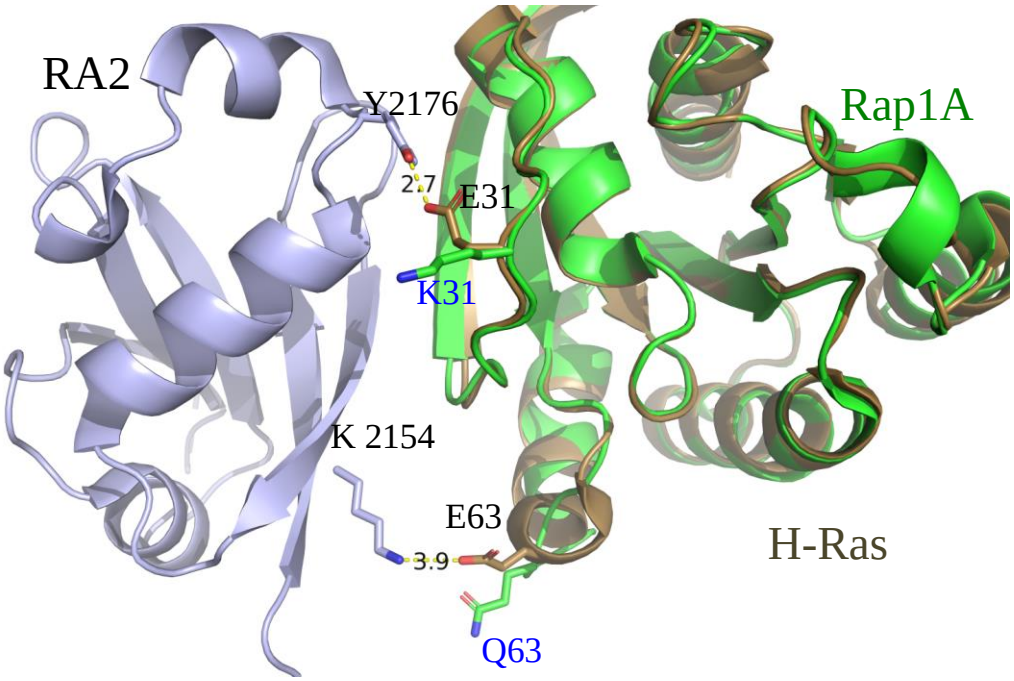

Figure 4.1 Comparison of the Rap1A and H-Ras interfaces with the RA2 domain. Superposition of the complex between H-Ras (brown) and RA2 (light blue, PDB ID 2C5L) [24] with Rap1A (green) of the Rap1A-RAFRBD (RAS-binding-domain OF C-RAF1 kinase, PDB ID 1C1Y) [95] complex. The residues involved in Ras^{G12V}-RA2 binding are labeled in black. K2154 and Y2176 of the RA2 domain make contacts with E63 and E31 of Ras, respectively. Residues of Rap1A that occupy analogous position in Ras are labeled in blue. Q63 and K31 of Rap1A may reduce the affinity between the RA2 domain and Rap1A. Rap1A and H-Ras align with an r.m.s.d of 0.458 Å for 143 residues.

4.2 Methods

4.2.1 Cloning and Expression of $Rap1A^{G12V}$ and the PLCε RA2 Domain

Human Rap1A in the pDNR-Dual vector was purchased from Harvard PlasmID and subcloned into pHis parallel 2 vector using the BamHI and SalI restriction sites. The G12V mutation, which makes the protein constitutively active, was introduced using Q5 mutagenesis kit (NEB). The PLCε RA2 domain, corresponding to residues 2111-2281, was subcloned into the into pHis parallel 2 vector using the EcoRI and SalI restriction sites. Both plasmids were independently transformed into BL21 (DE3) pLysS *E.coli*. $Rap1A^{G12V}$ expressed from BL21 (DE3) pLysS is soluble because these cells lack the machinery to add prenyl group to the C-terminal CaaX motif

of Rap1A^{G12V}. The transformed cells were then grown overnight at 37 °C on a plate containing carbenicillin and chloramphenicol. One colony was isolated and used to inoculated a 125 mL Luria broth (LB) starter culture overnight at 37 °C at a speed of 225 rpm. The following day, 8 L of LB was inoculated with ~15 mL of the starter culture per L. The cells were then induced with 0.2 M IPTG at an optical density (O.D) of 0.6-1.0 at 600 nm. Protein expression proceeded at 18 °C overnight. Cells were harvested by centrifugation at 8,671 x g for 6 min at 4 °C, flash frozen in liquid nitrogen, and stored at -80 °C. I expressed the RA2 domain and Rap1A^{G12V} in *E.coli* because the interaction of RA2 and Rap1A^{G12V} is not expected to be dependent on the prenylation state of the G protein [24].

4.2.2 Purification of Rap1A^{G12V} and the PLCε RA2 Domain

Cell pellets were resuspended in 300 mL of lysis buffer containing 20 mM HEPES pH 8.0, 150 mM NaCl, 10 mM β-mercaptoethanol (β-ME), 10% glycerol, 1 mM leupeptin (LL), and 1 mM PMSF (lysis buffer) and homogenized by dounce. The cells were then lysed by sonication. For sonication the sample was sonicated using a Q55 sonicator (Thermo Fischer) 40 to 50 times in 1-2 second pulses on ice. The lysate was then centrifuged at 4 °C at 100,000 g for 1 h. After centrifugation, the supernatant was filtered using a 40 μm glass fiber filter and loaded onto a 4 mL column volume Ni-NTA column pre-equilibrated with a buffer containing 20 mM HEPES pH 8.0, 300 mM NaCl, 10 mM β-ME, and 10% glycerol (Buffer A). The column was then washed with 10 CVs of Buffer A spiked with 20 mM imidazole. The protein was eluted with 15 CVs of Buffer A containing 250 mM imidazole (elution buffer). The elutate was then concentrated in an Amicon concentrator to 15-20 mL. To cleave the N-terminal His-Tag from the protein, 4 % (w/w) TEV protease was added and dialyzed overnight at 4 °C against 1.5-2 L of a buffer containing 20 mM HEPES pH 8.0, 150 mM NaCl, and 10 mM β-ME (dialysis buffer). The dialysate was then loaded

onto a Ni-NTA column pre-equilibrated with buffer A to remove the His-tag and uncleaved protein. The flow through was collected, and passed through the Ni-NTA column two more times. The final flow through was concentrated to 1 mL and loaded onto size exclusion columns pre-equilibrated with 20 mM HEPES pH 8.0, 150 mM NaCl, and 10 mM DTT (S200 buffer). Fractions corresponding to the RA2 domain were identified by SDS-PAGE, pooled, and concentrated to at least 5 mg/mL. The samples were flash frozen in liquid nitrogen and stored at -80°C for complex formation and crystallization trials. To purify $Rap1A^{G12V,}$ the same protocol was used with some modifications. 50 μM Guanosine-5′-triphosphate sodium salt hydrate (GTP) was added to the lysis buffer, 40 μM GTP and 5mM $MgCl_2$ were added to Buffer A and the dialysis buffer, and 40 μM GTP and 1 mM $MgCl_2$ were added to the S200 buffer.

4.2.3 $Rap1A^{G12V}$–RA2 Complex Formation

Purified $Rap1A^{G12V}$ and the PLCε RA2 domain filtered in a 0.2 μm Ultrafree filter (EMD Millipore) and then mixed at a 1.2:1 $Rap1A^{G12V}$: RA2 molar ratio. Incubation buffer containing 20 mM HEPES pH 8.0, 150 mM NaCl, 10 mM DTT, 50 μM GTP, and 5mM $MgCl_2$ was added for a final volume of 4 mL. The sample was then concentrated using a 10 kDa Amicon concentrator to a final volume of 500 μL at 4 ℃ at a speed of 3,260 x g. This step was repeated twice to ensure adequate buffer exchange and complex formation. The resulting 500 μL solution contained the complex in the incubation buffer. The mixture was then incubated on ice for 30 min., then diluted to 1 mL in incubation buffer and filtered through a 0.2 μm Ultrafree filter. The complex was then isolated over tandem size exclusion columns (Superdex 200 10/300 GL, GE Life Sciences) pre-equilibrated with incubation buffer. Fractions corresponding to the complex were identified by SDS-PAGE, pooled and concentrated to ~25 mg/mL. The complex was then screened for crystallization conditions.

4.2.4 Screening for Optimal Crystallization Conditions

Using the Mosquito HTS liquid handling robot (TTP LabTech), commercially available crystallization sparse matrix screens were screened at 20 °C. Hanging drop vapor diffusion was used for crystallization, and drops contained 0.2 μL of the protein complex and 0.2 μL of the well solution. The protein complex concentration ranged from 5-25 mg/mL (Table 4.2).

Table 4.1 Crystallization conditions screened for the Rap1A^{G12V}-RA2 complex.

VENDOR	SCREEN	His tag (Yes/ NO)	Protein concentration
Hampton Research	PEG-Ion	Yes	10.2 mg/mL, 17.1 mg/mL
Hampton Research	Index	Yes	11.6 mg/mL, 20.4 mg/mL
Hampton Research	MembFac	Yes	11.6 mg/mL, 17.1 mg/mL, 20.4 mg/mL
Jena Bioscience	PACT++HTS	Yes	8.2 mg/mL, 25.1 mg/mL
Jena Bioscience	JCSG++HTS	Yes	8.2 mg/mL
Jena Bioscience	Classic HTSI	Yes	11.6 mg/mL, 20.4 mg/mL, 25.1 mg/mL
Jena Bioscience	Membrane	Yes	11.6 mg/mL, 20.4 mg/mL
Molecular Dimension	Morpheus&Midasplus MD1-107	Yes	8.2 mg/mL, 11.6 mg/mL, 20.4 mg/mL
Molecular Dimension	Proplex	Yes	8.2 mg/mL, 11.6 mg/mL, 17.1 mg/mL, 20.4 mg/mL, 25.1 mg/mL
Molecular Dimension	Stura Footprint Combination/ Ecoscreen-BN 012-1-43	Yes	8.2 mg/mL
Molecular Dimension	PACT premier	No	5 mg/mL, 7 mg/mL
Molecular Dimension	Proplex	No	5 mg/mL, 7 mg/mL
Molecular Dimension	MemGold2	No	5 mg/mL, 7 mg/mL
Molecular Dimension	Morpheus&Midasplus MD1-107	No	5 mg/mL
Anatrace	MCSG4	No	7 mg/mL
Qiagen	PEGs	No	5 mg/mL, 7 mg/mL
Qiagen	PEGsII	No	5 mg/mL, 7 mg/mL

4.3 Results

4.3.1 $Rap1A^{G12V}$ and PLCε RA2 protein expression

The PLCε RA2 domain and $Rap1A^{G12V}$ were expressed and purified from *E.coli*. A constitutively active point mutant of Rap1A ($Rap1A^{G12V}$) was used because the RA2 domain only binds activated G proteins [27,96]. The first step in the purification of $Rap1A^{G12V}$ and PLCε RA2 was Ni-NTA affinity purification. As shown in the representative SDS-PAGE gels**,** $Rap1A^{G12V}$ (molecular weight of 25 kDa) and RA2 (molecular weight of 23 kDa) elute from the column at high imidazole concentrations. An unknown contaminant protein with a molecular weight greater than 48 kDa is also present in the elution sample from both proteins (**Fig. 4.2A**). After Ni-NTA purification, the N-terminal histidine tags were cleaved using TEV protease (**Fig. 4.2A).** The TEV-cleaved $Rap1A^{G12V}$ (molecular weight of 22 kDa) and RA2 (molecular weight of 20 kDa) were then purified by size exclusion chromatography. The RA2 domain is homogeneous, but appears to be dimeric when compared to the molecular weight standards (Biorad) separated on tandem SEC columns (**Fig. 4.2B, C**). Typical yields of the PLCε RA2 domain are between ~0.4-0.8 mg per liter of cell culture. $Rap1A^{G12V}$ is monomeric and homogeneous (**Fig 4.2D, E**) as shown by the SEC chromatogram (**Fig 4. D**) and SDS-PAGE gel analysis of pooled fractions (**Fig 4.2E**). Typical yields for $Rap1A^{G12V}$ are between ~0.4-0.8 mg.

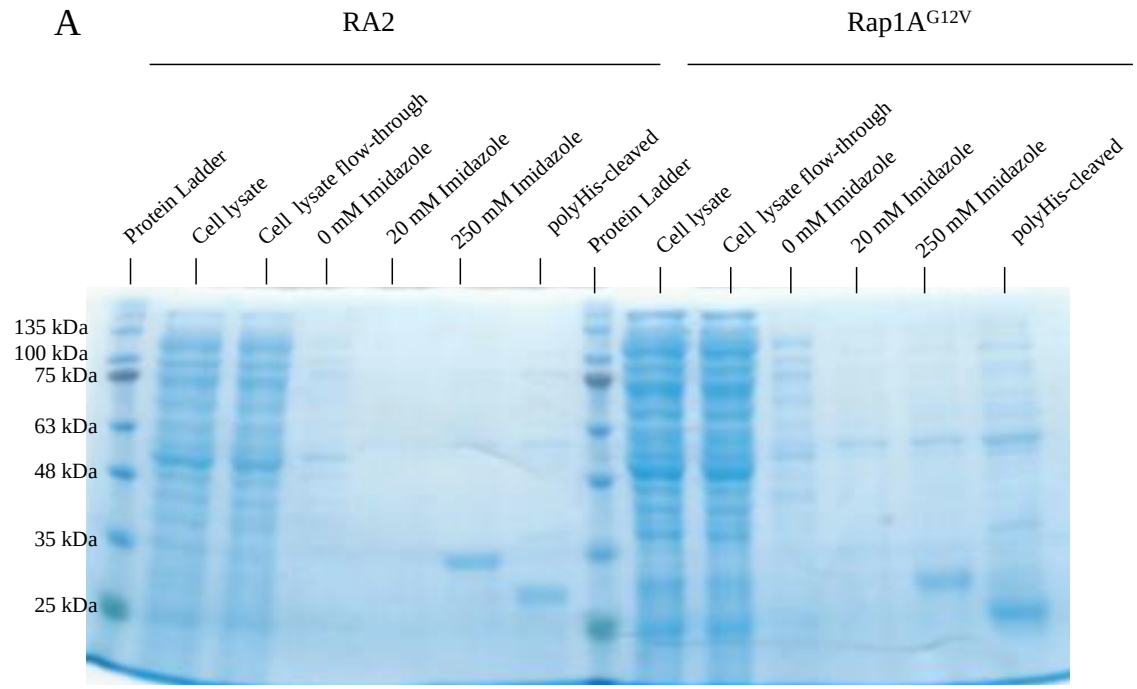

Figure 4.2 Purification of the PLCε RA2 domain and Rap1A^{G12V}.
A. The RA2 domain and Rap1A^{G12V} were first isolated by Ni-NTA affinity purification. After ultracentrifugation, the cell lysate was loaded onto a Ni-NTA the flow through was collected, and the resin was washed with buffer A (0 mM imidazole), buffer spiked with 20 mM imidazole (20 mM imidazole), and eluted with 250 mM imidazole (250 mM imidazole). The His-tags were removed by incubation with TEV protease (polyHis-cleaved). **B.** A representative SEC of the RA2 domain superimposed with the molecular weight standards separated on tandem size exclusion columns. RA2 (20 kDa) appears to be a dimer (44 kDa). **C.** Fractions 59-65 (corresponding to 30-35 mL) were pooled and concentrated for complex formation. The fractions number is indicated on the top of the gel. **D.** Rap1A^{G12V} was also separated by tandem size exclusion columns. Comparison of Rap1A^{G12V} chromatogram to the molecular weight standards reveals Rap1A^{G12V} (~22kDa) is a monomer in solution because it elutes at a molecular weight >17 kDa. **E.** Fractions 63-69 (corresponding to 32-38 mL) were pooled and concentrated for complex formation. The fractions number is indicated on the top of the gel. Each peak of the molecular weight standard is indicated to the right of the chromatogram.

Figure 4.2 Continued

B

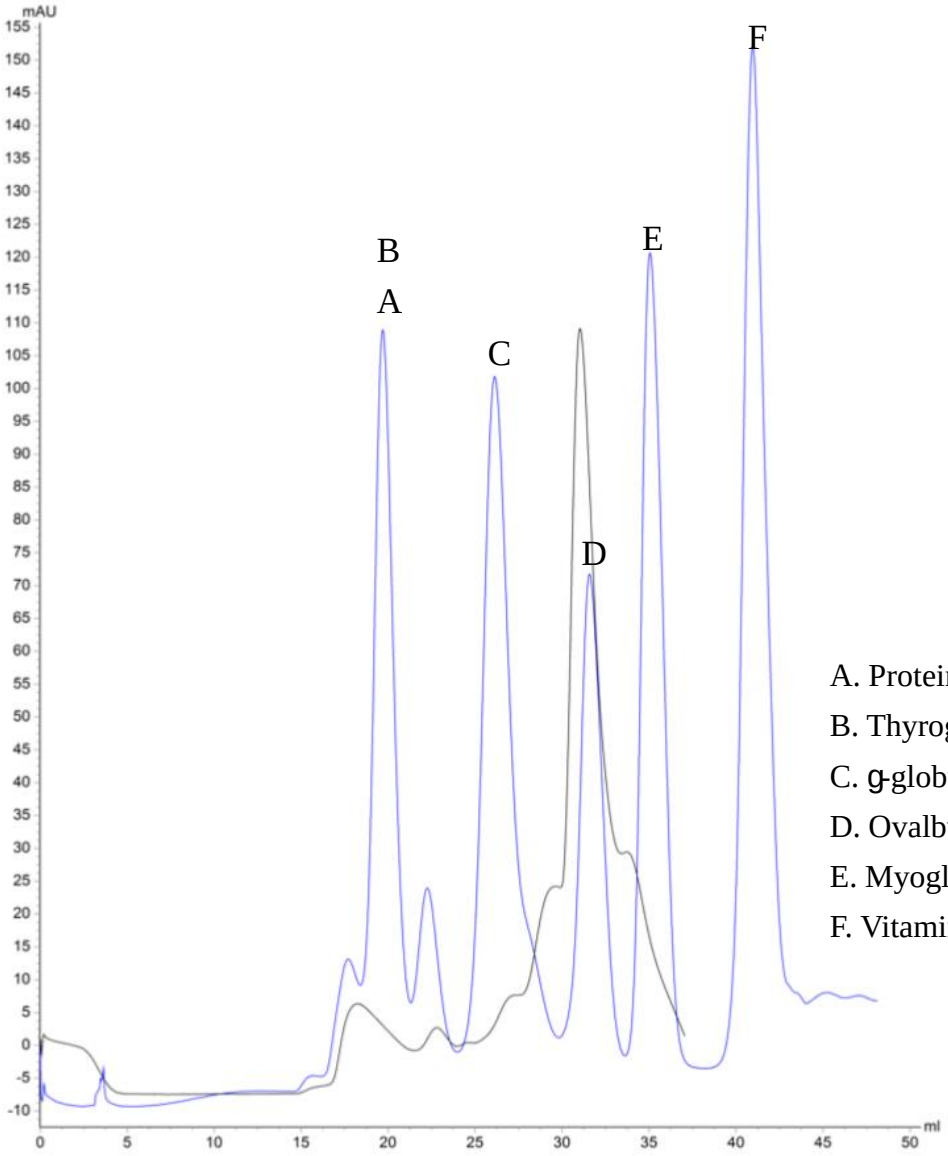

A. Protein aggregate
B. Thyroglobulin 670 kDa
C. g-globulin 158 kDa
D. Ovalbumin 44kDa
E. Myoglobin 17 kDa
F. Vitamin B 12 1.35 KDa

C

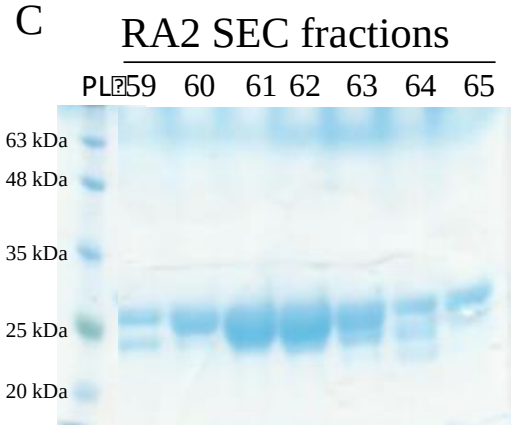

Figure 4.2 Continued

D

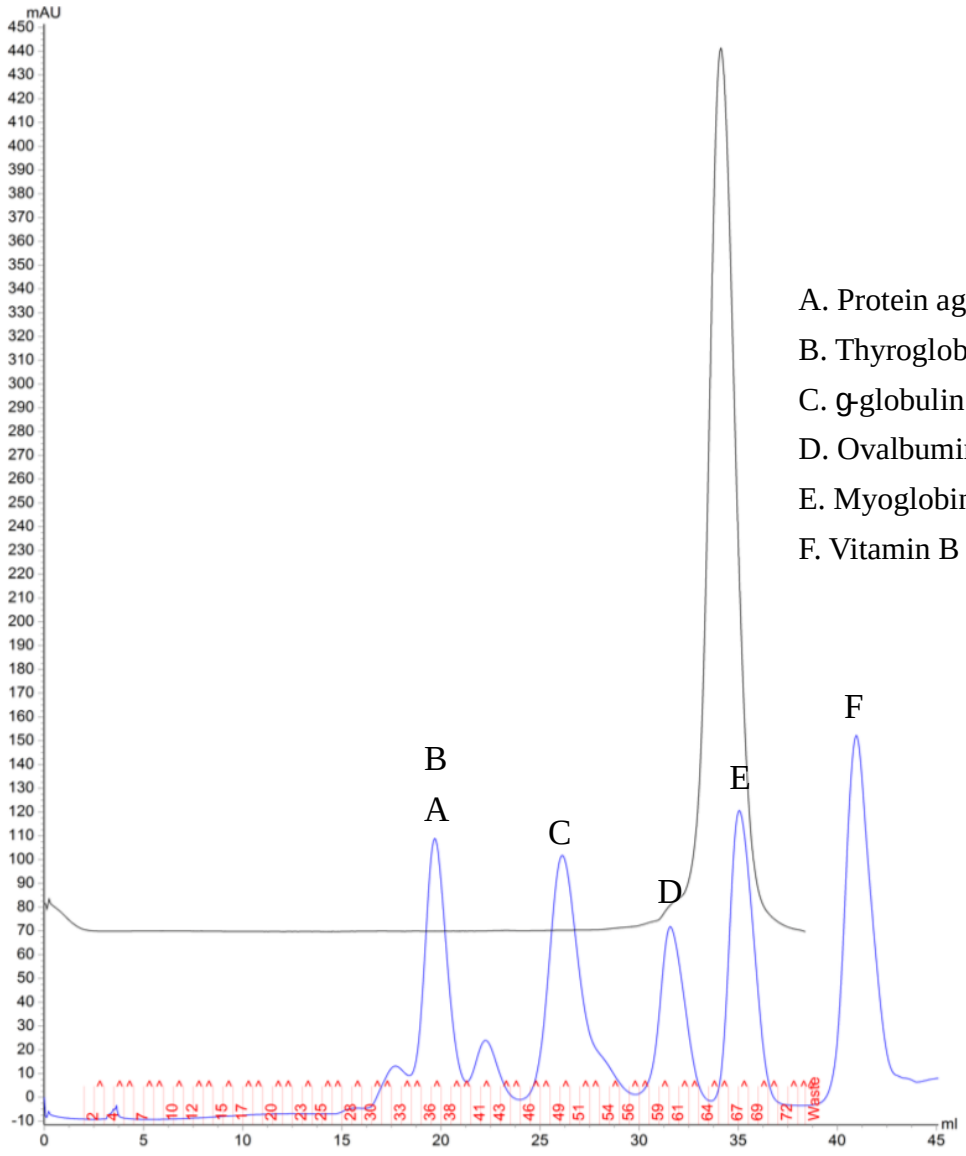

A. Protein aggregate
B. Thyroglobulin 670 kDa
C. g-globulin 158 kDa
D. Ovalbumin 44kDa
E. Myoglobin 17 kDa
F. Vitamin B 12 1.35 KDa

E

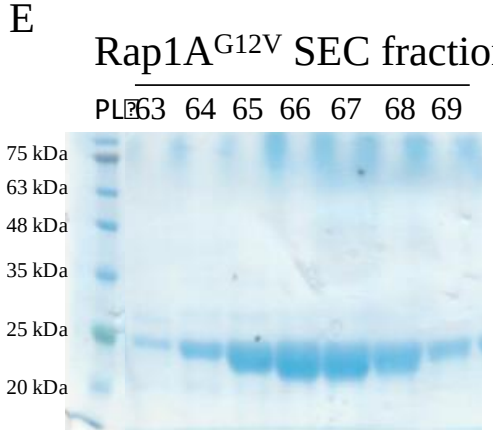

d

4.3.2 Rap1A^{G12V}–RA2 Complex Formation

After purification, the RA2 domain was incubated with Rap1A^{G12V} at a molar ratio of 1:1.2 in the presence of excess GTP. The mixture was concentrated and the complex isolated on tandem size exclusion columns (**Fig. 4.3**). A stable and stoichiometric complex was isolated (**Fig. 4. 3**). Typical yields are between ~0.5 mg and 0.6 mg per liter of Rap1A^{G12V} combined with a liter of RA2.

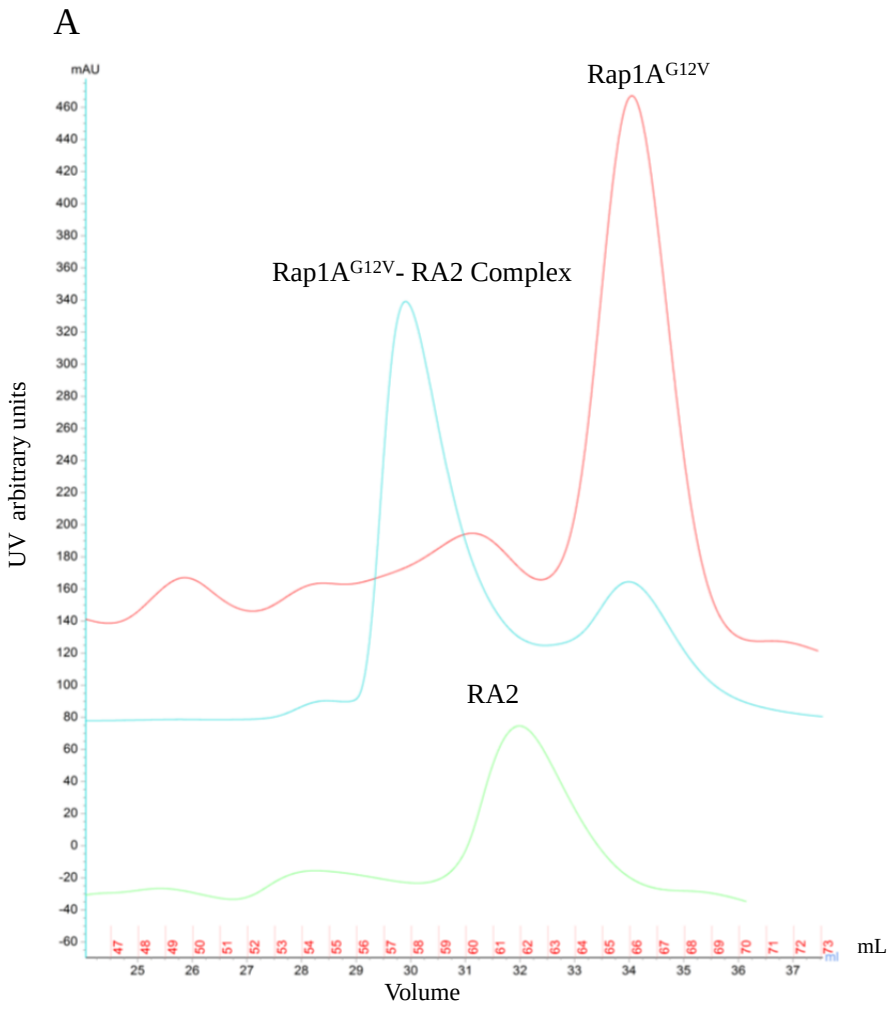

Figure 4.3 Rap1A^{G12V}–RA2 complex formation
A. Superposition of the elution profiles of RA2, Rap1A^{G12V}, and Rap1A^{G12V}–RA2 complex from SEC. **B.** Representative SDS-PAGE gel of the complex. Fractions 56-67 (corresponding to 29-35 mL) were analyzed, but only fractions 56-63 (corresponding to 29-31 mL) corresponded to the complex. The remaining fractions represent unbound Rap1^{G12V}.

Figure 4.3 Continued

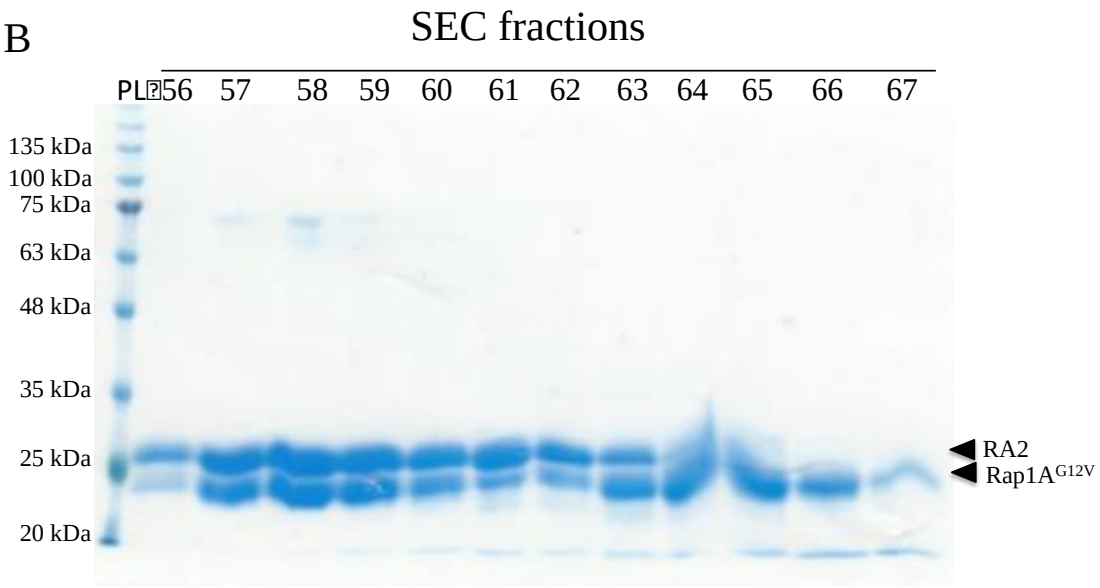

Despite RA2 being a dimer, examination of the complex elution profile indicates that the complex is made of one molecule of Rap1A^{G12V} and one molecule of RA2 (**Fig 4.4**). Comparison of the molecular weight standards to the Rap1A^{G12V}–RA2 complex elution profiles shows that the complex is approximately 44 kDa, consistent with a 1:1 ratio of the proteins (**Fig. 4.4**).

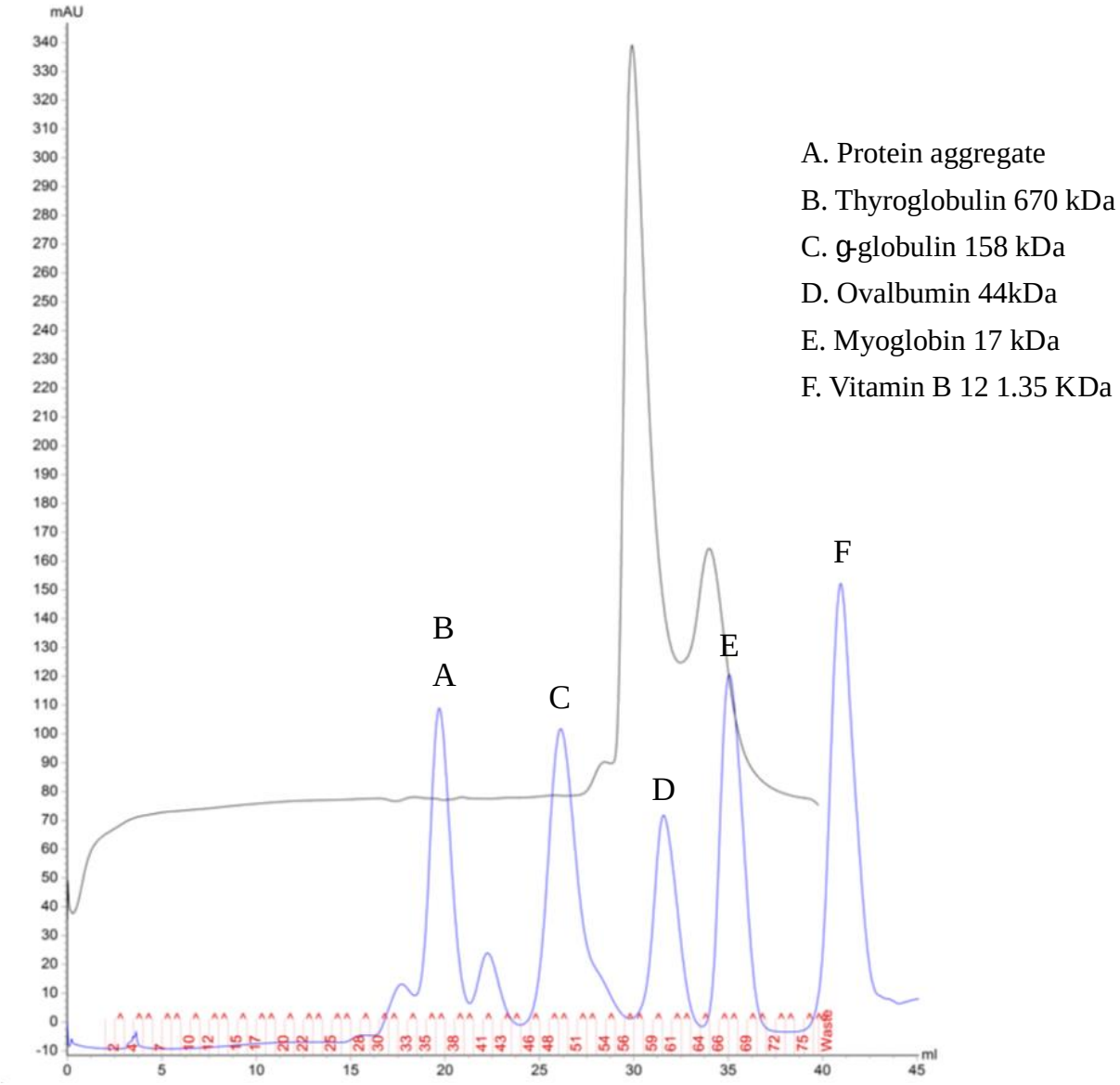

Figure 4.4 Approximation of the molecular weight of the Rap1A^{G12V}–RA2 Complex
A representative chromatogram of the Rap1A^{G12V}–RA2 complex, separated on tandem size exclusion columns, superimposed with the chromatogram of molecular weight standards. The Rap1A^{G12V}-RA2 complex has a predicted molecular weight of 45 kDa.

4.3.3 Crystallization Trials of the Rap1A^{G12V}–RA2 Complex

Initial screening was done using protein purified with the N-terminal His-tags at 20 °C. From these screens, granular precipitate formed in 0.1 M TRIS pH 8.0, 8% PEG 6,000, and 0.15 M NaCl using protein at 25.1 mg/mL. Optimization around this condition resulted in similar precipitate (**Fig. 4.5A**). When these conditions were visualized using a Korima PRS1000 ultraviolet (UV) light microscope, a weak UV signal was observed (**Fig. 4. 5B**). There are still ongoing efforts into optimizing these conditions.

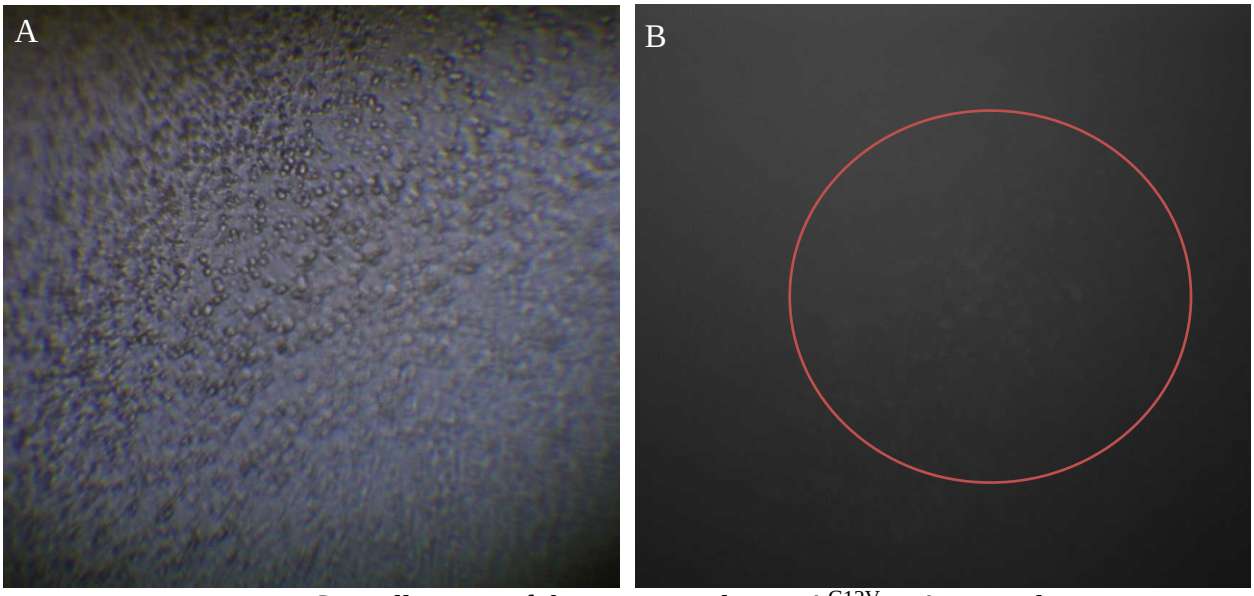

Figure 4.5 Crystallization of the His-tagged Rap1A^{G12V}–RA2 complex.
Granular precipitates of Rap1A^{G12V}–RA2 complex at a concentration of 12.6 mg/mL. The precipitates were observed at 20 °C in 100 mM TRIS pH 8.5, 12 % PEG 6000, and 150 mM NaCl. The photographs were taken using a Korima PRS1000 microscope under A. Visible light or B. ultraviolet light. The red circle indicates regions with a weak UV signal, consistent with protein.

I also screened crystallization conditions for the TEV-cleaved Rap1A^{G12V}–RA2 complex. These efforts are ongoing (**Fig. 4.6).** Spherulites were observed in 0.05 M MOPS pH 7.0, 0.05 M NaCl, 19% (w/v) and PEG 6,000 (**Fig. 4.6A)**, and in 0.1M SPG pH 9.0 (succinic acid, sodium phosphate monobasic monohydrate, and glycine buffer) and 25% PEG 1500, **Fig. 4.6B).** It is important to note that spherulites were only observed at a protein concentration of 7 mg/mL.

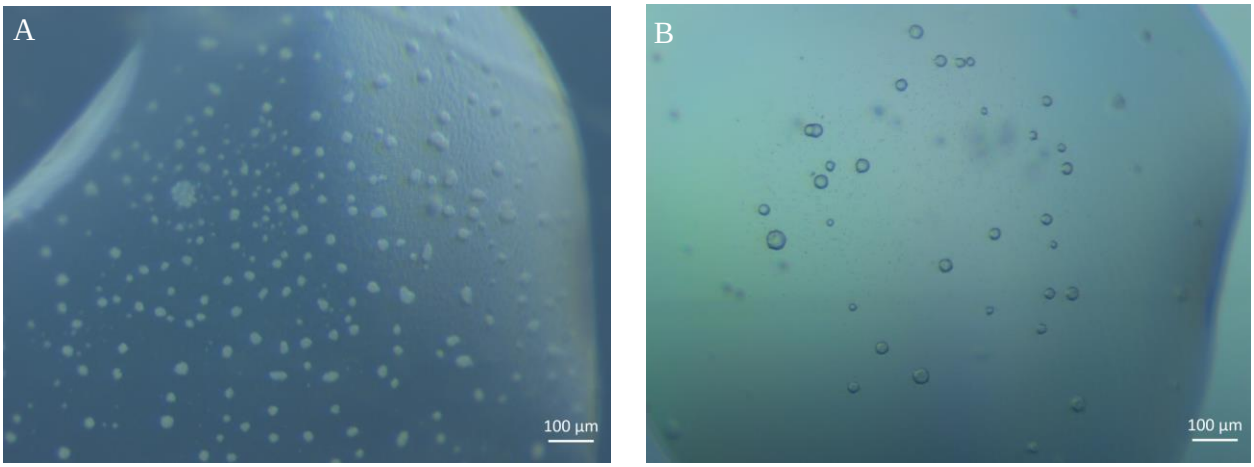

Figure 4.6 Crystallization of the TEV-cleaved Rap1A^{G12V}–RA2 complex.
Spherulites of Rap1A^{G12V}–RA2 complex are observed at a protein concentration of 7 mg/mL at 20 °C in **A**. 0.05 M NaCl, 0.05 M MOPS pH 7.0, and 19% PEG 6,000, **B**. or in 0.1 M SPG pH 9.0 and 25% PEG 1500. The photographs were taken using a Carl Zeiss visible light microscope. The scale bar is 100 µm.

4.4 Discussion and future directions

I have isolated a stable and stoichiometric complex between a constitutively active mutant of Rap1A^{G12V} and the PLCε RA2 domain. The SEC chromatograms of the Rap1A^{G12V} and the RA2 domain indicate the purified proteins are monomeric and dimeric in solution, respectively. These data are supported by observations made when the NMR solution of RA2 was determined [24]. It was shown that RA2 had a propensity to dimerize in solution. In fact, to determine the crystal structure of RA2 in complex with H-Ras, the authors mutated the surface exposed Y2176 to leucine to purify a RA2 monomer. The SEC chromatogram suggest that the complex is ~44 kDa, which is approximately equal to the expected molecular weight (~42 kDa) suggesting that the complex is made of one molecule of RA2 bound to one molecule of Rap1A^{G12V}.

Initial screening of crystallization conditions shows formation of granular precipitate or spherulites, both promising initial signs. A change in temperature might facilitate formation of crystals using these conditions. The H-Ras^{G12V}–RA2 complex was crystallized under oil using the

microbatch method[24], which may be another strategy I can use. A Ras D38N mutation has been shown to selectively activate PLCε [58]. Residue D38 of Ras corresponds to D38 of Rap1A. Therefore, I would be interesting to test whether $Rap1A^{G12V/D38N}$ also selectively activates PLCe. If so this would prove a very important tool to specifically study perinuclear translocation an sustained signaling of PLCε. A study of predicted interface and/or effector residues is required to further determine which Rap1A mutant is selective for PLCε. Since the physiological role of PLCε in the cardiovascular system depends on Rap1A-dependent activation of PLCε, determining the structure of the complex between RA2 and Rap1A is of paramount importance. Ultimately, structure-based therapies can be developed to target this interaction and improve cardiovascular health.

REFERENCES

1. Majerus, P. W. *et al.* The metabolism of phosphoinositide-derived messenger molecules. *Science* **234**, 1519–26 (1986).

2. Berridge, M. J., Lipp, P. & Bootman, M. D. The versatility and universality of calcium signalling. *Nat. Rev. Mol. Cell Biol.* **1**, 11–21 (2000).

3. Nakayama, H. *et al.* The IP3 receptor regulates cardiac hypertrophy in response to select stimuli. *Circ. Res.* **107**, 659–666 (2010).

4. Huang, K.-P. The mechanism of protein kinase C activation. *Trends Neurosci.* **12**, 425–432 (1989).

5. Lipp, P. & Reither, G. Protein Kinase C: The "Masters" of Calcium and Lipid. *Cold Spring Harb. Perspect. Biol.* **3**, (2011).

6. Krishna, S., Zhong, X.-P. & Sauer, K. Regulation of lipid signaling by diacylglycerol kinases during T cell development and function. (2013).

7. Smrcka, A. V, Brown, J. H. & Holz, G. G. Role of phospholipase Cε in physiological phosphoinositide signaling networks. *Cell. Signal.* **24**, 1333–1343 (2012).

8. Kadamur, G. & Ross, E. M. Mammalian Phospholipase C. *Annu. Rev. Physiol.* **75**, 127–154 (2013).

9. Suh, P.-G. *et al.* Multiple roles of phosphoinositide-specific phospholipase C isozymes. *BMB Rep.* **41**, 415–34 (2008).

10. Jezyk, M. R. *et al.* Crystal structure of Rac1 bound to its effector phospholipase C-b2 A R T I C L E S. *Nat. Struct. Mol. Biol.* **13**, 1135–1140

11. Snyder, J. T., Singer, A. U., Wing, M. R., Kendall Harden, T. & Sondek, J. The Pleckstrin Homology Domain of Phospholipase C-β2 as an Effector Site for Rac. *J. Biol. Chem.* **278**, 21099–21104 (2003).

12. Lyon, A. M. *et al.* An autoinhibitory helix in the C-terminal region of phospholipase C-β mediates $G\alpha_q$ activation. *Nat. Struct. Mol. Biol.* **18**, 999–1006 (2011).

13. Hicks, S. N. *et al.* Article General and Versatile Autoinhibition of PLC Isozymes. *Mol. Cell* **31**, 383–394 (2008).

14. Lyon, A. M., Dutta, S., Boguth, C. A., Skiniotis, G. & Tesmer, J. J. G. Full-length $G\alpha_q$-phospholipase C-β3 structure reveals interfaces of the C-terminal coiled-coil domain. *Nat. Struct. Mol. Biol.* **20**, 355–363 (2013).

15. Waldo, G. L. *et al.* Kinetic Scaffolding Mediated by a Phospholipase C-β and G_q Signaling Complex. *Science.* **330** (6006), 974–980 (2010).

16. Ferguson, K. M., Lemmon, M. A., Schlessinger, J. & Sigler, P. B. Structure of the high affinity complex of inositol trisphosphate with a phospholipase C pleckstrin homology domain. *Cell* **83** (6), 1037–1046 (1995).

17. Essen, L.-O., Perisic, O., Cheungt, R., Katant, M. & Williams, R. L. Crystal structure of a mammalian phosphoinositide-specific phospholipase Cβ Structure determination. *Nature* **380** (6575), 595-602 (1996).

18. Lars-Oliver Essen, *et al.* Structural Mapping of the Catalytic Mechanism for a Mammalian Phosphoinositide-Specific Phospholipase C. *Biochemistry* 36 (7), 1704-1718 (1997).

19. Hajicek, N., Charpentier, T. H., Rush, J. R., Harden, T. K. & Sondek, J. Autoinhibition and Phosphorylation-Induced Activation of Phospholipase C-γ Isozymes. *Biochemistry* **52** (28), 4810–4819 (2013).

20. Deng, L. *et al.* Structural basis for recognition of the T cell adaptor protein SLP-76 by the SH3 domain of phospholipase Cgamma1. *J. Mol. Biol.* **352**, 1–10 (2005).

21. McKercher, M. A., Guan, X., Tan, Z. & Wuttke, D. S. Multimodal Recognition of Diverse Peptides by the C-Terminal SH2 Domain of Phospholipase C-γ1 Protein. *Biochemistry* **56**, 2225–2237 (2017).

22. Rotin, D., Honeggers, A. M., Margolissll, B. L., Ullrich, A. & Schlessingers, J. Presence of SH2 Domains of Phospholipase Crl Enhances Substrate Phosphorylation by Increasing the Affinity toward the Epidermal Growth Factor Receptor *The Journal of Biological Chemistry*. **267** (14), 9678-9683 (1992).

23. Bunney, T. D. *et al.* Article Structural Insights into Formation of an Active Signaling Complex between Rac and Phospholipase C Gamma 2. *Mol. Cell* **34**, 223–233

24. Bunney, T. D. *et al.* Structural and Mechanistic Insights into Ras Association Domains of Phospholipase C Epsilon. *Mol. Cell* **21**, 495–507 (2006).

25. Zhang, L., Malik, S., Kelley, G. G., Kapiloff, M. S. & Smrcka, A. V. Phospholipase Cε Scaffolds to Muscle-specific A Kinase Anchoring Protein (mAKAPβ) and Integrates Multiple Hypertrophic Stimuli in Cardiac Myocytes *The Journal of Biological Chemistry.* **286** (26), 23012–23021 (2011).

26. Zhang, L. *et al.* Phospholipase Cε Hydrolyzes Perinuclear Phosphatidylinositol 4-Phosphate to Regulate Cardiac Hypertrophy. *Cell* **153**, 216–227 (2013).

27. Jin, T.-G. *et al.* Role of the CDC25 Homology Domain of Phospholipase Cε in Amplification of Rap1-dependent Signaling. *The Journal of Biological Chemistry.* **276**, 30301–30307 (2001).

28. Schmidt, M. *et al.* A new phospholipase-C–calcium signalling pathway mediated by cyclic AMP and a Rap GTPase. *Nat. Cell Biol.* **3** (11), 1020-1024 (2001).

29. Evellin, S. *et al.* Stimulation of Phospholipase Cε by the M3 Muscarinic Acetylcholine Receptor Mediated by Cyclic AMP and the GTPase Rap2B. *The Journal of Biological Chemistry.* **277** (19), 16805–16813 (2002).

30. Stope, M. B. *et al.* Rap2B-dependent stimulation of phospholipase C-epsilon by epidermal growth factor receptor mediated by c-Src phosphorylation of RasGRP3. *Mol. Cell. Biol.* **24** (11), 4664–4676 (2004).

31. Song, C. *et al.* Regulation of a Novel Human Phospholipase C, PLCε, through Membrane Targeting by Ras. *The Journal of Biological Chemistry.* **276** (4), 2752–2757 (2001).

32. Sorli, S. C., Bunney, T. D., Sugden, P. H., Paterson, H. F. & Katan, M. Signaling properties and expression in normal and tumor tissues of two phospholipase C epsilon splice variants. *Oncogene* **24**, 90–100 (2005).

33. Oestreich, E. A. *et al.* Epac-mediated Activation of Phospholipase C (epsilon) Plays a Critical Role in beta-adrenergic receptor-dependent enhancement of Ca^{2+} mobilization in Cardiac Myocytes . *The Journal of Biological Chemistry.* **282 (8)**, 5488–5495 (2006).

34. Oestreich, E. A. *et al.* Epac and Phospholipase Cε Regulate Ca^{2+} release in the heart by activation of Protein Kinase Cε and Calcium-Calmodulin Kinase II. *The Journal of Biological Chemistry.* **284** (3), 1514–1522 (2008).

35. Malik, S. *et al.* G protein βγ subunits regulate cardiomyocyte hypertrophy through a perinuclear Golgi phosphatidylinositol 4-phosphate hydrolysis pathway. *Mol. Biol. Cell* **26** (6), 1188–1198 (2015).

36. Smrcka, A. V. Regulation of Phosphatidylinositol-specific Phospholipase C at the Nuclear Envelope in Cardiac Myocytes. *J. Cardiovasc. Pharmacol.* **65** (3), 203–210 (2015).

37. Nash, C. A., Brown, L. M., Malik, S., Cheng, X. & Smrcka, A. V. Compartmentalized cyclic nucleotides have opposing effects on regulation of hypertrophic phospholipase Cε signaling in cardiac myocytes. *J. Mol. Cell. Cardiol.* **121**, 51–59 (2018).

38. Wang, H. *et al.* Phospholipase C epsilon modulates beta-adrenergic receptor-dependent cardiac contraction and inhibits cardiac hypertrophy. *Circ. Res.* **97**, 1305–13 (2005).

39. Citro, S. *et al.* Phospholipase C is a nexus for Rho and Rap-mediated G protein-coupled receptor-induced astrocyte proliferation. *Proc. Natl. Acad. Sci. U. S. A.* **104** (39), 15543–15548 (2007).

40. Dusaban, S. S., Kunkel, M. T., Smrcka, A. V & Heller Brown, J. Thrombin Promotes Sustained Signaling and Inflammatory Gene Expression through the CDC25 and Ras-associating Domains of Phospholipase Cε. *The Journal of Biological Chemistry.* **290** (44), 26776–26783 (2015).

41. Dusaban, S. S. *et al.* Phospholipase Cε links G protein-coupled receptor activation to inflammatory astrocytic responses. *Proc. Natl. Acad. Sci. U. S. A.* **110** (9), 3609–3614 (2013).

42. Dealmeida, A. C., Van Oort, R. J. & Wehrens, X. H. T. Transverse Aortic Constriction in Mice. *J. Vis. Exp.* **38**, (2010).

43. Lu, J., Mckinsey, T. A., Nicol, R. L., Olson, E. N. & Mcknight, S. L. Signal-dependent activation of the MEF2 transcription factor by dissociation from histone deacetylases. *Proc. Natl. Acad. Sci. U. S. A.* **97**, 4070–4075 (2000).

44. Zou, Y. *et al.* Heart Ryanodine Receptor Type 2 Is Required for the Development of Pressure Overload-Induced Cardiac Hypertrophy. *Hypertens.* **58**, 1099–1110 (2011).

45. Hains, M. D., Wing, M. R., Maddileti, S., Siderovski, D. P. & Harden, T. K. $G\alpha_{12/13}$-and Rho-Dependent Activation of Phospholipase C-epsilon by Lysophosphatidic Acid and Thrombin Receptors. *Mol. Pharmacol.* **69** (6), 2068–2075 (2006).

46. Kelley, G. G., Reks, S. E. & Smrcka, A. V. *Hormonal regulation of phospholipase Cε through distinct and overlapping pathways involving G_{12} and Ras family G-proteins. Biochem. J* **378** (1), (2004).

47. Lopez, I., Mak, E. C., Ding, J., Hamm, H. E. & Lomasney, J. W. A Novel Bifunctional Phospholipase C That Is Regulated by Galpha 12 and Stimulates the Ras/Mitogen-activated Protein Kinase Pathway. *The Journal of Biological Chemistry.* **276** (4), 2758–2765 (2001).

48. Wakita, M. *et al.* Phospholipase Cε Activates Nuclear Factor-B Signaling by Causing Cytoplasmic Localization of Ribosomal S6 Kinase and Facilitating Its Phosphorylation of Inhibitor κB in Colon Epithelial Cells. *The Journal of Biological Chemistry.* **291** (24), 12586–12600 (2016).

49. Whiteside, T. L. The tumor microenvironment and its role in promoting tumor growth. *Oncogene* **27**, 5904–5912 (2008).

50. Cui, X.-B. *et al.* Targeting oncogenic PLCE1 by miR-145 impairs tumor proliferation and metastasis of esophageal squamous cell carcinoma. *Oncotarget* **7**, 1777–95 (2016).

51. Chen, Y. *et al.* Epigenetically upregulated oncoprotein PLCE1 drives esophageal carcinoma angiogenesis and proliferation via activating the PI-PLCε-NF-κB signaling pathway and VEGF-C/ Bcl-2 expression. *Mol. Cancer* **18**, 1–19 (2019).

52. Bijli, K. M. *et al.* Phospholipase C-ε signaling mediates endothelial cell inflammation and barrier disruption in acute lung injury. *Am. J. Physiol. Lung Cell. Mol. Physiol.* **311**, L517-24 (2016).

53. Du, H. *et al.* Nuclear factor-κB signaling pathway is involved in phospholipase Cε-regulated proliferation in human renal cell carcinoma cells. *Mol. Cell. Biochem.* **389**, 265–275 (2014).

54. Li, M., Edamatsu, H., Kitazawa, R., Kitazawa, S. & Kataoka, T. Phospholipase Cε promotes intestinal tumorigenesis of $Apc^{Min/+}$ mice through augmentation of inflammation and angiogenesis. *Carcinogenesis* **30**, 1424–1432 (2009).

55. Song, C. *et al.* Differential roles of Ras and Rap1 in growth factor-dependent activation of phospholipase Cε. *Oncogene* **21**, 8105–8113 (2002).

56. Martins, M. *et al.* Activity of PLC contributes to chemotaxis of fibroblasts towards PDGF. *J. Cell Sci.* **125**, 5758–5769 (2012).

57. Kelley, G. G., Kaproth-Joslin, K. A., Reks, S. E., Smrcka, A. V. & Wojcikiewicz, R. J. H. G-protein-coupled Receptor Agonists Activate Endogenous Phospholipase Cε and Phospholipase Cβ3 in a Temporally Distinct Manner. *The Journal of Biological Chemistry.* **281** (5), 2639–2648 (2006).

58. Kelley, G. G., Reks, S. E., Ondrako, J. M. & Smrcka, A. V. Phospholipase C(epsilon): a novel Ras effector. EMBO J, 20(4), 743-754. (2001).

59. Bos, J. L., Rehmann, H. & Wittinghofer, A. GEFs and GAPs: Critical Elements in the Control of Small G Proteins. *Cell* **129**, 865–877 (2007).

60. Lopez, I., Mak, E. C., Ding, J., Hamm, H. E. & Lomasney, J. W. A Novel Bifunctional Phospholipase C That Is Regulated by Galpha12 and Stimulates the Ras/Mitogen-activated Protein Kinase Pathway. *The Journal of Biological Chemistry.* **276 (4)**, 2758–2765 (2001).

61. Boriack-Sjodin, P. A., Margarit, S. M., Bar-Sagi, D. & Kuriyan, J. The structural basis of the activation of Ras by Sos. *Nature* **394**, 337–343 (1998).

62. Altschul, S. F., Gish, W., Miller, W., Myers, E. W. & Lipman, D. J. Basic local alignment search tool. *J. Mol. Biol.* **215**, 403–410 (1990).

63. Cole, C., Barber, J. D. & Barton, G. J. The Jpred 3 secondary structure prediction server. *Nucleic Acids Res.* **36**, 197–201 (2008).

64. Seifert, J. P., Zhou, Y., Hicks, S. N., Sondek, J. & Kendall Harden, T. Dual Activation of Phospholipase C-ε by Rho and Ras GTPases. *The Journal of Biological Chemistry.* **283** (44), 29690–29698 (2008).

65. Seifert, J. P. *et al.* RhoA Activates Purified Phospholipase C-ε by a Guanine Nucleotide-dependent Mechanism. *The Journal of Biological Chemistry.* **279**, 47992–47997 (2004).

66. Wing, M. R. *et al.* Activation of Phospholipase C-ε by Heterotrimeric G Protein βγ-Subunits. *The Journal of Biological Chemistry.* **276**, 48257–48261 (2001).

67. Leinonen, R. *et al.* UniProt archive. *Bioinforma. Appl. Note* **20**, 3236–3237 (2004).

o68. Bienert, S. *et al.* The SWISS-MODEL Repository—new features and functionality. *Nucleic Acids Res.* **45**, D313–D319 (2017).

69. Athena Enzyme Systems. *Protein Refolding Kit Application Manual V 2.1*.

70. Lea, W. A. & Simeonov, A. Fluorescence Polarization Assays in Small Molecule Screening. *Expert Opin Drug Discov.* **6**, 17–32 (2011).

71. Arkin, M. R., Glicksman, M. A., Fu, H., Havel, J. J. & Du, Y. Inhibition of Protein-Protein Interactions: Non- Cellular Assay Formats. *Assay Guid. Man.* (2012).

72. Evelyn, C. R. *et al.* High-Throughput Screening for Small-Molecule Inhibitors of LARG-Stimulated RhoA Nucleotide Binding via a Novel Fluorescence Polarization Assay. *J. Biomol. Screen.* **14**, 161–172 (2009).

73. Yamaguchi, H. & Miyazaki, M. Refolding Techniques for Recovering Biologically Active Recombinant Proteins from Inclusion Bodies. *Biomolecules* **4**, 235–251 (2014).

74. Vallejo, L. F. & Rinas, U. Microbial Cell Factories Strategies for the recovery of active proteins through refolding of bacterial inclusion body proteins. *Microb. Cell Fact.* **3**, (2004).

75. Thomson, C. A., Olson, M., Jackson, L. M. & Schrader, J. W. Simplified Method for the Efficient Refolding and Purification of Recombinant Human GM-CSF. *PLoS One* **7**, 1–6 (2012).

76. Rudolph' And, R. & Lilie, H. In vitro folding of inclusion body proteins. *FASEB J.* **10**, 49–56 (1996).

77. Korlach, J. *et al.* Spontaneous nucleotide exchange in low molecular weight GTPases by fluorescently labeled-phosphate-linked GTP analogs. *PNAS* **101**, 2800–2805 (2004).

78. Kelley, G. G., Reks, S. E., Ondrako, J. M. & Smrcka, A. V. Phospholipase Cepsilon: a novel Ras effector. *EMBO J.* **20**, 743–754 (2001).

79. Garland-Kuntz, E. E. *et al.* Direct observation of conformational dynamics of the PH domain in phospholipases Cϵ and β may contribute to subfamily-specific roles in regulation. *The Journal of Biological Chemistry.* **293**, 17477–17490 (2018).

80. Sieng, M., Garland-Kuntz, Elisabeth, E. & Lyon, Angeline, M. Characterization of Rap1A-dependent activation of PLCε. *Submitted to the Journal of Bioogical Chemistry*

81. Vollrath, F., Hawkins, N., Porter, D., Holland, C. & Boulet-Audet, M. Differential Scanning Fluorimetry provides high throughput data on silk protein transitions. *Sci. Reports* **4**, 5625 (2014).

82. Ullmann, A., Jacob, F. & Monod, J. Characterization by in vitro complementation of a peptide corresponding to an operator-proximal segment of the beta-galactosidase structural gene of Escherichia coli. *J. Mol. Biol.* **24**, 339–43 (1967).

83. Vieira, J. & Messing, J. The pUC plasmids, an M13mp7-derived system for insertion mutagenesis and sequencing with synthetic universal primers. *Gene* **19**, 259–268 (1982).

84. Vonrhein, C. *et al.* Data processing and analysis with the autoPROC toolbox. *Acta Crystallogr. D. Biol. Crystallogr.* **67**, 293–302 (2011).

85. Emsley, P., Cowtan, K. & IUCr. Coot : model-building tools for molecular graphics. *Acta Crystallogr. Sect. D Biol. Crystallogr.* **60**, 2126–2132 (2004).

86. Adams, P. D. *et al.* PHENIX: a comprehensive Python-based system for macromolecular structure solution. *Acta Crystallogr. Sect. D Biol. Crystallogr.* **66**, 213–221 (2010).

87. Vagin, A. A. *et al.* REFMAC5 dictionary: organization of prior chemical knowledge and guidelines for its use. *Acta Crystallogr. Sect. D Biol. Crystallogr.* **60**, 2184–2195 (2004).

88. Winn, M. D. *et al.* Overview of the CCP 4 suite and current developments. *Acta Crystallogr. Sect. D Biol. Crystallogr.* **67**, 235–242 (2011).

89. Chen, V. B. *et al.* MolProbity : all-atom structure validation for macromolecular crystallography. *Acta Crystallogr. Sect. D Biol. Crystallogr.* **66**, 12–21 (2010).

90. Lyon, A. M., Begley, J. A., Manett, T. D. & Tesmer, J. J. G. Molecular Mechanisms of Phospholipase C β3 Autoinhibition. *Cell Struct.* **22**, 1–11 (2014).

91. Jurrus, E. *et al.* Improvements to the APBS biomolecular solvation software suite. *Protein Sci.* **27**, 112–128 (2018).

92. Lyon, A. M. & Tesmer, J. J. G. Structural Insights into Phospholipase C- Function. *Mol. Pharmacol.* **84**, 488–500 (2013).

93. Wing, M. R., Snyder, J. T., Sondek, J. & Harden, T. K. Direct Activation of Phospholipase C-ε by Rho*. *J. Biol. Chem.* **278**, 41253–41258 (2003).

94. Ponting, C. P. & Benjamin, D. R. A novel family ofras-binding domains. *Trends Biochem. Sci.* **21**, 422–425 (1996).

95. Nassar, N. *et al.* The 2.2A crystal structure of the Ras-binding domain of the serine/threonine kinase c-Raf1 in complex with Rap1A and a GTP analogue. *Nature* **375**, 554–60 (1995).

96. Zhang, H., Chang, Y.-C., Brennan, M. L. & Wu, J. The structure of Rap1 in complex with RIAM reveals specificity determinants and recruitment mechanism. *J. Mol. Cell Biol.* **6**, 128–139 (2014).